A New Physical Shape Synthesis Method for Planar Microwave Circuits

Amal Emammar Al Ma Mohammed

Thesis submitted in partial fulfillment of the requirements for the
Doctorate in Philosophy degree
in Electrical & Computer Engineering

Ottawa-Carleton Institute for Electrical and Computer Engineering
School of Electrical Engineering and Computer Science
Faculty of Engineering
University of Ottawa

Abstract

Many microwave (RF) circuit designs require passive distributed sub-components with prescribed scattering parameters. These sub-components have typically been realised by cascading building-block configurations (eg. transmission lines of specific lengths, bends in transmission lines, coupled lines, and so on) of standard shape, and then adjusting the dimensions of selected prescribed features of these building-blocks. The problem with this approach is that the resulting sub-component may take up more "real-estate" on the overall circuit board than can be tolerated, may require tolerances that are too tight and hence be more costly than product developers can allow, can lead to less-than-best performance because we select the building-blocks (that we think are needed) ahead of time, and so on. The research in this thesis contributes to the shape synthesis approach of physical microstrip circuit design. The shape synthesis process is usually contrasted to traditional design by recognizing that it does not merely adjust the dimensions of a set of prescribed geometrical features on pre-selected shapes, but allows the electromagnetic physics to tell us what the sub-component layout needs to be (and it can be unconventional) in order to obtain the required performance. Existing shape synthesis techniques are based on the discrete- or continuous-pixelation method. Each of these approaches, however, have disadvantages (eg. too many degrees of freedom required to achieve the geometrical resolution necessary; the need for arbitrary decisions to fix material properties) that have prevented shape synthesis from being accepted for widespread use in design practice. In this thesis we develop, implement and apply a completely new shape synthesis approach, called the subtractive approach, that overcomes many of the above-mentioned disadvantages of pixelation-based methods It reduces the number of variables (degrees of freedom) needed in spite of the fact that the "design space" is significantly broadened by this approach. The latter is confirmed by the fact that it produces physical circuit geometries that we would not have come up with using traditional design methods. Examples are provided of the application of the new subtractive shape synthesis method. This new method involves continuous variables directly related to the physical circuit geometry, and thus could be used with surrogate modelling, unlike some existing shape synthesis procedures.

Acknowledgements

I thank God for giving me the strength, knowledge, ability, and opportunity to initiate this study and complete it successfully. I pray that my work be of benefit for those who come after me.

I am grateful to my supervisor, Professor Derek McNamara, for his support, guidance, advice, and many suggestions throughout the course of my research, and for allowing me to liberally use some review material on S-parameters for Chapter 2, from the notes of various courses he presents at the University of Ottawa. I am extremely fortunate to have had a supervisor who cares so much about my work and who responds so quickly to my questions and inquiries.

In addition, I would like to thank my PhD Advisory Committee members (Professors Aldo Petosa and Mustapha Yagoub) for their insightful and constructive advice on my thesis proposal.

Moreover, I would like to extend my appreciation to my colleagues Mohammed Nassor and Abdullah Aljanah for their support and for many enjoyable discussions.

Finally, I must express my gratitude to my family (especially my mother) for their continued support and encouragement.

TABLE OF CONTENTS

List of Figures

List of Tables

List of Acronyms

AI	Artificial Intelligence
ANN	Artificial Neural Network
CEM	Computational Electromagnetics
DNN	Deep Neural Network
FDTD	Finite-Difference Time-Domain (Method)
FEM	Finite Element Method
FSS	Frequency Selective Surface
GA	Genetic Algorithm
TL	Transmission Line
MIMO	Multiple-input Multiple-output
ML	Machine Learning
MM	Moment Method
NN	Neural Network
PEC	Perfect Electric Conductor
Q	Quality Factor
RWG	Rao-Wilton-Glisson expansion function

CHAPTER 1
Introduction

1.1 MICROWAVE CIRCUITS & THEIR SHAPE SYNTHESIS

Irrespective of the features and sophistication of any wireless communications device, or the extent of the "digitization" of the information processing, there must be an RF[1] front-end and antenna that is analog. The front-end is that portion that requires microwave circuit design of the kind described in texts such as [COLL 92], [POZA 90], [STEE 13], [DAVI 84] and [SORR 10]. In the recent past, it used to be the antenna designers that bemoaned the fact that radiators were often an afterthought as far as the system/product design was concerned, with little room and often inappropriate locations designated for these antennas. Fortunately, this latter challenge spawned new research in antenna engineering that resulted in improved understanding (eg. of electrically small antennas) and some new design methods. Some now claim that similar curtailments are now also placed on RF front-end circuits, even as performance demands on these tighten (eg. inclusion of an ability to electronically reconfigure the antennas). Few doubt that RF engineering will overcome these hurdles in a number of ways.

Many microwave (RF) circuit designs require passive two- and multi-port distributed sub-components with prescribed scattering parameters[2]. Until now these sub-components have typically been realised by cascading building-block configurations (eg. transmission lines of specific lengths; bends in transmission lines; coupled lines; more complex combinations of such lines as in hybrids; and so on[3]) of standard shape, and then adjusting the dimensions of known features of these building-blocks[4]. The problem with this approach is that the resulting sub-component may take up more "real-estate" on the overall circuit board than can be tolerated, may require tolerances that are too tight and hence be more costly than product developers can allow, and/or can lead to less-than-best performance because we select the building-blocks (that we

[1] Although the acronym "RF" used to stand for "radio-frequency", a word that in earlier times implied frequencies lower than what we would now call microwave or milliemetrewave, the acronym RF is now most often meant to mean circuits that operate anywhere between about 30 MHz and 300 GHz. We will use it in this way.
[2] S-parameters are reviewed in Section 2.4.
[3] This is often referred to as a known *design library*. It will be useful terminology in the present work.
[4] As will be stated in Section 2.10, this "adjustment" is usually done automatically using numerical optimization, a process we will term *feature optimization*.

think are needed) ahead of time[5]. The *shape synthesis process* is usually contrasted to traditional design by recognizing that it does not merely adjust the dimensions of a set of prescribed geometrical features on pre-selected shapes, but allows the electromagnetic physics to tell us what the sub-component layout needs to be (and it can be unconventional) in order to obtain the required performance.

Existing shape synthesis techniques are based on the discrete- or continuous-pixelation method. Each of these approaches, however, have disadvantages (eg. too many degrees of freedom required to achieve the geometrical resolution necessary; the need for arbitrary decisions to fix material properties) that have prevented shape synthesis from being accepted for widespread use in design practice. As its **contribution to shape synthesis** this thesis develops, implements and applies a completely new shape synthesis approach, called the subtractive approach, that overcomes many of the above-mentioned disadvantages of pixelation-based methods It reduces the number of variables (degrees of freedom) needed in spite of the fact that the "design space" is significantly broadened by this approach. The latter is confirmed by the fact that it produces physical circuit geometries that we would not have come up with using traditional design methods. Examples are provided of the application of the new subtractive shape synthesis method. This new method involves continuous variables directly related to the physical circuit geometry, and thus could be used with surrogate modelling, unlike some existing shape synthesis procedures.

1.2 OVERVIEW OF THE THESIS

The research described in this thesis deals with the shape synthesis of passive distributed circuits realized in a microstrip medium[6].

■ **Chapter 2** broadly reviews the subject of microwave circuit design. This is needed to be able to show the context into which to fit the subject of the shape synthesis of microstrip circuits.

■ **Chapter 3** places into perspective what has already been achieved on the shape synthesis of microwave circuits and antennas by other researchers. It allows us to identify the problem issues, and speculate why shape synthesis has not become widely-used yet; the literature on the subject is somewhat sparse compared to other research topics. A new interpretation of the physical RF

[5] In other words, there might be better possibilities that are not even known about.
[6] Although it could also be used with other media.

circuit/antenna shape synthesis problem is described, and a framework into which to place existing and future shape synthesis work, proposed.

■ **Chapter 4** introduces the new subtractive shape synthesis method. It enables us to retain the geometrical resolution needed for the shape synthesis of good performance physical circuits, and yet keep the number of degrees of freedom to a manageable value. The mesh density required to achieve accuracy in the computational electromagnetics analysis of the physical (eg. microstrip) circuit is separate from the geometry resolution aspects. Reasons for adopting such an approach, and its benefits, are described.

■ **Chapter 5** demonstrates the implementation of the subtractive shape synthesis method by applying it to the shape synthesis of several microstrip circuits.

■ Finally, **Chapter 6** summarizes the contributions of the thesis, and suggests possible future work.

CHAPTER 2
Review of Passive Microstrip Circuit Analysis & Design

2.1 INTRODUCTION

The actual device hardware that one can place on a laboratory bench we can call the physical circuitry. This physical circuitry, consisting of interconnected components, is described completely by the equations of macroscopic electromagnetic theory (and the other branches of continuum physics if necessary[7]), which we call the physical model or full-wave model. We are able to analyse any piece of physical circuitry, in principle, using this physical model. In engineering we analyse principally in order to be able to synthesize (or design). Because the physical model often provides a far more complete description of the physical circuit than is often required for conceptual design purposes, a more tangible and pictorial (or diagrammatic) model, namely a network model[8] consisting of interconnected elements[9], with which the said physical circuitry can be thought about during conceptual design work, is used. Once the conceptual design has been completed, a full-wave model of the physical circuit is usually used to finalize the design.

A proper appreciation for the direction taken in the development of a new shape synthesis technique that is the principal contribution of this thesis (and described in Chapter 4) is most easily achieved through the considerations laid out in Chapter 3. In order to offer Chapter 3 in a succinct way, a brief review of some basic concepts and tools used in traditional RF/microwave physical circuit design is given in the present chapter. Section 2.2 reminds us what we mean by lumped elements[10]. Section 2.3 sets down some well-known distributed circuit theory so that we can carefully define S-parameters in Section 2.4; the performance of all the physical circuits

[7] A physical system is in general a combination of electromagnetic, mechanical, thermodynamic, and other processes. If the material for some reason changes its electromagnetic properties (namely permittivity, permeability or conductivity), say, due to mechanical forces or heating, then it might be necessary to couple to the electromagnetic model other physical theories that account for the change in the electromagnetic properties or mechanical dimensions of the material. This is would then be known as a *multi-physics* problem. It would not necessarily be a linear time-invariant problem. We do not consider such multi-physics problems in this thesis, but the novel shape synthesis process introduced in Chapter 4 could be adapted to such problems; it can use whatever physics is needed for accurate analysis of the physical circuit.

[8] A network model is most often called an "equivalent circuit model", or simply the use of circuit theory.

[9] These are the familiar resistors, capacitors, inductors and ideal transformers (lumped elements), and transmission lines (distributed elements).

[10] So that we can refer to them in Section 2.9.

shape synthesized in Chapter 5 will be expressed in terms of S-parameters. The shape synthesis will utilize optimisation algorithms and methods of computational electromagnetics (as existing resources); thus some facts about these are written down in Section 2.5 and 2.6. What is meant by surrogate modelling (and how it is in fact a form of machine learning) is described in Sections 2.7 and 2.8. Past and current approaches to the design of physical microstrip circuits are appraised in Sections 2.9 and 2.10. Section 2.11 concludes the chapter.

2.2 LUMPED NETWORK MODEL ('EQUIVALENT CIRCUIT') ELEMENTS

A lumped linear network model consists of some combination of three types of passive components : resistances (R), capacitances (C) and inductances (L). Any electromagnetic system contains two types of energy, namely electric and magnetic. Depending on the circumstances, part of this energy may be converted into some other type of energy (eg. heat), in which case it is no longer electromagnetic and we say that power has been dissipated. Or power can be radiated away from the physical circuit in the form of electromagnetic waves; from the point of view of physical circuits that are not intended to be antennas[11] this has the same status as power dissipation. Resistors can be used to model such power dissipation. Inductors and capacitors can be used to model the two types of energy storage. Booker[12] notes that at lower frequencies the above-mentioned components have a physical structure not radically different from the way they are drawn in network model diagrams. At higher frequencies practicalities very often prevent this from being so.

The actual values of R, L and C for a given physical circuit cannot be found from within the network model (that is, from within "circuit theory"). They have to be found using either electromagnetic theory or through measurement *before being used as part of any network model*. When designing circuits (usually at low frequencies) for which lumped element network models are all that is needed, we implicitly assume that a range (or specific values) of R, L and C will be physically available to us.

[11] In this thesis we are concerned with physical circuits that are not intentionally designed to radiate, and preferably do not. The new shape synthesis method devised in Chapter 4 can, however, be applied to antenna problems as well.
[12] H.G.Booker, *Energy in Electromagnetism* (Peter Peregrinus Ltd., 1982) pp.176.

2.3 DISTRIBUTED NETWORK MODEL ('EQUIVALENT CIRCUIT') ELEMENTS

Fig.2.3-1 shows a distributed network model[13] for a single eigenmode[14] of a waveguiding structure. Usually, such waveguiding structures are designed so that, over some operating frequency band of interest, only one eigenmode is able to propagate (the dominant or lowest-order mode) and all others not. The non-propagating (evanescent) modes can be excited and store energy locally in the vicinity of their point of excitation, but cannot transport this energy. Only the lowest-order modes can move power from one point to another. The TL model describes the latter type of mode and no other. Localized energy storage due to evanescent modes can be modelled using the lumped components mentioned in Section 2.2.

The TL network model of any physical waveguiding structure requires knowledge of four parameters that, *before the network model can be used*, need to be found for that particular structure using either electromagnetic theory or measurements. These are the parameters:

- ❖ L : (Series) Inductance per unit length (Henries/Metre)
- ❖ C : (Shunt) Capacitance per unit length (Farads/Metre)
- ❖ R : (Series) Resistance per unit length (Ohms/Metre)
- ❖ G : (Shunt) Conductance per unit length (Siemens/Metre)

These are all physical properties of the waveguiding structure being represented by the TL network model, and so vary from one structure to another.

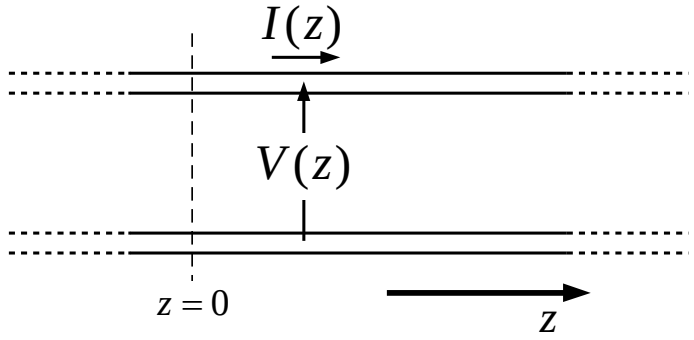

Fig.2.3-1 : Voltage and current on a distributed network model (also called a transmission line model) of a waveguiding structure.

[13] Which we can also refer to as the transmission line (TL) model.
[14] Eigenmodes are essentially wave-types that are able to exist on their own (and hence in combination if necessary) on the waveguiding structure.

Circuit theory can be used to show that a voltage-wave of the form

$$V(z) = V_0^+ e^{-\gamma z} + V_0^- e^{+\gamma z} \tag{2.3-1}$$

can exist on the source-excited (Thevenin source) and impedance-terminated (loaded) TL shown in Fig.2.3-2[15]. The term $V_0^+ e^{-\gamma z} = V^i(z)$ is a voltage wave travelling in the positive z-direction, and $V_0^- e^{+\gamma z} = V^r(z)$ such a wave travelling in the negative z-direction. V_0^+ and V_0^- are the complex amplitudes (constants independent of z) that can only be determined once the source and load have been specified. The quantity

$$\gamma = \alpha + j\beta = \pm\sqrt{(R + j\omega L)(G + j\omega C)} \tag{2.3-2}$$

is the propagation factor of the TL, and is clearly a property of the waveguiding structure. The *characteristic impedance* of the TL is defined as $Z_0 = V_0^+ / I_0^+ = -V_0^- / I_0^-$, from which it can be shown that

$$Z_0 = \sqrt{\frac{R + j\omega L}{G + j\omega C}} \tag{2.3-3}$$

Clearly, Z_0 is also a property of the waveguiding structure being modelled via the TL network model; it has to be determined from an electromagnetic analysis of the said waveguiding structure. The associated current wave on the TL is

$$I(z) = \frac{V_0^+}{Z_0} e^{-\gamma z} - \frac{V_0^-}{Z_0} e^{\gamma z} \tag{2.3-4}$$

For completeness, we mention that [POZA 90]

$$V_0^+ = V_g \left(\frac{Z_0}{Z_0 + Z_g} \right) \left\{ \frac{e^{-\gamma d}}{1 - \Gamma_L \Gamma_G e^{-2\gamma d}} \right\} \tag{2.3-5}$$

where

$$\Gamma_L = \frac{Z_L - Z_0}{Z_L + Z_0} \tag{2.3-6}$$

[15] The thin lines connected to the terminals of the TL network model do not occupy any space; they are lumped and not part of the distributed network model.

and

$$\Gamma_G = \frac{Z_g - Z_0}{Z_g + Z_0} \tag{2.3-7}$$

$$V_0^- = \Gamma_L V_0^+ \tag{2.3-8}$$

One final useful relation, obtained from (2.3-6), is

$$\frac{Z_L}{Z_0} = \frac{1+\Gamma_L}{1-\Gamma_L} \tag{2.3-9}$$

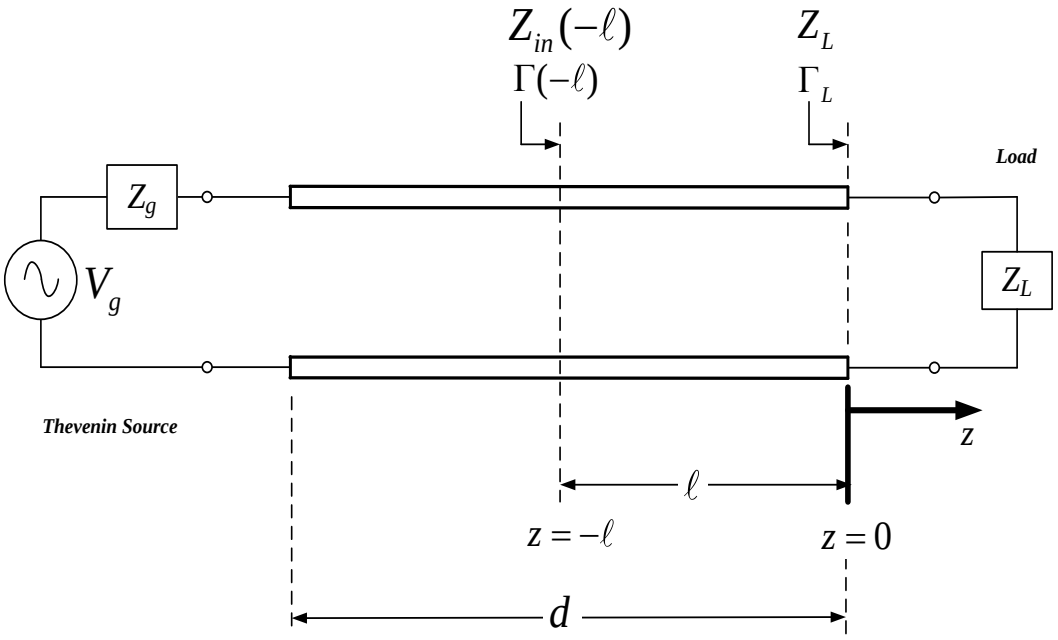

Fig.2.3-2 : TL network model of specified length (d), that has a source and load connected.

2.4 PERFORMANCE MEASURES FOR PASSIVE RF CIRCUITS

2.4.1 Transmission Lines Accessing the Ports of a Two-Port Network

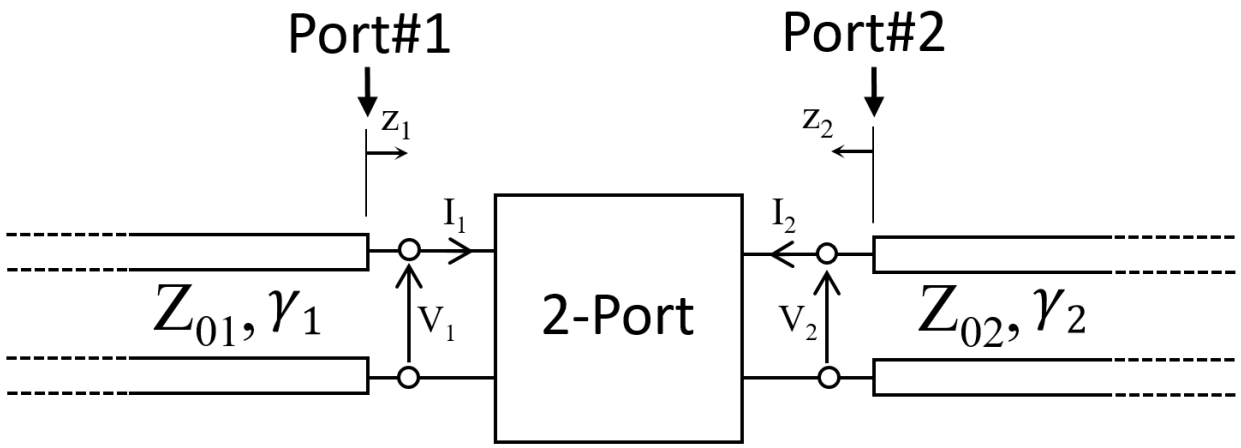

Fig.2.4-1 : Two-port network with ports accessed by transmission lines that may have different characteristic impedances.

The symbols z_1 and z_2 denote general locations on the TLs connected to port#1 and port#2 of the 2-port network. They should not be interpreted as specific values of some variable z. Once more, the thin lines connected to the terminals of the two-port network in Fig.2.4-1 do not occupy any space; they are lumped and not distributed. The TLs that are shown accessing the terminals do occupy space; they are part of the distributed network models of the actual waveguiding structures used to access the ports of the 2-port network.

The voltage on the two TLs can be written (purposefully adopting symbols similar to those in Section 2.3) as

$$V_1(z_1) = V_{01}^{+}\, e^{-\gamma_1 z_1} + V_{01}^{-}\, e^{+\gamma_1 z_1} = V_1^{i}(z_1) + V_1^{r}(z_1) \tag{2.4-1}$$

and

$$V_2(z_2) = V_{02}^{+}\, e^{-\gamma_2 z_2} + V_{02}^{-}\, e^{+\gamma_2 z_2} = V_2^{i}(z_2) + V_2^{r}(z_2) \tag{2.4-2}$$

So-called ‘power wave’ quantities are defined as [POZA 90]

$$a_1(z_1) = \frac{1}{\sqrt{Z_{01}}} V_1^{i}(z_1) \tag{2.4-3}$$

$$a_2(z_2) = \frac{1}{\sqrt{Z_{02}}} V_2^i(z_2) \tag{2.4-4}$$

$$b_1(z_1) = \frac{1}{\sqrt{Z_{01}}} V_1^r(z_1) \tag{2.4-5}$$

and

$$b_2(z_2) = \frac{1}{\sqrt{Z_{02}}} V_2^r(z_2) \tag{2.4-6}$$

We will write

$$a_1 = a_1(z_1)\big|_{z_1=0} \tag{2.4-7}$$

$$b_1 = b_1(z_1)\big|_{z_1=0} \tag{2.4-8}$$

$$a_2 = a_2(z_2)\big|_{z_2=0} \tag{2.4-9}$$

and

$$b_2 = b_2(z_2)\big|_{z_2=0} \tag{2.4-10}$$

It is important to recognize the notation in (2.4-7) through (2.4-10). Note that b_1 and b_2 represent waves exiting the respective ports, whereas a_1 and a_2 represent waves entering the ports.

2.4.2 Definition of the Scattering Parameters

The performance of all the devices of interest in this thesis can be completely characterized in terms of the scattering parameters (S-parameters). They are defined here for 2-port networks. The scattering parameters of the 2-port are defined as

$$b_1 = S_{11}a_1 + S_{12}a_2 \tag{2.4-11}$$

and

$$b_2 = S_{21}a_1 + S_{22}a_1 \tag{2.4-12}$$

In matrix form this is

$$\begin{bmatrix} b_1 \\ b_2 \end{bmatrix} = \begin{bmatrix} S_{11} & S_{12} \\ S_{21} & S_{22} \end{bmatrix} \begin{bmatrix} a_1 \\ a_2 \end{bmatrix} \tag{2.4-13}$$

$[S]$ is the scattering matrix of the two-port, and the S_{ij} are its scattering parameters. We can use (2.4-11) and (2.4-12) to write

$$S_{11} = \left.\frac{b_1}{a_1}\right|_{a_2=0} \qquad S_{12} = \left.\frac{b_1}{a_2}\right|_{a_1=0} \qquad S_{21} = \left.\frac{b_2}{a_1}\right|_{a_2=0} \qquad S_{22} = \left.\frac{b_2}{a_2}\right|_{a_1=0} \tag{2.4-14}$$

The condition $a_2 = 0$ prevails when Port #2 is terminated in a load impedance $Z_{L2} = Z_{02}$ and the source is on the Port#1 side of the network, whereas $a_1 = 0$ whenever Port #1 is terminated in a load impedance $Z_{L1} = Z_{01}$ and the source is on the Port#2 side of the network.

It is instructive to relate the power wave quantities to the voltage amplitudes mentioned earlier. We begin with

$$S_{11} = \left.\frac{b_1}{a_1}\right|_{a_2=0} = \left.\frac{V_{01}^-}{V_{01}^+}\right|_{a_2=0} \tag{2.4-15}$$

and similarly

$$S_{12} = \left.\sqrt{\frac{Z_{02}}{Z_{01}}}\,\frac{V_{01}^-}{V_{02}^+}\right|_{a_1=0} \tag{2.4-16}$$

$$S_{21} = \left.\sqrt{\frac{Z_{01}}{Z_{02}}}\,\frac{V_{02}^-}{V_{01}^+}\right|_{a_2=0} \tag{2.4-17}$$

$$S_{22} = \left.\frac{V_{02}^-}{V_{02}^+}\right|_{a_1=0} \tag{2.4-18}$$

Expressions (2.4-16) and (2.4-17) of course simplify when $Z_{01} = Z_{02}$.

2.4.3 Amplitude and Phase of the S-Parameters

The scattering parameters $S_{ij}(\omega)$ are complex quantities[16] and thus each has a magnitude $\left|S_{ij}(\omega)\right|$ and phase $\arg\left\{S_{ij}(\omega)\right\}$.

[16] The angular frequency $\omega = 2\pi f$, with f the frequency, has been shown explicitly to recall that the S-parameters are also frequency dependent.

2.4.4 Scattering Parameter Attributes

On a continuous basis (for example the shaping controller script mentioned later in this proposal) it is easy to monitor the accuracy of the CEM model output by checking that the predicted S-parameters satisfy certain known properties.

All the passive circuits considered in this thesis are made of isotropic passive materials, and so must be reciprocal. As a result, we must have

$$S_{12} = S_{21} \tag{2.4-19}$$

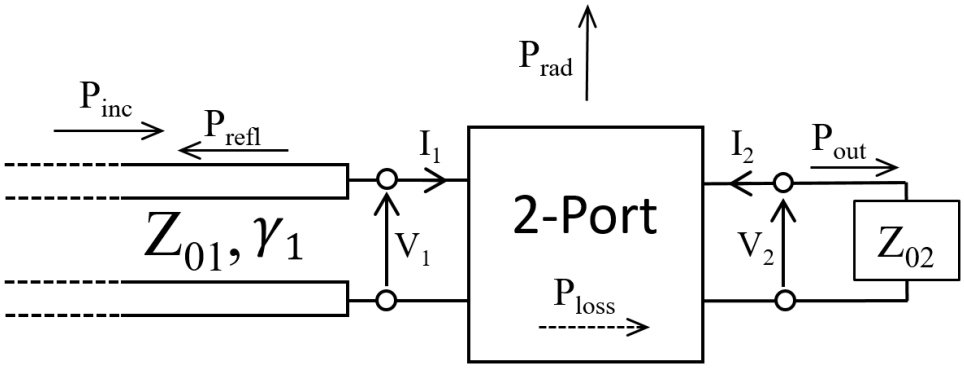

Fig.2.4-2 : Diagram to illustrate power budget.

With reference to Fig.2.4-1, a source connected on the Port#1 side, and the reference impedance terminates Port#2, we can write a power budget

$$P_{out} = P_{inc} - P_{refl} - P_{ohmic} - P_{rad} \tag{2.4-20}$$

P_{out} is the time-averaged power exiting Port#2, P_{inc} the power incident on Port#1, P_{refl} the power reflected at Port#1, P_{ohmic} the power dissipated in the 2-port network, and P_{rad} the power radiated by the 2-port network. We can manipulate (2.4-20) to read

$$\frac{P_{out}}{P_{inc}} = 1 - \frac{P_{refl}}{P_{inc}} - \frac{P_{ohmic}}{P_{inc}} - \frac{P_{rad}}{P_{inc}} \tag{2.4-21}$$

Using the definition of the S-parameters, (2.4-21) can be rewritten as

$$|S_{11}|^2 + |S_{21}|^2 = 1 - \frac{P_{ohmic}}{P_{inc}} - \frac{P_{rad}}{P_{inc}} \tag{2.4-22}$$

If all the materials involved are lossless, then

$$P_{ohmic} = 0 \tag{2.4-23}$$

and

$$|S_{11}|^2 + |S_{21}|^2 = 1 - \frac{P_{rad}}{P_{inc}} \tag{2.4-24}$$

If there is no power loss due to radiation[17] $P_{rad} = 0$, and

$$|S_{11}|^2 + |S_{21}|^2 = 1 \tag{2.4-25}$$

Similarly,

$$|S_{22}|^2 + |S_{12}|^2 = 1 \tag{2.4-26}$$

and

$$S_{11}^* S_{12} + S_{21}^* S_{22} = 0 \tag{2.4-27}$$

These expressions can be used to show [SAZO 82] that any lossless non-radiating two-port satisfies the conditions

$$|S_{11}| = |S_{22}| \tag{2.4-28}$$

and

$$\angle S_{11} + \angle S_{22} = \angle S_{21} + \angle S_{12} \pm \pi \tag{2.4-29}$$

For the reciprocal two-ports of interest here $\angle S_{21} = \angle S_{12}$, and the latter expression reduces to

[17] In circuits that are not meant to be antennas, a low radiated power is a necessity.

$$\angle S_{11} + \angle S_{22} = 2\angle S_{21} \pm \pi \quad \Rightarrow \quad \angle S_{22} = 2\angle S_{21} - \angle S_{11} \pm \pi \tag{2.4-30}$$

2.5 OPTIMIZATION ALGORITHMS - CLASSIFICATION

Consider a real-valued quantity $F_{obj}(a_1, a_2, ..., a_q, ..., a_Q)$ that is a function of quantities a_q, which may be complex. If the purpose in using an optimization algorithm is the minimization of F_{obj} by selecting the values of the elements of the set $\{a_1, a_2, ..., a_q, ..., a_Q\}$, then F_{obj} is called the objective function for the optimization[18]. The quantities a_q are the optimization variables (**degrees of freedom of the optimization**), and their values are systematically adjusted by the optimization algorithm until the combination of such quantities that makes F_{obj} smallest is found. When optimization algorithms are used in microwave circuit design the performance goals must be translated into an objective function[19].

The methods used to perform optimization are classified as either *evolutionary* or *gradient-based*. The thesis will use existing optimization algorithms[20].

There are many types of evolutionary[21] optimization algorithms, the most widely used of which is the genetic algorithm (GA) [HAUP 10][WEIL 97][RAHM 12][MITC 99]. All such heuristic algorithms have a performance governed by the so-called "no free lunch theorem" [WOLP 97] [CAPE 19]. The implication is that, because they do not use (do not know) any information about the objective function except its values at particular "points" $\{a_1, a_2, ..., a_q, ..., a_Q\}$, no such optimization algorithm will always perform better than any other such optimization algorithm, on average. The only way to possibly speed up the optimization is if additional knowledge on the objective function is exploited. Such additional knowledge (namely the gradient of the objective function) is used in gradient-based optimization algorithms. In basic calculus courses we are shown how to find the maximum or minimum of a function $F_{obj}(a)$ of a single variable a

[18] In the evolutionary optimisation algorithm context the objective function is often called the fitness function, but it needs to be recognised that these are one and the same thing [JOHN 99b]. In some disciplines it is also referred to as the penalty function.
[19] The shape synthesis of physical circuits makes use of optimization algorithms. Appropriate objective functions are defined in Chapter 5, for the shape synthesis application examples described there.
[20] These optimization algorithms will, of course, be used in a different way in the new shaping algorithm than what has been done previously.
[21] Also referred to as heuristic algorithms by some.

through use of its derivative information. If F_{obj} is a function of many variables[22] the derivative is generalised to the gradient concept, and sophisticated ways have been developed of using this to find one's way to the Q-dimensional point $\{a_1, a_2, ..., a_q, ..., a_Q\}$ that minimises F_{obj}. Different gradient-based algorithms "hike" a path to this point in different ways. Use of such gradient-based algorithms requires that we be able to define and compute the gradients of F_{obj} as the algorithm demands. Tutorial accounts of such algorithms can be found in [BAND 69] and [BAND 88], references that remain relevant in spite of their age.

The work of this thesis does not do research on such optimization algorithms themselves; it views these algorithms, and their implementation (in [MATLAB]), as an available resource.

2.6 COMPUTATIONAL ELECTROMAGNETICS (CEM) MODELLING OF PHYSICAL CIRCUITS

The research in this thesis uses computational electromagnetics (CEM), in particular the method of moments (MM), extensively to achieve its goals. However, it does not do research on such CEM methods themselves, but on how these are used in physical circuit shape synthesis. Indeed, it uses the commercially available computational engines FEKO[23] [FEKO 21] and SONNET [SONN 21]. Some selected background on the CEM approach used, by FEKO in particular, will allow us to more easily explain reasons for some decisions that are taken in this work. Details on the method of moments are adequately described in books/papers such as [PETE 97], [VOLA 12] and [RAO 82].

With reference to the microstrip circuit in Fig.2.6-1, we wish to compute electromagnetic scattering parameters of the lowest order waveguide mode at the input/output ports. In the electromagnetic model an incident field, consisting of the fields of the lowest order mode on an infinitely long microstrip line of width t_1 is allowed to impinge on Port#1. As a result there will be surface electric conduction currents on the conducting material ("tracks") on the upper surface of the substrate and on the conducting groundplane, and volume polarization current densities in the substrate. If these can all be determined the scattered fields, and hence the total fields, can be

[22] As in most engineering design work, and certainly the shape synthesis work that is the subject of the present thesis.

[23] These codes on their own do not allow one to perform the shape synthesis of microstrip circuits. They are merely part of the overall tool whose development is used to implement a new shape synthesis approach.

found, and the S-parameters S_{11} and S_{21} then determined. Thereafter the incident field is specified as those of the lowest order mode on an infinitely long microstrip line of width t_2 (on which Port#2 resides), and S_{22} and S_{12} found from the field solution. Because such analysis effectively uses the full form of Maxwell's equations (no terms are assumed negligible) it is usually referred to as a full-wave analysis.

In order to lighten[24] the computational load, the substrate and conducting groundplane are assumed to be infinitely large, although the substrate is of finite thickness (*h*). The conductor arrangement on the upper surface of the substrate remains finite, as in Fig.2.6-1. These assumptions allow the MM to be based on an integral equation model that uses a modified Green's function[25] that analytically accounts for the presence of the substrate and groundplane. The "only" unknowns are the current densities on the conductors on the top of the substrate. This is the reason the MM is often preferred[26] for the analysis of microstrip (and other) geometries that consist of thin conducting tracks within and on layered dielectric substrates.

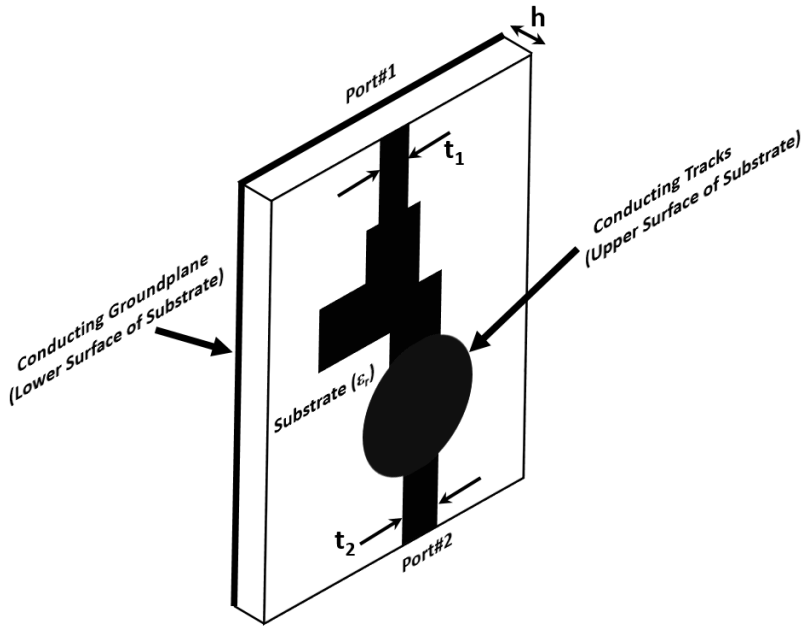

Fig.2.6-1 : Two-port microstrip physical circuit layout of finite size.

[24] It is not implied that the load becomes light; just lighter!
[25] As opposed to the free-space Green's function.
[26] Compared to other CEM methods such as the finite element method (FEM) and finite-difference time-domain (FDTD) method.

The MM describes the unknown equivalent electric current densities in terms of a set of expansion functions, and then finds the complex coefficients of each of these expansion functions, from which all field quantities can be determined, thereby solving the electromagnetics problem. The most widely-used expansion functions[27] are the so-called RWG expansion functions, defined over a triangular mesh. Fig.2.6-2 shows the conductor layout meshed into 12 triangles[28], the numbering being shown encircled. We note that some triangles have one or more edges in common with an adjacent triangle. There is an RWG expansion function [PETE 97] associated with each such common edge, whose numbering in this case is given by the digit located on each common edge. We can say that the electric surface current density $\bar{J}_s(\bar{r})$ at locations $\bar{r}$ on the top conductor are represented in terms of RWG expansion function $\bar{J}_n(\bar{r})$, $n = 1, 2, ..., N_{\text{MM}}$, with $N_{\text{MM}} = 10$ in Fig.2.6-2.

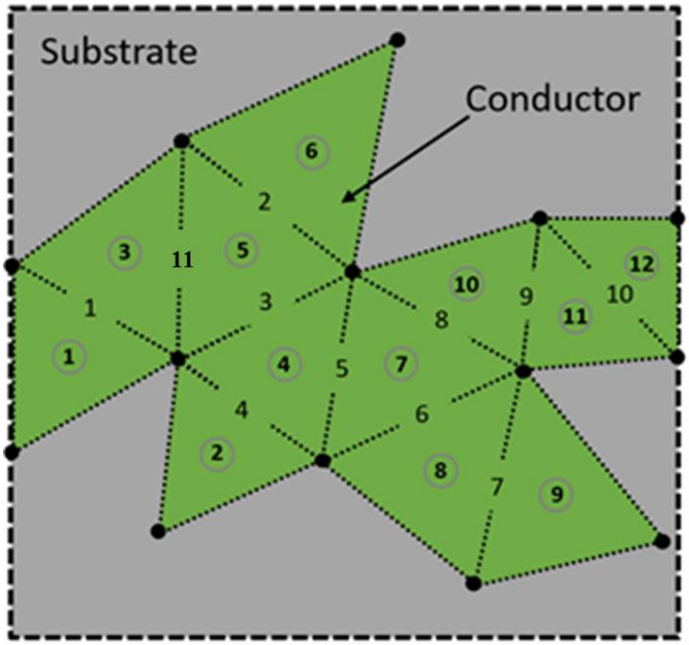

Fig.2.6-2 : Conducting tracks on the top surface of the substrate. This does not depict an actual designed microstrip circuit. It will be used for explanatory purposes only. Thus it contains a small number of triangles forming a mesh into which the circuit is divided.

[27] The description here is needed to explain some comments made in Chapter 3.
[28] In practice the number of such triangles will be very much larger. This simplified case is shown for explanatory purposes.

2.7 SURROGATE[29] MODELLING

If we have all the details (viz. geometrical dimensions; material properties) of the physical circuit in Fig.2.6-1, then CEM modelling can be used to compute everything we wish to know about it. This has to be done at each frequency of interest. The computational burden is high, and need to be executed hundreds or thousands of times during any design process. Engineers therefore often use surrogate models, based on CEM model data, that are not as computationally burdensome. Surrogate models have been used for many years.

In the interests of explanatory simplicity, suppose we have a real function $g_{\mathrm{fw}}(\mathrm{w})$ whose values for a specific value of a real variable w we can only determine using an extremely computer-time-consuming process (we will call this the "full-wave model" for the function). If we perform such burdensome computations for a selected number of different w-values over some range $[\mathrm{w}_1, \mathrm{w}_N]$, we can plot the graph shown in Fig.2.7-1. We can then use some method to "fit" a curve through these points, as indicated by the dashed line in Fig.2.7-1. The fitted curve is an example of a surrogate model of the more complicated process.

Next, suppose that the surrogate model has been set up. If we select a w-value (not part of the original full-wave data used to "train" the surrogate model) that lies within the interval $[\mathrm{w}_1, \mathrm{w}_N]$, and obtain the value $g_{\mathrm{su}}(\mathrm{w})$, we are using interpolation. If we select a w-value that lies outside $[\mathrm{w}_1, \mathrm{w}_N]$ to obtain $g_{\mathrm{su}}(\mathrm{w})$ we are using extrapolation.

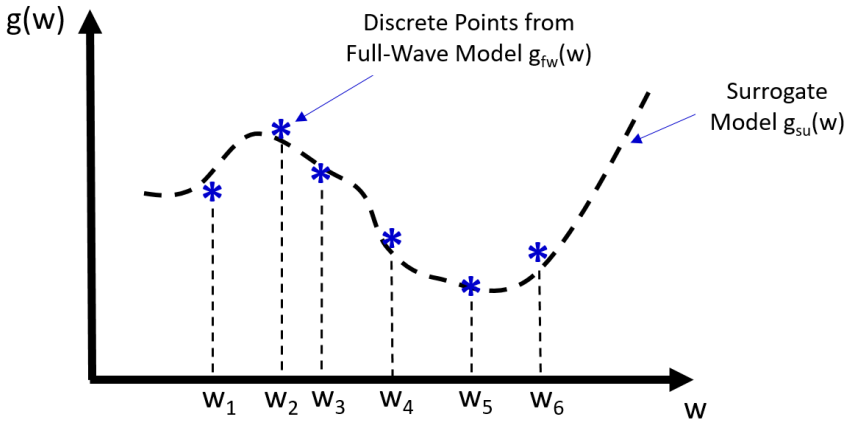

Fig.2.7-1 : Diagram for simple illustration of the surrogate modelling idea.

[29] The word "surrogate" simply means "substitute".

Modern surrogate modelling methods exist that allow multiple (multi-dimensional) inputs. One successful and widely-used surrogate modelling method is that using an artificial[30] neural network (ANN). Just as numerical methods such as the FEM and MM have been developed into a computational technology, so too has the subject of ANNs. In essence, a neural network (depicted in Fig.2.7-2) is composed of multiple layers (stages), each of which performs a certain transformation (weighting and adding) on information from the previous layer. The combined transformations throughout all layers make the neural network capable of representing functions. In RF design work to date, the input consists of the selected geometrical features of the physical circuit, say $[A]=\{a_1, a_2, a_3, a_4\}$ in the case of four such features. The output consists of performance quantities, say $[B]=\{|S_{11}|, \angle S_{11}, |S_{21}|, \angle S_{21}\}$. By "value of $[A]$" we mean a specific combination of the values $\{a_1, a_2, a_3, a_4\}$. The weights associated with the specific neural network are determined by training[31] the neural network. This training is done using input and output that are connected using full-wave CEM analyses. The fully-trained NN surrogate model can then be used for "interpolation" – the output can give the performance for different[32] values of $[A]$ without having to run the full-wave CEM model for the different $[A]$ values (that is, set of geometrical features). If there are many internal[33] (hidden) layers it is referred to as a deep neural network (DNN), and schemes using DNNs are considered to be using of deep-learning[34].

[30] They are "artificial" because the "real" neural networks are the ones in our brains!
[31] Determining the said weights.
[32] That is, those that were not used for training and for which a full-wave CEM
[33] That is, layers other than the input and output layer.
[34] Brief comments on the use of the term "learning" are made in Section 2.8.

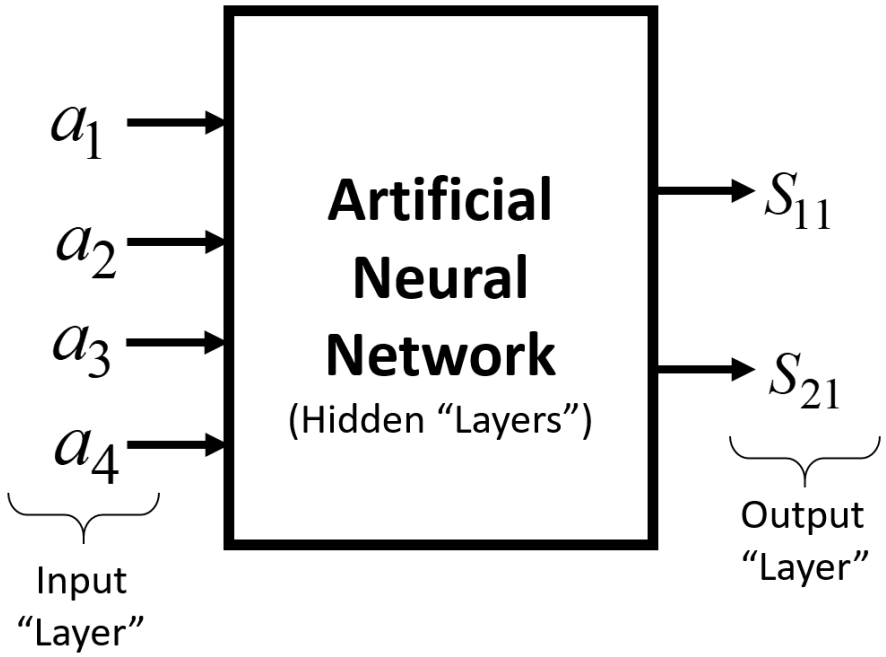

Fig.2.7-2 : Principle of an artificial neural network (ANN).

There are other ways to generate surrogate models [SUMO 21], but neural networks have been the most widely and successfully used in traditional RF design. It has not been used with existing shape synthesis methods, for reasons that will be provided in Chapter 3.

2.8 MACHINE LEARNING, COMPUTATIONAL INTELLIGENCE & ARTIFICIAL INTELLIGENCE

Surrogate modelling using neural networks (as well as other surrogate modelling approaches) is an example of *machine learning (ML) methods*. It is trendy in the electrical engineering literature at present to try to view one's work as an application of ML. It is important to realise that, recognizing (as will be noted in Section 2.9) the work on the use of NN's in RF engineering for the past 20 years, current ML work is a continuation and not a revolution. Thus it would be wise to take to heart a cautionary phrase from the announcement[35] of an IEEE Microwave Magazine Special Issue on Machine Learning in Microwave Engineering, namely that it is

[35] Extracted from announcement written by special issue editors C.Sarris & Q.J.Zhang, *IEEE Microwave Magazine*, 2021.

important to “tell apart hope from hype”. Fortunately, useful new work on the use of ML in RF engineering is indeed continuing, through ways of improving the accuracy of surrogate models for instance.

Another popular term that has emerged is “computational intelligence”. It is also not a brand new topic that has suddenly burst onto the RF design field. It is merely a term that now encompasses the use of optimization algorithms (especially evolutionary ones) and surrogate modelling. In fact, it is so encompassing that much of what is being done in RF design today can be considered to be using some type of computational intelligence.

Finally, there is the subject of artificial intelligence (AI). As per [CAMP 21], “AI can be considered as intelligence displayed by machines, which imitate cognitive tasks that humans associate with natural intelligence”, and therefore ML is a sub-domain of AI. Reference [CAMP 21] continues[36] to note that “while AI and ML have recently become increasingly mainstream concepts, they actually have a long history”. Indeed, we are urged[37] not to try consider too much to be AI.

2.9 THE EVOLUTION OF MICROSTRIP CIRCUIT ANALYSIS METHODS

Before computational electromagnetics modelling became computationally possible, and then widely available, microstrip circuits such as that shown in Fig.2.9-1 were analysed using TL models of the type discussed in Section 2.3 for those portions in Fig.2.9-1 labelled as such. The lengths of the TL sections were those of the physical circuit, and their characteristic impedance values were found using approximate formulas[38] that included the substrate permittivity and thickness, and the microstrip track width. It was recognized that the junctions/discontinuities (eg. steps, bends, open ends) stored energy locally because of the excitation of non-propagating higher-order modes, and this was accounted for though the inclusion of lumped element T or PI equivalent circuits (which in some cases reduced to simple lumped shunt or series elements) where the TL models joined. The values of the lumped components in these discontinuity models

[36] For the reader’s convenience, although [CAMP 21] is in the list of references at the end of the thesis, we repeat its details here : S.D.Campbell, R.P.Jenkins, O.J.O’Connor and D.H.Werner, “The explosion of artificial intelligence in antennas and propagation”, *IEEE Antennas and Propagation Magazine*, pp.16-27, June 2021.

[37] K.Pretz, “Stop calling everything AI, machine-learning pioneer says”, *IEEE Spectrum*, March 2021 [Headline of Interview with AI pioneer M.I.Jordan].

[38] These were catalogued. If a completely different discontinuity was needed, this implied a substantial research effort.

were found from approximate analytical solutions to an electromagnetic formulation of the particular discontinuity [EDWA 01]. Eventually CEM methods were used to more accurately characterize discontinuities, which were then represented by their computed S-parameter matrices. As computational resources grew it became possible to analyse complete physical microstrip circuit layouts using a CEM model, without some recourse to more approximate modelling being absolutely necessary.

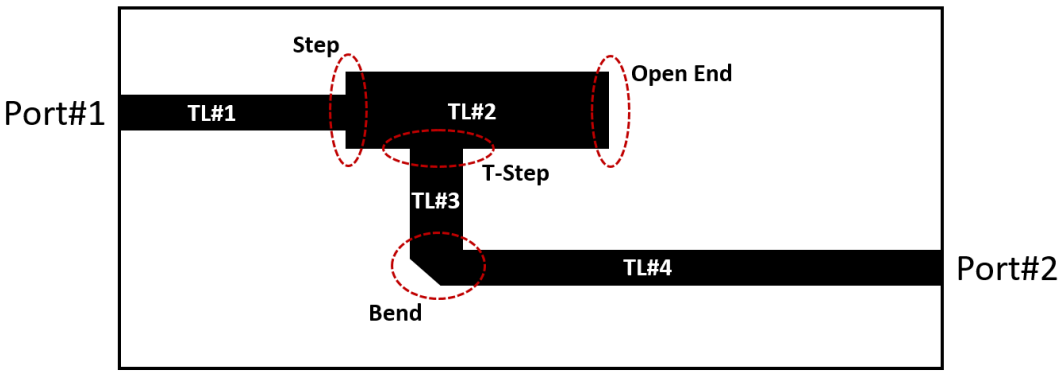

Fig.2.9-1 : Fictitious physical microstrip circuit seen by inspection to consist of lengths of transmission line (TL) and discontinuities.

2.10 CURRENT CONVENTIONAL ('TRADITIONAL') MICROSTRIP CIRCUIT DESIGN METHODS : FEATURE OPTIMISATION

If we have all the dimensions and material properties of some microstrip circuit, such as that shown in Fig.2.6-1, and we use CEM modelling to compute the S-parameters, this process is known as a *forward problem*. It has a unique (only one) solution. Design is the *inverse problem* to this – we know what S-parameters we want, and wish to determine the physical circuit that will provide this. This does not have a unique solution because more than one collection of induced sources (viz. the electric current densities on the conductors on the top of the substrate and the groundplane, as well as the polarization current densities in the substrate) can produce the same scattered field outside the region occupied by these sources, and hence the S-parameters at the ports. Even using the same substrate and port locations/dimensions, two or more different conductor layouts on the top surface of the substrate could give us the same [S] over a limited frequency range.

Traditional physical microstrip circuit design methods begin with a library of well-understood components, described in terms of their distributed circuit TL models[39] as mentioned in the previous paragraph and Section 1.1. These components are pieced together in order to obtained some desired functionality. This is the route one finds in mainstream texts such as [COLL 92], [POZA 90], [STEE 13], [DAVI 84] and [SORR 10]. These TL-modelled configurations are then "translated" into physical layouts depending on the selected transmission medium (eg. microstrip medium in Figs. 2.6-1 and 2.9-1). Once these have been translated into a physical microstrip layout we might, in the case of a bandstop filter for example [POZA 90], end up with the layout depicted in Fig.2.10-1. It is recognized that simply connecting the TL models do not account for all the physical effects, and so a CEM model of the layout in Fig.2.10-1 is set up. Some of the geometrical features (eg. the microstrip line widths and/or spacings shown) are selected, and an optimization algorithm, using the CEM full-wave model for forward analyses, is used to automatically adjust the selected geometrical features until the physical circuit displays a behavior close to that desired. This approach we will, for want of a better term, call the *feature optimization* approach to design.

In the case of Fig.2.10-1, if d_1, d_2, the three h_i values, and the three b_i values, are selected for automatic adjustment, we can say that the feature optimization involved 8 degrees of freedom. It is important to note that the conceptual design obtained (before applying feature optimisation) will usually provide a performance that is already 'close' to what is desired. The optimisation used for the feature optimisation has a 'warm start'. This allows the use of gradient-based optimisers without having to be overly concerned with the problem the latter have of stagnating in the vicinity of 'local minima' of the associated F_{obj}.

When engineers began to use this design approach it was soon threatened by the computational burden due to the need for full-wave CEM analysis. Fortunately, clever methods were devised to accommodate such full-wave analysis in a way that significantly alleviated some of this computational burden. One such method was that of surrogate modelling[40], especially the training of neural networks using a restricted (albeit not insignificant) number of full-wave electromagnetic analyses, and then relying on the trained neural network to predict predict other cases (eg. different combinations of circuit feature dimensions) without having to run the full-

[39] Not yet an actual physical layout.
[40] Already outlined in Section 2.7.

wave analysis for such new case. This approach allowed feature optimization based RF circuit design to be pushed to the next limit. It has underpinned the success of modern wireless communications systems, and more.

But technology is insatiable, and further developments are needed on several fronts to meet fresh demands[41] for even more and complex RF circuit design [ZHAN 21]. The particular "front" of interest in this thesis is design using what we will term *shape optimization* (as opposed to feature optimization).

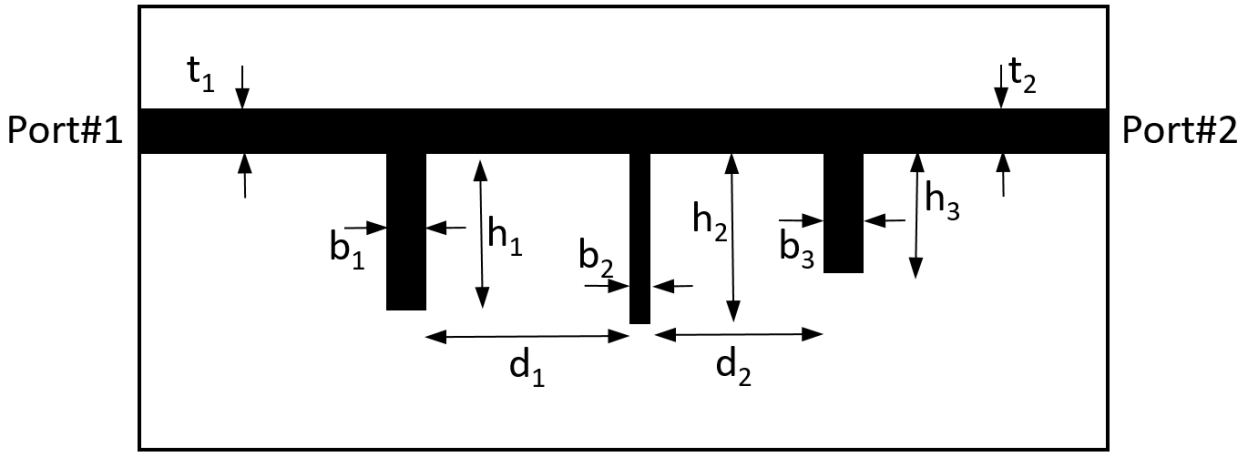

Fig.2.10-1 : Physical circuit design using feature optimization versus shape optimisation

2.11 CONCLUDING REMARKS

Most importantly, the present chapter has described a context into which we can place the subject of shape synthesis for physical microstrip circuit design. In addition, it has defined the performance measures (eg. S-parameters) that will be used in the thesis in the definition of associated objective functions. It has also briefly introduced terminology (eg. optimisation algorithm, CEM, surrogate modelling) that can now, in the interests of clarity, be used in the remainder of the thesis.

[41] Some of which were mentioned in Section 1.1.

CHAPTER 3
A Framework for the Shape Synthesis of Physical Circuits

3.1 INITIAL REMARKS & OVERVIEW

Section 2.10 indicated that the traditional design approach uses libraries of well-understood components, along with feature optimization, with surrogate modelling used to lighten the computational burden. Surrogate modelling has been under constant improvement, with such models being able to accommodate increasing numbers of inputs (eg. more geometrical features), can be constructed using less full-wave data than before, can "interpolate" highly-resonant responses that are sensitive to small changes in certain geometrical features, and so forth. The success of the above methods has been extraordinary, but the number of input variables possible with surrogate models is in the tens rather than the hundreds or more. Furthermore, because feature optimization begins with selection of known sub-components from a known library[42], there might be better possibilities (for a given set of requirements) that are not even known about.

Designers are looking to alternative approaches to be able to satisfy requirements already being expected[43] in the future [MATT 21]. One design approach that could be complementary to traditional design is that of shape synthesis. The use of shape synthesis is not new; it has been written about (somewhat sporadically, compared to other topics) for more than 20 years. This raises the question : "Why has shape synthesis via pixelation (or voxelation) not become part of standard practice in microwave circuit design"? The present chapter attempts to provide some answers to this question.

Sections 3.2 through 3.4 describes what is usually meant by shape synthesis. The straightforward tutorial-like description given there is not available elsewhere, and will help place the new subtractive shape synthesis method of this thesis into the proper perspective. Sections 3.5 through 3.7 review the literature in which shape synthesis has already been applied, and immediately conjectures why shape synthesis use is not more widespread. This is further

[42] It is also difficult to keep pace with additions to the "library" that appear in a plethora of publications.
[43] [MATT 21] : M.Matthaiou, O.Yurduseven, H.Q.Ngo, D.Morales-Jimenez, S.L.Cotton and V.F.Fusco, "The road to 6G : Ten physical layer challenges for communications engineers", IEEE Communications Magazine, pp.64-69, Jan.2021.

discussed in Section 3.8. Arising from this study of existing applications, Section 3.9 proposes a fresh framework in which to think about the shape synthesis process that we believe will be of benefit in future work on topic, and concludes that some shape synthesis method, "between" feature-optimisation and pixelation-based shape synthesis, will be of benefit in RF circuit design[44].

3.2 EXTERNAL BOUNDARY SHAPE VARIATION APPROACH TO SHAPE SYNTHESIS

A more general method of design has used optimization algorithms to modify the boundary of some starting shape[45] to attempt the achievement of some desired performance. We can understand the essentials by referring to Fig.3.2-1. The top drawing shows a physical microstrip 2-port circuit, with the port feedline geometries fixed, but a central region occupied by conductor. The boundary of this region is defined using a mathematical parameterization[46] expressed in terms of a set of real coefficients $\{a_1, a_2, ..., a_q, ..., a_Q\}$. The S-parameter performance of the two-port can be found[47] for any set of values of these coefficients, the S-parameter values being used to find the value of an objective function F_{obj}. Minimisation of F_{obj} by varying the values of $\{a_1, a_2, ..., a_q, ..., a_Q\}$, and hence the shape of the boundary, constitutes a shape synthesis process that results in a shaped physical circuit such as that in the bottom drawing of Fig.3.2-1. In such a process no "holes" are possible inside the boundary of the original starting shape.

[44] This is the subject of Chapter 4.
[45] Also called the "design area".
[46] For example, multi-segment spline fitting.
[47] Using some CEM method.

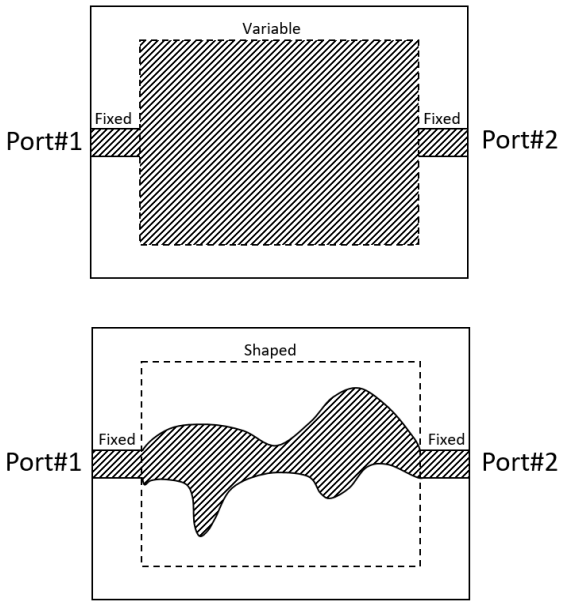

Fig.3.2-1 : Starting form (top), and shaped synthesized (bottom) microstrip physical circuit. The hatched regions represent conductor regions.

3.3 EXTERNAL & INTERNAL BOUNDARY SHAPE VARIATION APPROACH TO SHAPE SYNTHESIS

We here describe an approach, which is a slight generalization on that in Section 3.2, *but has not actually been described by others*. The reason for our doing so is that it will help us develop the new framework in which to think about shape synthesis, which will then spawn the new subtractive shape synthesis method described in Chapter 4 for the first time.

It is possible to define a starting shape that has an external boundary and internal boundaries, parameterize these as in Section 3.2, and then perform shape synthesis as in Section 3.2. This is easily illustrated by referring to Fig.3.3-1, in which the top drawing shows the starting arrangement, and the bottom one the resulting shape synthesized microstrip circuit. In this case the parameterization coefficients of both the external and internal boundaries form the optimization variables. But decisions need to be taken on the locations of the internal boundaries; it is not clear on what basis this could be done. Although “holes” are now possible, which might cause some to refer to this as our being able to change not just the shape but in fact the topology, we will not use such terminology.

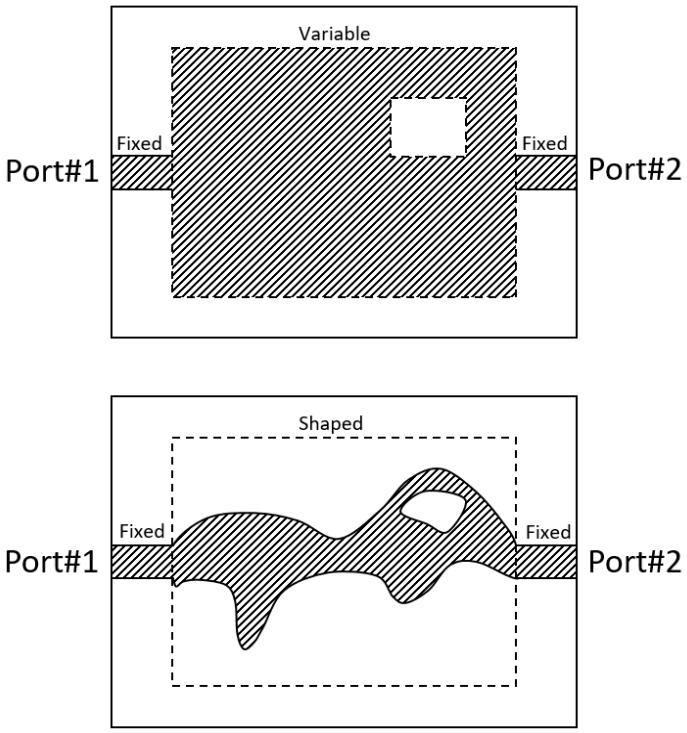

Fig.3.3-1 : Starting form (top), and shaped synthesized (bottom) microstrip physical circuit. The hatched regions represent conductor regions.

3.4 PIXELATION APPROACH TO SHAPE SYNTHESIS

3.4.1 Discrete Design Variable

The starting shape S_0, denoted by "variable" in Fig.3.4-1(a), is divided into geometry elements (pixels[48]), as in Fig.3.4-1(b), and an element design variable defined that controls the material properties of the specific element[49] (or pixel). The discrete design variable for the e-th element can be designated as

$$\Lambda_e = \begin{cases} 1 & \text{Material Present in } e\text{-th Element} \\ 0 & \text{No Material Present in } e\text{-th Element} \end{cases} \tag{3.4-1}$$

[48] In the case of the microstrip circuits of interest in this thesis we need only refer to pixelation. In situations such as the shaping of dielectric resonator antennas [ALRO 20] the structure to be shaped is volumetric in nature, and so is divided into voxels, with the starting shape some volume V_0.

[49] These are not the "elements" associated with the mesh required by the CEM full-wave analysis being used.

The shaping problem is to find the distribution of the materials over S_o to achieve the desired response. The material distribution can be written as a binary quantity[50]

$$\tilde{\Lambda}_{\text{mat}} = [\Lambda_1, \Lambda_2, .., \Lambda_e, .., \Lambda_N] \tag{3.4-2}$$

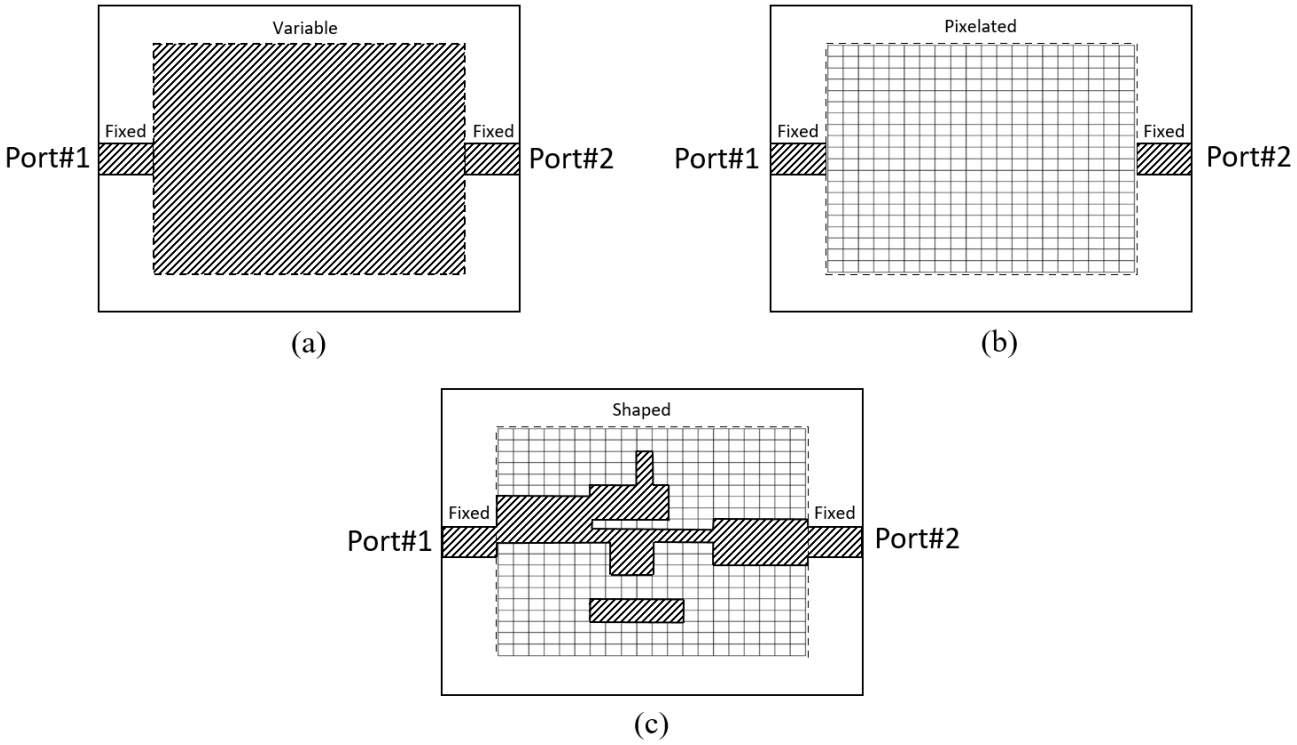

Fig.3.4-1 : Physical circuit shape synthesis using a pixelation approach - The pixelation of the starting shape (a) is shown in (b), with (c) depicting some resulting (fictitious in this case) shaped structure. The hatched regions represent conductor regions.

In the case of microstrip circuits the material referred to in (3.4-1) is conductor, as implicitly assumed in Fig.3.4-1. The conductor geometry undergoes shaping through the removal or retention of conducting pixels into which the starting shape is divided, so that the binary quantity[51] in expression (3.4-2) describes the conductor shape. This is illustrated by the binary

[50] The specified starting shape has $\Lambda_e = 1$ for all $e = 1, 2, ..., N$. The number of quantities whose value may be altered during any shape optimization process (in this case N) is of course what we have called (Section 2.5) the number of degrees of freedom assigned to the shaping process.

[51] In the terminology of the genetic (optimization) algorithm, or GA, this is called a chromosome that consists of a string of N bits.

chromosomes [1 1 1 1 1 1 1] and [0 1 1 1 0 1 1] shown below each of the greatly simplified layouts in Fig.3.4-2; clearly by altering the binary values of each bit a different conducting geometry can be defined.

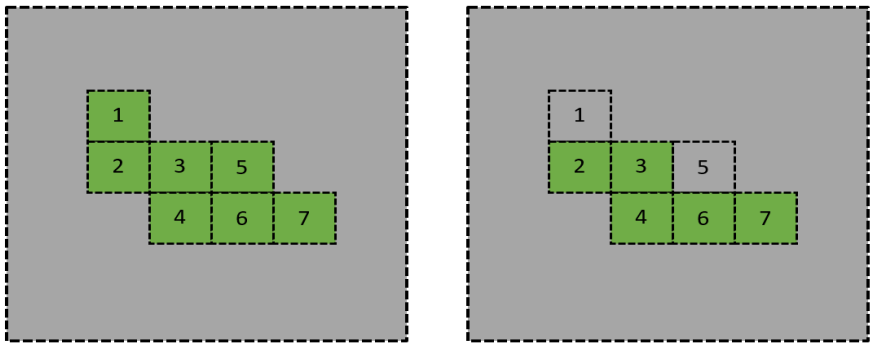

Fig.3.4-2 : Simplified pixelated conducting shape on the top surface of the microstrip substrate. The shaded (green) areas are those occupied by conductor.

Since each different binary quantity (3.4-2) defines a particular conductor layout, and it is possible to use full-wave analysis to compute the circuit performance for such a conductor layout, an objective function F_{obj} can be effectively defined as a function whose dependent variables are the bits in the said binary quantity and hence control the shape of the structure.

This is well-suited to use of binary versions of evolutionary algorithms such as the GA. However, in feature-optimisation design methods, it is the use of gradient-based optimisation algorithms that have made this approach sufficiently fast (but recall it always has a 'warm start') and hence used in practice. Evolutionary optimisation algorithms are slower. If we wish to use a gradient-based optimization algorithm the discrete (binary) element variables describing the geometry must be converted into continuous ones, so that gradients of the F_{obj} with respect to such variables can be defined and determined.

3.4.2 Continuous Design Variable[52]

In order to convert the geometry variables into continuous ones, we need to have[53]

$$0 \le \Lambda_e \le 1 \qquad (3.4\text{-}3)$$

[52] The approach becomes one that could be called a density-based pixelation approach to shape synthesis.
[53] Scaling into the range $0 \le \Lambda_e \le 1$ is always possible.

However, this means we have to devise[54] some "material interpolation law" that gives the material properties (in the microstrip case it is the conductivity) of the *e*-th element for different values of Λ_e (and hence conductivity) over its range $0 \le \Lambda_e \le 1$. In other words, one needs to define some conductivity function

$$\sigma_e = f_\sigma(\Lambda_e) \tag{3.4-4}$$

defined so that $f_\sigma(0) = 0$ and $f_\sigma(1) \approx \sigma_{Cu}$ or $f_\sigma(1) \to \infty$ (the PEC case). The selection of this material interpolation law can be quite complicated [NOMU 13][HASS 14][LIU 16][HASS 20] and somewhat arbitrary. Furthermore, the disadvantage of doing this, for the physical microstrip circuit case, is that the introduction of continuous geometry variables makes it possible that the shaped designs consist of conducting regions of many different conductivity values. This is depicted in Fig.3.4-3; in practice there may be many more non-PEC regions that arise and some conductivities may be low. In other words if we think of zero conductivity (no conductor) and infinite conductivity[55] (PEC) as the only available conducting materials, then materials of intermediate conductivity must be eliminated if we are to end up with a desirable shaped circuit[56]. This elimination has been attempted in a number of ways. For example, some authors [JENS 11] [EREN 11] use a "penalization technique" by adding a term to F_{obj} that penalizes (by making F_{obj} larger) pixels with $\Lambda_e \neq 0$ and $\Lambda_e \neq 1$. If F_{obj} already contains terms that provide a measure of the power loss one would think that such "self-penalization" would do the trick; but [HASS 20] observes that this "tends to aggressively terminate the optimisation quickly, resulting in designs with poor performance". Some use a "biasing function" technique that does not alter F_{obj} but instead, at each gradient update of the optimisation algorithm, moves each Λ_e closer to 0 or 1, depending on its current value. Others [HASS 20] use a "blurring filter" technique where, at each gradient update of the in the optimization algorithm, the value of Λ_e of each element is replaced by a weighted average of the neighbouring elements' values. The penalization, biasing

[54] It is not possible to have only zero or infinite conductivity when requiring a continuous material variable.
[55] Or some practical material of high-conductivity (such as Cu).
[56] We would also not want to deposit conducting material with conductivities ranging from almost zero to that of Cu, for instance, over different parts of the shaped geometry. At any rate, such materials would impose unacceptable loss on the resulting circuit.

function and blurring filter approaches all have a certain arbitrariness[57] since the numerical values of various weights and factors have to be selected "by the user". The question of what values to use always arises. And even then [JENS 11], we may still end up with a shaped design for which there are elements whose Λ_e values are not 0 or 1. One route taken is to re-run the shape synthesis with different values assigned to the above-mentioned weights and factors until the number of elements for which Λ_e is not close to 0 or 1 is small.

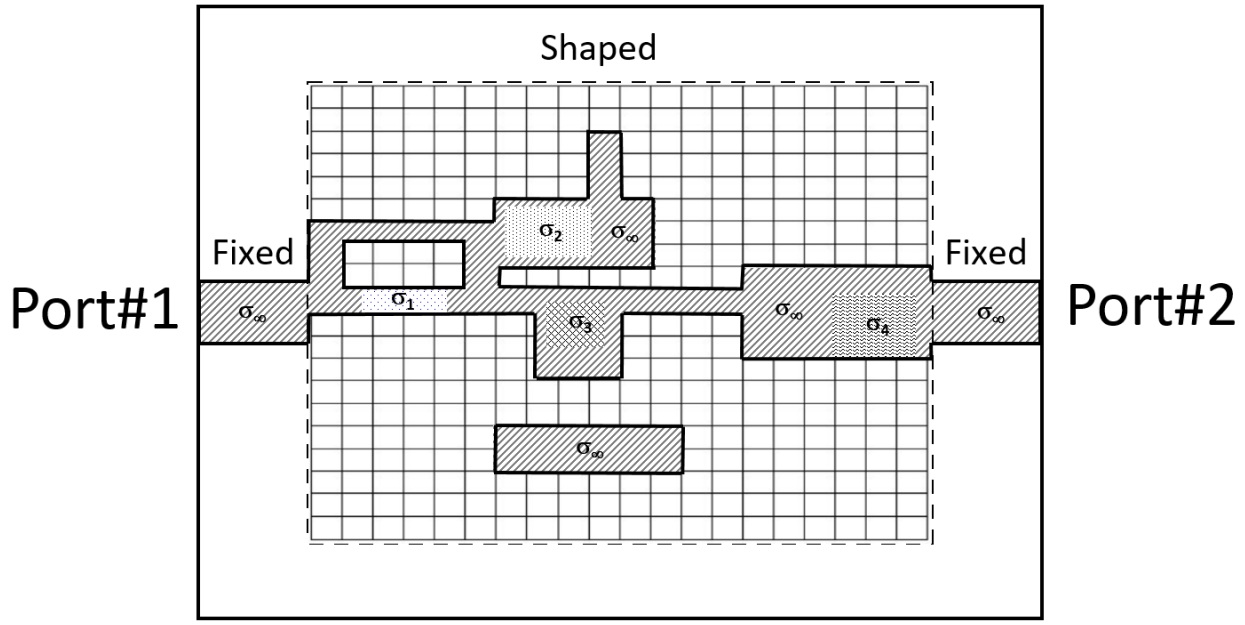

Fig.3.4-3 : Illustration (for explanatory purposes) of a fictitious outcome of the continuous-variable pixilation shape synthesis method applied to a microstrip circuit problem. The hashed sections are meant to depict PEC portions (σ_∞) of the shaped physical circuit whereas the process has arrived at other areas (shown differently shaded) which must have finite-conductivity values (σ_1 through σ_4).

3.4.3 Remarks on Some Terminology

The use of pixelation along with a "material interpolation law" such as (3.4-4), so as to allow the computation of gradient information, is called "topology optimization" by many[58], for varied reasons. Some use this terminology because the gradients used are often called topological

[57] The proponents of the continuous-variable pixelation approach often imply that, because it uses gradient-based optimization with so-called topological or adjoint-sensitivity derivatives, it is somehow more rigorous than "heuristic" methods (eg. discrete-variables pixelation methods) that use evolutionary optimizers. However, as pointed out in [CAPE 19], the need to make (*sometimes problem-dependent*) choices regarding the discrete-to-continuous variable conversion, makes it no more rigorous.

[58] Especially those in structural mechanics, and those who have transferred methods from that field into the electromagnetics area.

derivatives. Others appear to do so because they see the activity of Section 3.2 as "shape optimization", whereas the pixelation approach to be "topology optimization" because internal holes can come about[59], and the mathematical study of topology is concerned with the properties of a geometrical object that are preserved under continuous deformations (eg. stretching, bending) without closing holes or opening holes. Thus if a shaping procedure allows holes to develop in the starting structure we are changing its topology. This author considers that *shape optimization is the better terminology for anything other than feature optimization*, for reasons that will be explained in Section 3.9.

3.5 EXISTING APPLICATIONS OF SHAPE SYNTHESIS TO ANTENNAS

In the antenna field, shape synthesis research appears to have begun in the mid-1990's. Although it has not been an area in which there has been a copious number of publications, such work has been steady but intermittent. This is the reason some references may seem "old" to the reader.

3.5.1 Boundary Shaping Approach

The shaping of antennas (monopole-like and microstrip patch-like) whose geometry is defined in terms of splines has been described in [TOIV 10] and [SALU 18]. The spline parameters are adjusted using a gradient-based optimisation process, and hence the boundary shapes the antennas[60]. This corresponds to what was outlined in Section 3.2.

3.5.2 Discrete-Variable Pixelation Approach

This has been used to shape synthesise low directivity[61] microstrip patch [JOHN 99a][JOHN 99b][THOR 05], and wire [YAMA 09], antennas. This has allowed miniaturization and bandwidth increases of these planar structures. Fully three-dimensional shaping of thin-wire monopole-like antennas is performed in [ALTS 02][LIND 99][CHOO 05], with some restrictions placed on the allowed occupied volume, for obvious practical reasons. The above references all

[59] Borrowing the terminology from the mathematical discipline of topology.
[60] So this might be considered to fall somewhere between feature optimization and shape synthesis.
[61] The shaping of high-directivity reflector antenna surface geometries for directivity maximisation, or to provide contoured beams, has been done for many years [RAO 13, Vol.I] [RAHM 07], and should also be considered to be shape synthesis of this type because the reflecting surfaces are represented by spline-type functions whose coefficients are adjusted.

used the GA as the optimisation method in a discrete-variable pixelation approach. More recently [MIRH 16] used a binary particle swarm optimisation algorithm, [GOUD 17] a binary differential evolution optimization algorithm, and [WANG 20a][WANG 20b] a binary bat algorithm, in such discrete-variable pixelisation-based shaping of monopole-like antennas, but for problems already satisfactorily tackled with the GA.

A discrete-variable pixelation-based method for the shape synthesis of single electrically-small antennas, in which the feed location need only be selected after the shaping has been performed, was described in [ETHI 14b]. A related approach was later used in [YANG 19] for MIMO antennas, and has been termed a "shape-first, feed-next" approach by its authors. It relies on a characteristic mode analysis of the structure in order to define objective functions independent of the feedpoint position. This work applies only to electrically small or intermediate-size antennas that are "single-mode" in the sense that only one characteristic mode completely describes the antenna's behaviour. If the antenna proper radiates in the presence of other objects (that need not be electrically small) the approach of [ETHI 14b] can still be used, except that the sub-structure characteristic modes [ETHI 12] of the antenna proper (with the other objects in place) must be used. The shape-first feed-next approach has more recently been extended to fully 3D conducting surface antennas [ALAK 21].

The shape synthesis of dielectric resonator antennas has recently been reported [ALRO 20]. Although a discrete-variable voxelation-based approach, it separates the voxels used to control the geometry from any meshing used for the purposes of full-wave CEM modelling.

Shape synthesis has been done in antenna-related work such as frequency selective surfaces (FSS)[62] with specific passband or stopband performance in [OHIR 07], and for the shape synthesis of reflectarray elements in [AOKI 11][ETHI 14a]. In the latter reference the elements are shaped in such a way that adjacent reflectarray elements, although not identical, can be selected to have a geometrical similarity that in the end endows the resulting reflectarray with improved aperture efficiency. The use of shape synthesis for transmitarray elements has been reported in [ALJA 17][ALJA 18][ALJA 21]. It is important to note that the assumption of an element being resident in an infinite periodic structure of identical elements means the full-wave CEM model (through use of a modified Green's function in the MM formulation) needs to have

[62] A periodic structure of identical elements. This is unlike reflectarrays and transmitarrays that do not have all elements identical, but whose individual element properties are found on a per element basis by assuming each element lies in a periodic structure of identical elements.

unknowns on a single element (unit cell) only, which has per-side dimensions usually much less than a half-wavelength.

3.5.3 Continuous-Variable Pixelation Approach

[EREN 11] shape synthesizes an electrically small ("sub-wavelength") conducting antenna with conductor located on a spherical surface, to obtain as low an antenna *Q* as possible. They use more than 16000 degrees of freedom, made possible by the fact that a gradient-based optimization algorithm can be used with a continuous-variable pixelation approach, but report difficulties with the penalization method[63]. From an electromagnetics viewpoint, it seems that so many design variables represent far more degrees of freedom than would be necessary for an electrically small antenna. [HASS 14] shape synthesizes a coaxially-fed monopole antenna and microstrip patch antenna for input reflection coefficient minimisation. [LIU 16] performs the shaped design of a planar metallic dipole for maximum efficiency; the material interpolation law is expressed in terms of a surface impedance that is used in the electric field integral equation[64] that is solved using the MM for the full-wave analysis. Post-processing is needed to crop off parts of the shaped antenna that exhibit surface impedances that are not zero (no conductor) or that of the material (eg. copper) intended for actually fabricating the antenna. The latter appears somewhat arbitrary.

3.5.4 Remarks on Antenna Shape Synthesis

All the antenna shape synthesis work surveyed, irrespective of the details of the method used, has been done for antennas that are electrically small, or structures whose largest dimension is less than (usually much less than) a half-wavelength.

3.6 EXISTING APPLICATION OF PIXELATION-BASED SHAPE SYNTHESIS TO MICROWAVE CIRCUITS : SEPTA IN RECTANGULAR WAVEGUIDES

3.6.1 Discrete-Variable Pixelation Approach

[JIN 21] describes the shape synthesis of microwave filters consisting of transverse septa in rectangular waveguide. The authors acknowledge the inability to use surrogate modelling and

[63] See Section 3.4.2.

[64] This is the usual way conductor loss is included (albeit approximately) in integral equation / moment method models involving good conductors.

gradient-based optimizers (they use a GA) with such a discrete-variable pixelation approach, and so delve into ways to accelerate the solution of the FEM[65] matrix equation at many multiple frequencies, in an effort to reduce the time to perform the shape optimization by accelerating the full-wave solution.

3.6.2 Continuous-Variable Pixelation Approach

In [AAGE 17] a finite-length centrally-located, E-plane conducting septum is placed inside a rectangular waveguide, and then shaped to provide a bandpass filter. The process is complicated by the difficulties that result from the need to select some discrete-to-continuous conversion, as described in Section 3.4.2; this appears to be the nemesis of such methods when used in applications requiring conductor shaping.

3.7 EXISTING APPLICATION OF PIXELATION-BASED SHAPE SYNTHESIS TO MICROWAVE CIRCUITS : MICROSTRIP MEDIA

3.7.1 Continuous-Variable Pixelation Approach

Recall that the authors of the references referred to in this sub-section would describe their work as using topology optimization. As stated in Section 3.4, we prefer to call it shape optimisation using a continuous-variable pixelation approach.

A. [ASSA 06] [ASSA 08]

Fig.3.7-1(a) shows a conventional gap-coupled (capacitively coupled) microstrip line resonator with $L_{\text{ref}} = \lambda_g / 2$ at f_o, considered as a reference case. The authors perform a number of different shaping experiments, using first the starting shape in Fig.3.7-1 (b) that shows a fixed line that is not altered during shaping, and a second starting shape shown in Fig.3.7-1(c) where such a fixed line is not included. The primary goal was to shape synthesize a gap-coupled resonator with $L_{\text{ref}} < \lambda_g / 2$ (that is, achieve size reduction[66]). The resulting shape synthesized "compact" shape[67] is that in Fig.3.7-2, obtained using Fig.3.7-1(c) as the starting shape. It is

[65] The full-wave analysis is done using the finite element method (FEM).
[66] Dimension *d* is smaller as well.
[67] Caused to have the same S-parameters as the conventional resonator.

difficult to draw any general conclusions from the paper, but it shows that shaping can be used for circuit layout "miniaturization". The pixelation approach is an additive one.

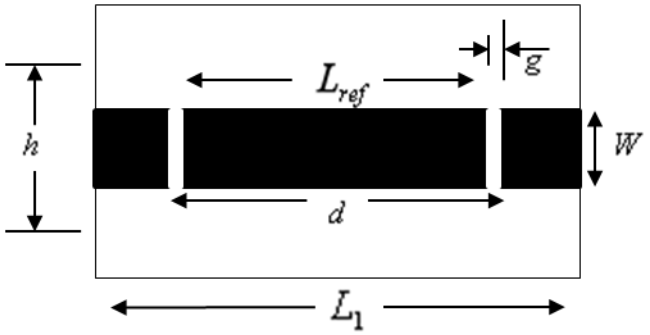

(a)

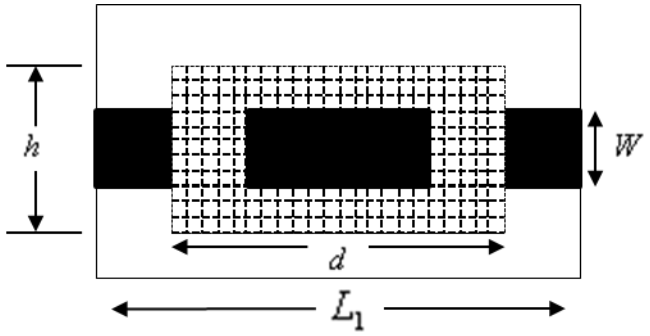

(b)

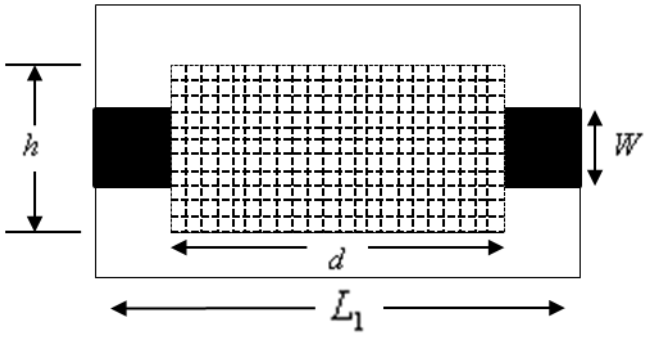

(c)

Fig.3.7-1 : Physical circuit layout diagrams for a description of [ASSA06]. (a). conventional gap-coupled (capacitively coupled) microstrip line resonator with $L_{\text{ref}} = \lambda_g / 2$ at f_o; (b). starting shape consisting of cells that can potentially be populated by the conductor during shaping, and some that are permanently occupied by conductor (and remain so during shaping); (c). starting shape consisting of cells that can potentially be populated by the conductor during shaping (but are initially all "empty").

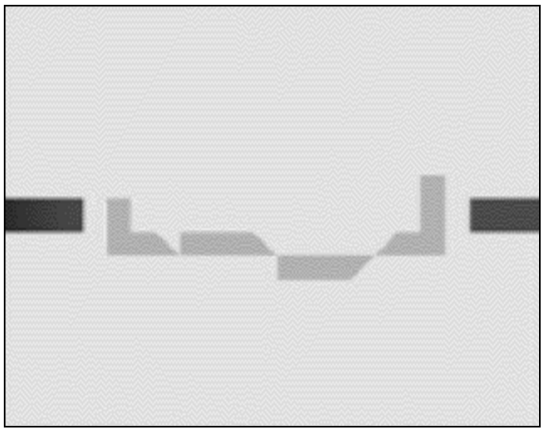

Fig.3.7-2 : Physical circuit layout of gap-coupled resonator miniaturized through the use of shape synthesis. (Adapted from [MAHD 15]).

B. **[NOMU 13]**

The emphasis in this reference was on the issues associated with the discrete-to-continuous conversion required (as discussed in Section 3.4.2) to apply a continuous-variable pixelation approach to the shaping of a microstrip bandpass filter.

3.7.2 Discrete-Variable Pixelation Approach

Surprisingly, there are only a limited number of references on the shape synthesis of microstrip RF circuits directly related to the work of the present thesis. We here mention a number of these, selected either to indicate what circuit types shape synthesis has been applied to, or if they provide valuable information on the objective function definitions used.

A. **[JOHN 96]**

Physical RF circuit shape synthesis appears to have first been described in [JOHN96]. The authors use magnitudes $\left|S_{ij}(\omega)\right|$ and $\left|S_{ii}(\omega)\right|$ in the definition of their objective function F_{obj}. They synthesize notch-stop (transmission less than -14dB at a single frequency) and notch-pass (full transmission at two specified frequencies) filters. The physical circuits are realized in microstrip, and a GA is used as the underlying optimization algorithm.

B. **[DELA 97]**

The goal of this paper was to shape synthesize a resonant structure with an improved *Q*-factor over that of a conventional rectangular patch. The authors thus use the *Q*-factor in the definition of their objective function. The rectangular resonator in Fig.3.7-3(a), which is the starting shape, has $Q = 7$ at a resonant frequency of 8.6 GHz, while the slightly altered shape in Fig.3.7-3(b) has $Q = 12$. When shape optimization is used (with left-right and top-down symmetry enforced) the authors obtained the resonator in Fig.3.7-3(c) that has $Q = 92$, albeit at a shifted resonant frequency of 8.4 GHz. The optimizer used was a GA.

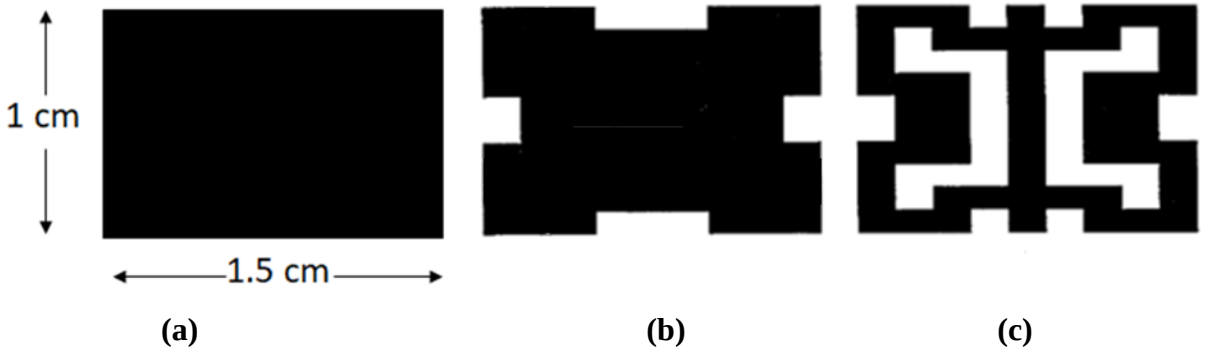

Fig.3.7-3 : Physical resonator circuit layout - (a). conventional rectangular resonator; (b). notched rectangular resonator, and (c). resonator shape synthesized for Q maximization. (Adapted from [DELA 97]).

D. **[OHIR 07]**

The aim of this paper was to shape synthesize a microstrip bandpass filter, with the passband and stopband characteristics specified by defining F_{obj} in terms of the S-parameter magnitude masks. The authors found that the required filter could be synthesized in fewer iterations of GA used if F_{obj} is a weighted linear combination of $|S_{11}(f)|$ and $|S_{21}(f)|$, expressed in dB. Two examples where shown. In the first, whose result is that in Fig.3.7-4(a), a microstrip line of the same width as that at the ports was fixed between input and output (the lightly shaded portion in the said figure), and was not allowed to be altered during the shaping process. The resulting filter was apparently slightly reduced in size compared to a conventional bandpass filter design with the same characteristics. In contrast, in the second example, whose shaped layout in shown in

Fig.3.7-4(b), a gap was enforced[68] between the input and output (as indicated). Either top/down and left/right symmetry was enforced during shaping. The required frequency response was similar to that in Fig.3.7-4(a), namely one close to that of a conventionally design bandpass filter with a 2nd-order Chebyshev characteristic, albeit slightly smaller in layout. The number of degrees of freedom needed was 288. Nevertheless, this serves to show how shape synthesis is able to access possible designs not reachable using traditional procedures.

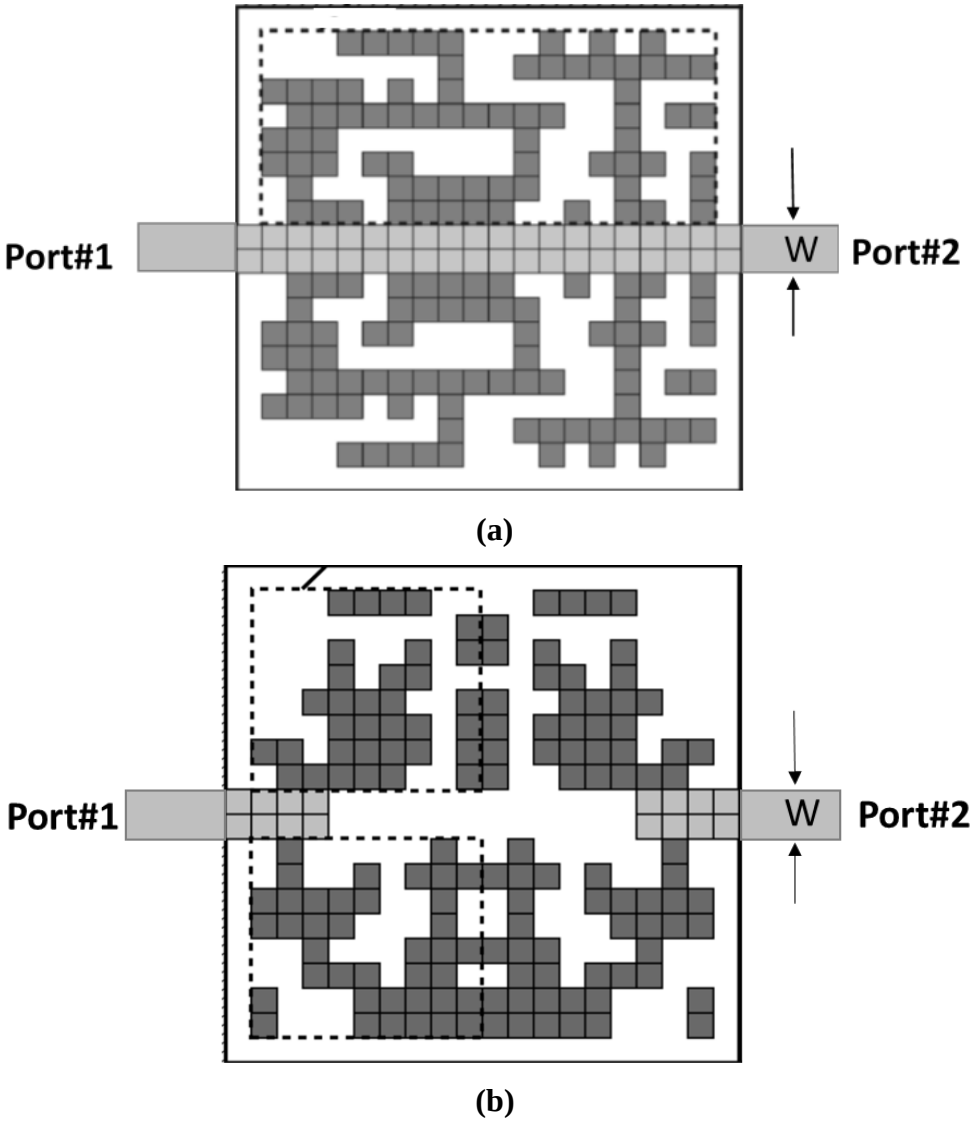

Fig.3.7-4 : Physical microstrip bandpass filter circuit examples. (Adapted from [OHIR 07]).

[68] No conductor located there in the starting shape.

E. [KIDO 07]

The order of a filter is determined by the number of resonances possessed by the physical circuit. The goal in this paper was to synthesize, in microstrip, bandpass filters with up to four resonances. The authors note that it is not easy to control the "order" (that is, number of resonances) when shape synthesis is used if only the S-parameter magnitudes are used in the definition of F_{obj}. They show that if F_{obj} is a weighted linear combination of two parts, one related to the S-parameter magnitudes, and the other to the deviation of the phase (namely $\arg\{S_{21}(\omega)\}$) from some desired phase behavior[69], then the required filter order can be obtained through shape synthesis. The desired phase behavior was taken to be that of a prototype Chebyshev filter of the same order as that intended for the shape-synthesized filter. Left/right geometrical symmetry was enforced. It was found that the relative weights of the two parts of the F_{obj} may need to be adjusted to synthesize a filter with the desired response in a reasonable number (eg. 200) of iterations. The resulting filter layout is that shown in Fig.3.7-5. The number of degrees of freedom needed was roughly 300, even with the left/right symmetry used.

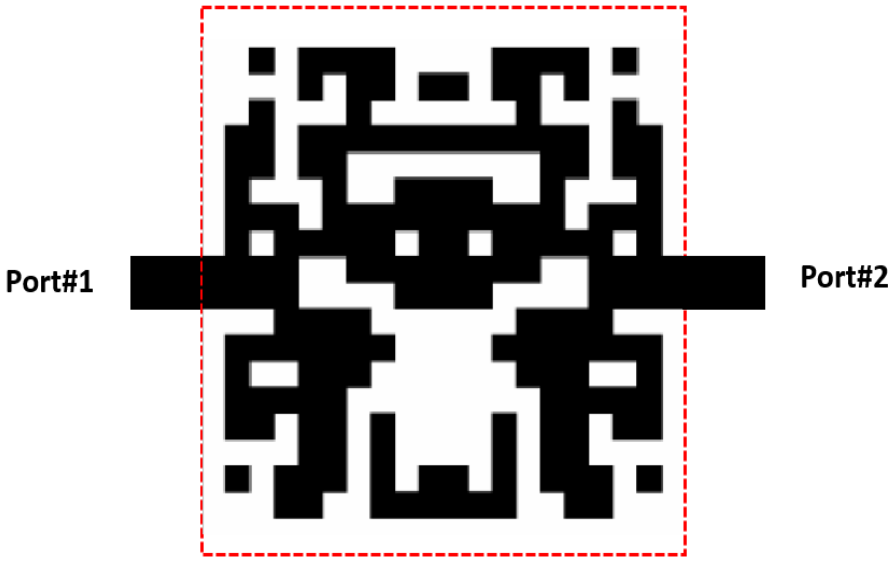

Fig.3.7-5 : Physical microstrip bandpass filter circuit layout. (Adapted from [KIDO 07]).

[69] Which has to be selected in some way.

F. [KIDO 08]

The authors of [KIDO 07] here extend their work to that of a microstrip bandpass filter where the portion of the groundplane "under the filter" is also shaped (and hence becomes a defected groundplane structure) in order to obtain a more compact filter than that in [KIDO 07]. They use S-parameter magnitude masks, and enforce top/down symmetry.

G. [MAHD 15]

This is an example where only one portion of a conventional microstrip filter (one of the resonators) is separately shaped rather than the complete filter. The authors begin with a conventional five-pole bandpass hairpin filter design that provides the passband characteristics they desire, but not the required rejection at a specific frequency (the 2nd harmonic $2f_o$ of the centre-frequency f_o of their passband). An individual resonator, of which several are used in the complete filter, is shown in Fig.3.7-6(a). This can be considered to be a starting shape. Shaping is then done[70] on such an individual resonator until its $|S_{21}(2f_o)|$ is below a certain threshold (or rejection) level. The shaping is effectively additive[71]. The resulting shaped resonator is that in Fig.3.7-6(b). The shaping procedure could be halted at this point. However, the authors essentially infer (albeit qualitatively[72]) that the shaping process is "telling" us that the perturbation should be as shown in Fig.3.7-6(c), which they call the approximated "smoothed" shape. They then fine-tune dimensions W and L of this smoothed resonator shape until its $|S_{21}(2f_o)|$ is below the required threshold. These resonators are then used successfully in the hairpin filter[73] that provides the required pass band behaviour *and* the 2nd harmonic rejection. In the shape synthesis process only S-parameter magnitudes are used in the definition of F_{obj}. Left/right symmetry is exploited.

[70] The authors of [MAHD 15] used several different optimisation algorithms, but concluded that the GA is the best for their application. But see comments on the "no free lunch theorem" in Section 2.5.
[71] In other words, pixels are added to the starting shape but never removed.
[72] How this is concluded is not completely clear to the present author, as details are not provided in [MAHD 15].
[73] But the complete filter was not shape synthesized from scratch.

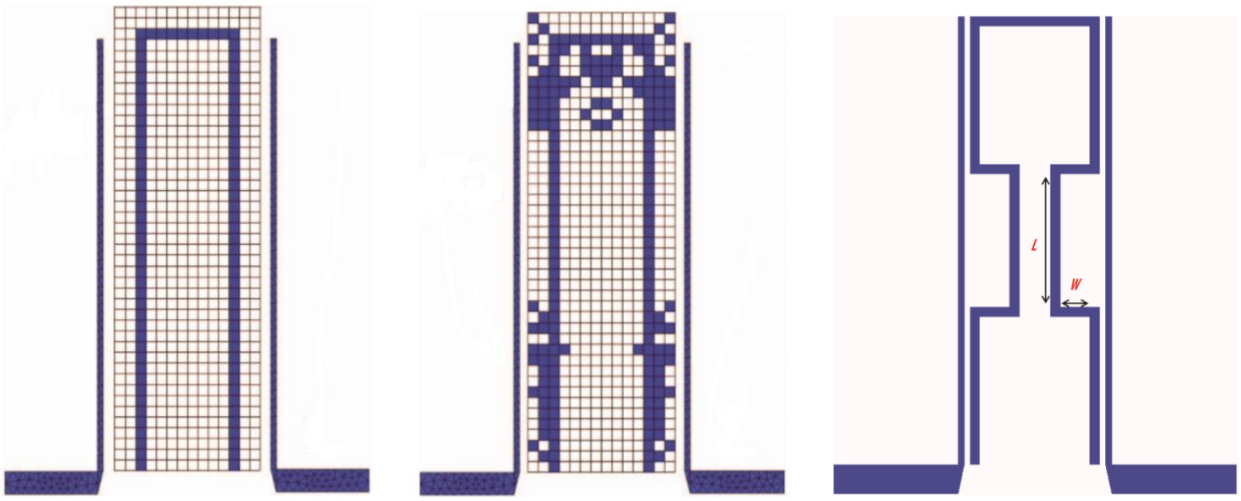

Fig.3.7-6 : Hairpin (single) resonator physical circuit shape perturbation example showing (a). the starting shape; (b). the perturbed shape; and (c). the "smoothed" shape. (After [MAHD 15])

H. Direct Experiences with the Discrete-Pixelation Shape Synthesis Method

The author applied[74] the discrete-variable pixelation approach to shape synthesis to several microstrip circuit problems. Some of these were repetitions of cases from references mentioned above in the present section; we will draw on this experience in the conclusions we will reach in Section 3.10 as to the shortcomings of pixelation-based shape synthesis methods. Due to the fact that we wish to refer to one specific case[75] in our deliberations in Section 3.10, that confirmed the conclusions we will draw in Section 3.10, we relate it here. We began by studying the "hairpin" bandpass filter configuration [HONG 01] shown in Fig.3.7-7, and is representative of what we want a shape synthesis method to do. The geometry in Fig.3.7-7 was obtained using feature optimisation. We noted that changes of only 0.1mm in the lengths of the coupled

[74] Using the commercially-available full-wave MM-based code SONNET [SONN 21] for the "forward problem". When using the discrete-variable pixelation approach with SONNET, it was only possible to use the same pixels for geometry shaping and for the MM expansion function mesh (cells less than $\lambda/20$ per side are recommended), due to restricted access to various workspace files (for proprietary reasons). Also, in SONNET, the actual conductor geometry must always fit into the defined cells layout like pieces of a puzzle. The GA script used in the shaping process was that available in the MATLAB optimisation toolbox. Use of this discrete-pixelation based shape synthesis implementation was used only for the "gaining experience" study by the author; this experience spawned the completely new subtractive shape synthesis method that is the main contribution of this thesis; its implementation (described in Section 4.6) did not use the code SONNET as the CEM engine.

[75] Quantitative details (eg. geometrical dimensions; computed S-parameter performance) have been relegated to Appendix I, since they distract from the point we wish to make.

resonators in Fig.3.7-7 caused the S-parameter performance to change by noticeable amounts; this is indicative of the level of resolution that is often required for microstrip circuits. When performing discrete pixelation based shape synthesis, if the pixel size were consequently selected to 0.1mm per side to realise such a geometrical resolution, the number of pixels required[76] (degrees of freedom assigned for shaping) is roughly 10000, which is too large for a GA algorithm. In order to at least attempt a shape synthesis we increased the pixel size to reduce the degrees of freedom to 1584, which provided a resolution of 0.5 mm. Even with this much smaller number (still too large for use with evolutionary optimisation algorithms), the shape synthesis runs for several weeks without the shaped designs[77] satisfying the specified masks. The GA optimizer simply stagnates[78]. An alternative to pixelation-based shape synthesis is needed. Before collating the reasons for the latter statement in Section 3.10, we wish to present a "design-space" viewpoint to facilitate such further discussion.

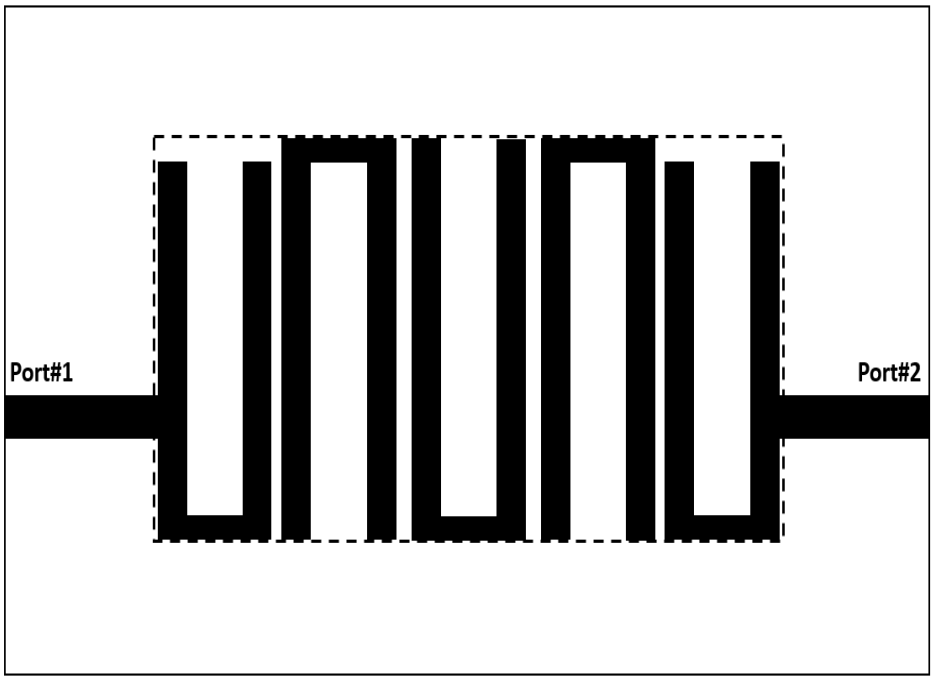

Fig.3.7-7 : Geometry of a conventional hairpin bandpass filter.

[76] This is also then the resulting chromosome length when using the GA optimiser.
[77] The best shape synthesized design is shown in Fig.I-4 of Appendix I.
[78] It may be for this reason that (see Part G of Section 3.7.2) the authors of [MAHD 15] shaped the resonators of their hairpin filter individually to obtained the special performance they required, rather than the complete hairpin filter, although they do not say this. Also, if we were to be able to speed up the full-wave CEM computations involved, using parallelization for example, we would simply "know sooner that the GA is stagnating"!

3.8 A DESIGN-SPACE VIEWPOINT FOR SHAPE SYNTHESIS

No RF circuit design task begins with a set of S-parameter specifications[79] and allows the designer unlimited design freedom. There are always size (eg. allowed occupied surface area, or occupied volume), tolerance, port location, and other constraints. Thus no shaping method used for design purposes allows unlimited design freedom either. We depict this in Fig.3.8-1 by showing that the available "design space" (the outer boundary shown, and which does not refer to physical space here) may be large but is constrained and not unlimited. Different design methods may be used to attempt a design, but none of these will be able to access the complete available design space, and different design approaches may access different parts of the available design space.

In Fig.3.8-1 we show the design space accessed by the feature-optimisation approach to design. It is limited because, as noted in Section 2.10, in this approach designers pick well-understood sub-components of conventional geometrical shape from a library of canonical shapes, connect these (usually with a good amount of ingenuity and experience), and then automatically adjust a handful of key dimensions to obtain acceptable performance.

Shape synthesis is not tied to some known design library (depicted as the "design space for feature optimization" in Fig.3.8-1), and so has the potential to allow one to explore a broader design space. In a sense, it gets closer to allowing the electromagnetics decide on the shape of the final physical circuit in order to obtain the performance desired under the restrictions set by the starting shape. The number of degrees of freedom assigned to the shaping process will determine the size of the design space used. In discrete-variable pixelation methods (say Method#A in Fig.3.8-1) the number of degrees of freedom is the number of pixels into which the starting shape has been divided. In continuous-variable pixelation shaping (say Method#B), the choices made regarding the discrete-to-continuous conversion process (viz. material interpolation law, penalization, biasing function, blurring filter) will result in these using different design spaces even for the same number of pixels.

[79] Or S-parameter specifications plus radiation pattern requirements in the case of antennas.

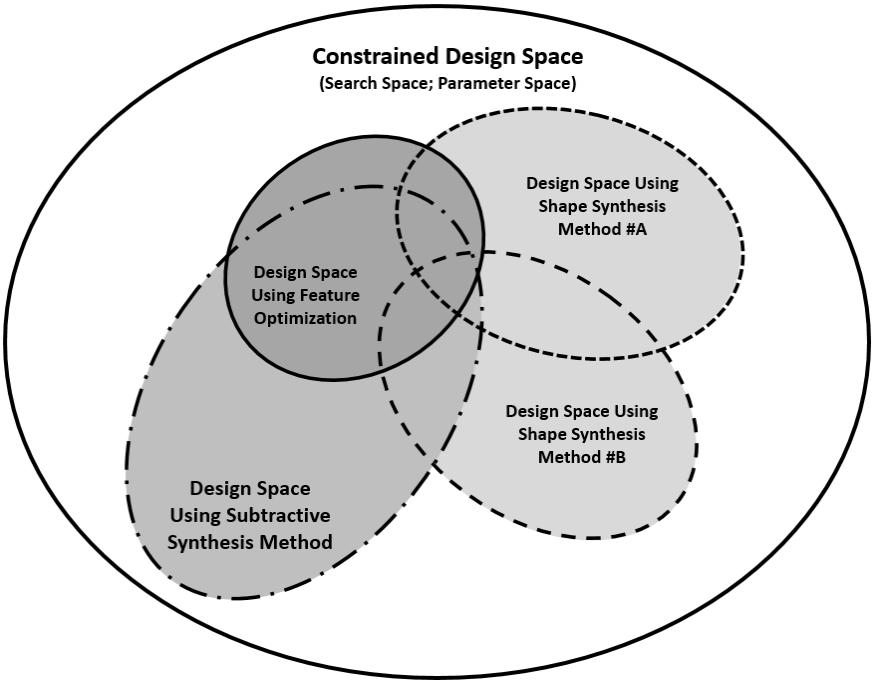

Fig.3.8-1 : Framework in which to think about various shape synthesis methods.

3.9 CONCLUSIONS

Physical microstrip circuits are not electrically small; even the simple quarter-wave transformer is exactly that, namely on the order of a quarter-wave (the effective wavelength being referred to) in dimension. In discrete-variable pixelation based shaping this means that the number of pixels needed (and hence the number of degrees of freedom) is in the hundreds[80]. The author's reproducing of cases of the type reviewed in Section 3.7.2 revealed that the evolutionary optimization algorithm struggled to converge with so many degrees of freedom. Indeed, this author's experience is that each problem has to be handcrafted with much effort in order to "manipulate" the method to a solution. We would prefer a method that could be used in more of a production line manner; only then would its use become more widespread in practice. As a means of achieving this we prefer to have a greatly **reduced number of degrees of freedom** (to ensure better convergence of the optimizer), and yet retain a **geometrical resolution** that is capable of providing high-quality physical circuit performance. Apart from slow evolutionary optimisation algorithm convergence (due to a very large number of degrees of freedom), it is the

[80] Not necessarily to ensure sufficiently accurate CEM computations (as the pixels can be defined different from the elements of the mesh used in the CEM computation, though this is not necessarily possible using commercially-available CEM engines), but to ensure sufficient geometrical resolution during shaping.

computer-time taken for copious CEM simulations that prevents faster shaping outcomes. A shortcoming of the discrete-pixelation based method is that it cannot be used with surrogate modelling in an attempt to decrease the CEM simulation time. We would prefer a shaping approach that involved continuous geometrical variables to permit **surrogate modelling** usage[81]. Continuous-pixelation methods are not the answer because of the need for somewhat arbitrary problem-dependent "fixes" mentioned in Section 3.4.2. In Chapter 4 we will develop a new shape synthesis method (the subtractive shape synthesis method) that allows the preferences, highlighted in bold earlier in this paragraph, to be realized. It will be shown to increase the extent of the design space, as portrayed shown in Fig.3.8-1. The context of the new subtractive shape synthesis method is depicted in the chart of Fig.3.9-1.

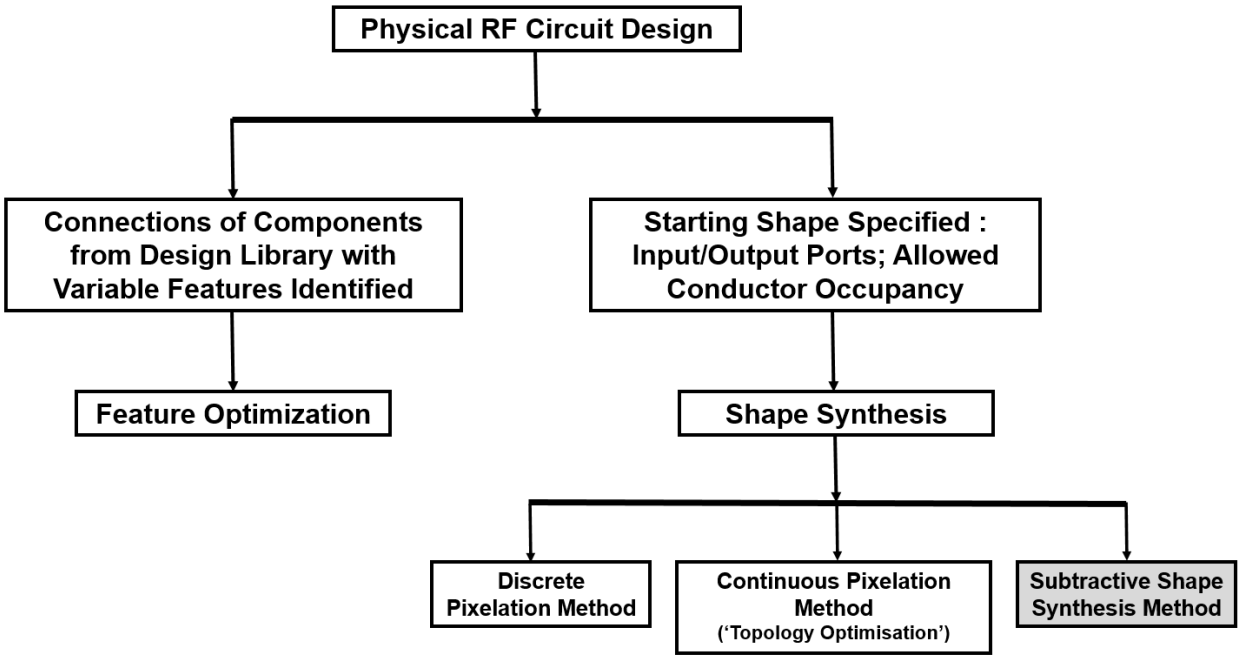

Fig.3.9-1 : Chart that indicates (bottom right) the relation of the new subtractive shape synthesis design method (developed in Chapter 4) to other design methods.

[81] This would also permit the use of gradient-based, and not only evolutionary, optimization algorithms in order to exploit the benefits of each if possible (eg. combined used at various stages of the shaping process).

CHAPTER 4
A New Subtractive Shape Synthesis Method

4.1 INITIAL REMARKS & MOTIVATING IDEAS FOR THE SUBTRACTIVE SHAPE SYNTHESIS METHOD

Chapter 3 placed the topic of shape synthesis into perspective. Section 3.9 summarised the shortcomings of existing shaping methods, and stated what the preferred characteristic would be for an alternative shape synthesis method. In this chapter we propose and develop an alternative shape synthesis approach, that we will call the **subtractive shape synthesis method** for purposes of identification. It allows the design space to be enlarged, but will avoid the dimensionality issues, would permit the use of surrogate modelling (eg. ML-based techniques), and allow either evolutionary or gradient-based optimization algorithms (or even a combination) to be used. Yet it will offer a "wider" design space than feature-optimisation does.

Section 4.2 describes the basis of the subtractive shape synthesis method, including the imposition of fabrication tolerance constraints. Section 4.3 shows how symmetry (either left/right, top/down, or quadrantal) can be enforced. Section 4.4 shows that different types of subtractive elements can be used, whereas section 4.5 reveals the flexibility of the method in accommodating constraints that may exist when a particular physical circuit is to be used with other components on the same substrate, for example. Some technicalities on the particular implementation of the subtractive shape synthesis method, developed as part of this thesis, are outlined in Section 4.6.

The new subtractive shape synthesis idea was spawned (after much hands-on experience with the discrete-variable pixelation method) by a number of observations. Firstly, the realisation that microstrip circuits shape synthesized using the pixelation method reveal many isolated collections of electrically small pixels that contribute little to the actual S-parameter performance (eg. the fact that the pixelated and "smoothed" layouts [MAHD 15] have almost similar performance). Secondly, if one pages through the design libraries used as the basis for feature-optimization design, with the hairpin filter in Fig.3.7-7 as just one of many examples, it is clear that the geometry of many passive microstrip components could be arrived at from some starting shape of conductor with designated ports, and then removing (subtracting) rectangles, circles and triangles from the starting shape to arrive at the actual physical circuits. If the size-dimensions of

these subtractive shapes could be used as the degrees of freedom, this number will be greatly reduced. It would also permit very fine geometrical resolution. However, we do not know beforehand where these subtractive shapes should be located. We therefore allow the coordinates of the locations of their centroids to also be degrees of freedom. Since the quantities now constituting the degrees of freedom are continuous geometrical variables, surrogate modelling of precisely the kind used in feature optimization can be employed, and gradient-based optimization algorithms are an option (along with evolutionary ones) if they can be used to advantage. This approach also allows one to separate the meshing needed for an accurate full-wave analysis from the geometrical resolution with which shaping can be done. The new shaping approach is next introduced for the first time here in Chapter 4. Its implementation, described in Section 4.6, will be used in Chapter 5 to demonstrate its successful application and show that it significantly broadens the design space compared to pure feature optimization design.

4.2 DESCRIPTION OF THE BASIC SUBTRACTIVE SHAPING METHOD

4.2.1 Geometry Manipulation

The dimensions of the two feedlines are fixed. These feedlines are unaltered by the shaping process. The known starting shape shown in Fig.4.1 is rectangular, but it need not be. The coordinates of the four corners of the rectangular starting shape are (x_a, y_a), (x_b, y_b), (x_c, y_c) and (x_d, y_d). We denote this starting shape by S_{start}. There are $n = 1, 2, ..., N$ rectangles, that we refer to as subtractive rectangles. The n-th rectangle has height H_n and width W_n, with its centroid located at (x_n, y_n). We denote the n-th rectangle by $\Re_n$ and completely specify it by its designator $[H_n, W_n, x_n, y_n]$.

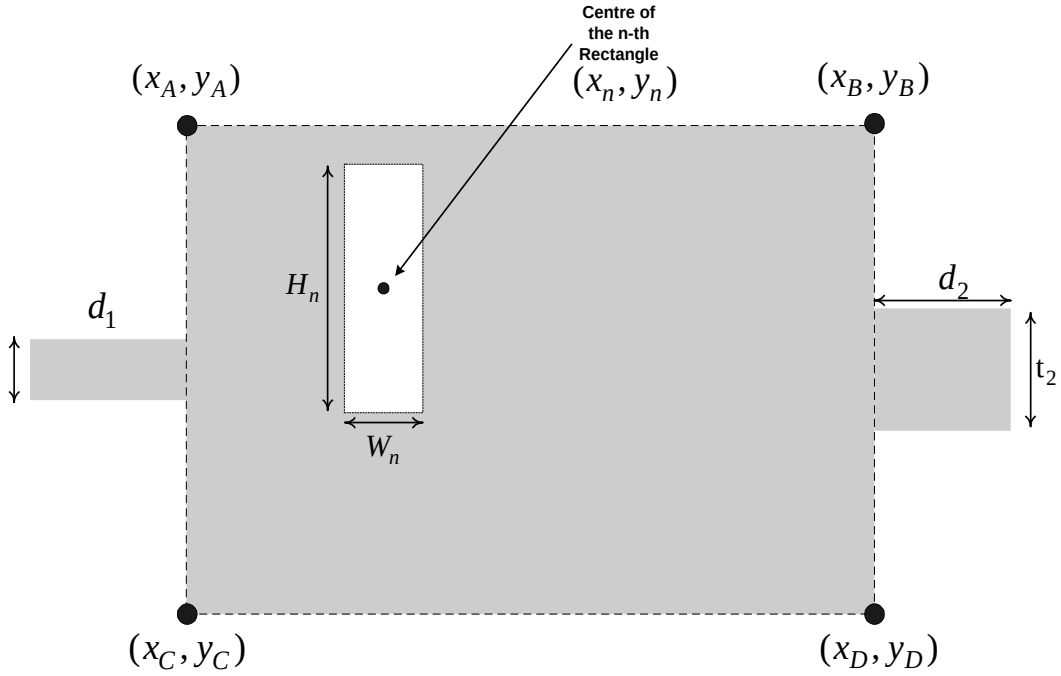

Fig.4.2-1 : Physical microstrip circuit layout, seen from above. The shaded areas are conducting material on the top surface of the finite thickness substrate. The substrate is backed by a conducting groundplane.

4.2.2 Rectangular Subtractive Elements

We define so-called subtractive element geometries. The location and size of each subtractive element is defined by its designator. In particular, we consider a rectangular subtractive element (say the n-th one), as indicated in Fig.4.2-1. It has a designator $[H_n, W_n, x_n, y_n]$ and occupies a region $\Re_n$. Each of the four quantities in the designator will be a variable in the shape synthesis process.

4.2.3 Subtractive Shaping Process

We begin by specifying starting shape[82] (or design area) $\{S_{start}\}$, that has its corners at (x_A, y_B), (x_B, y_B), (x_C, y_C) and (x_D, y_D), as shown in Fig.4.2-1. The feedline locations and dimensions are specified, as well as these coordinates of the corners of the starting shape. We specify that there are N subtractive rectangular elements, and hence there are $4N$ shaping

[82] As will be noted later, the starting shape need not be rectangular.

variables. The objective function F_{obj} is defined in terms of the complex S-parameters, and its definition includes the frequency range information, and so on, as discussed in Sections 3.10 through 3.12. Initial values have to be specified for the quantities in each designator. At each step of the optimisation[83] iterations we have the values of each designator $[H_n, W_n, x_n, y_n]$. The shape of the physical circuit is $\{S_{start}\} - \{\Re_1 \cup \Re_1 \cup ..... \cup \Re_N\}$, where the negative sign denotes removal of the conductor from those potions of $\{S_{start}\}$ occupied by the subtractive shape.

4.2.4 Constraints on the Subtractive Rectangle Dimensions & Locations

At each step of optimization, we have the values of the designators $[[H_n, W_n, x_n, y_n]]$ of each subtractive rectangle. A number of constraints are needed to make the process sensible in practice. These can be listed as:

(a). We do not want any rectangle to be located outside the (in this case rectangular) starting shape, that has its corners at (x_A, y_B), (x_B, y_B), (x_C, y_C) and (x_D, y_D).

(b). So as not to end up with conducting tracks that are too narrow for the etching process a designer might have in mind, we want to limit the lowest values of the quantities $\{D_{x\ell}^{(n)}, D_{xr}^{(n)}\}$ and $\{D_{yt}^{(n)}, D_{xb}^{(n)}\}$, where the second subscripts denote left, right, top and bottom, respectively. We must have (with reference to Fig.4.2-2)

$$D_{x\ell}^{(n)} > t_{\min} \text{ or } D_{x\ell}^{(n)} = 0 \qquad (4.2\text{-}1)$$

$$D_{xr}^{(n)} > t_{\min} \text{ or } D_{xr}^{(n)} = 0 \qquad (4.2\text{-}2)$$

$$D_{yt}^{(n)} > t_{\min} \text{ or } D_{yt}^{(n)} = 0 \qquad (4.2\text{-}3)$$

and

$$D_{yb}^{(n)} > t_{\min} \text{ or } D_{yb}^{(n)} = 0 \qquad (4.2\text{-}4)$$

It is readily established that

[83] When using the GA optimisation algorithm, as we will initially do, there are at each iteration step, of course several shapes (that is, members of the population), for which all designators are known.

$$D_{x\ell}^{(n)} = \left(x_n - \frac{W_n}{2} \right) - x_A = \left(-\frac{1}{2} \right) W_n + x_n - x_A \qquad (4.2\text{-}5)$$

$$D_{xr}^{(n)} = x_B - \left(x_n + \frac{W_n}{2} \right) = \left(-\frac{1}{2} \right) W_n - x_n - x_A \qquad (4.2\text{-}6)$$

$$D_{yt}^{(n)} = y_A - \left(y_n + \frac{H_n}{2} \right) = \left(-\frac{1}{2} \right) H_n + y_n - y_A \qquad (4.2\text{-}7)$$

and

$$D_{yb}^{(n)} = \left(y_n - \frac{H_n}{2} \right) - y_C = \left(-\frac{1}{2} \right) H_n + y_n - y_C \qquad (4.2\text{-}8)$$

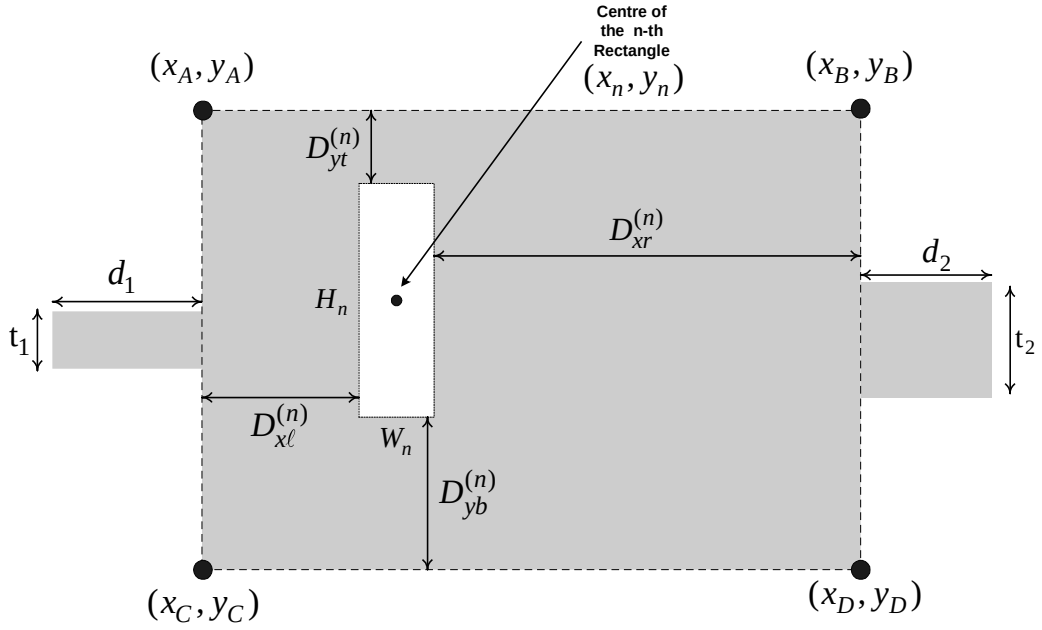

Fig.4.2-2 : Physical microstrip circuit, seen from above, in order to define the subtractive rectangular element size/location constraints.

Expressions (4.2-1) through (4.2-8) can be used to write the constraints in matrix form for inclusion in the optimization algorithm.

Considering any pair of subtractive rectangles, say the *m*-th and *n*-th ones, we will have the values in the corresponding designators $[H_m, W_m, x_m, y_m]$ and $[[H_n, W_n, x_n, y_n]]$. A further constraint is then as follows:

(c). With reference to the separation quantities $\{T_x^{(mn)}, T_y^{(mn)}\}$ shown in Fig.4.2-3 and Fig.4.2-4, so as not to end up with conducting tracks that are too narrow for the etching process a designer might have in mind, we want

$$T_x^{(mn)} \geq t_{\min} \quad \text{or} \quad T_x^{(mn)} = 0 \tag{4.2-9}$$

and

$$T_y^{(mn)} \geq t_{\min} \quad \text{or} \quad T_y^{(mn)} = 0 \tag{4.2-10}$$

Inspection of Fig.4.2-3 and Fig.4.2-4 allows us to establish that

$$T_x^{(mn)} = \left| |x_m - x_n| - \left(\frac{W_m + W_n}{2} \right) \right| \tag{4.2-11}$$

and

$$T_y^{(mn)} = \left| |y_m - y_n| - \left(\frac{H_m + H_n}{2} \right) \right| \tag{4.2-12}$$

Use of the two modulus signs in expression (4.2-11), and in (4.2-12), ensures that (4.2-9) and (4.2-10) are correct irrespective of whether the m-th subtractive rectangle is to the left or right of the n-th one, and will also allow the overlapping of subtractive rectangles depicted in Fig.4.2-5.

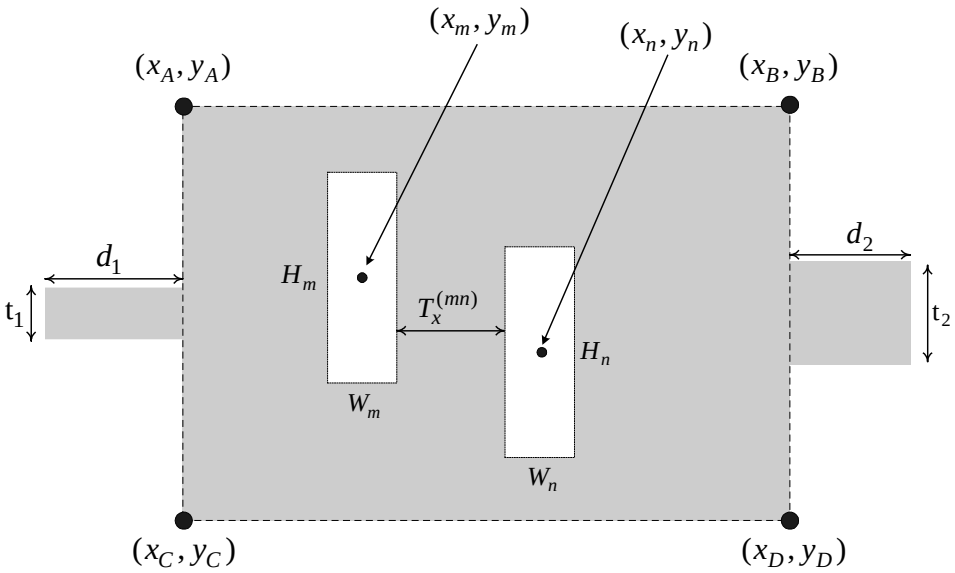

Fig.4.2-3 : Physical microstrip circuit, seen from above, in order to define the subtractive rectangular element x-axis separation constraints.

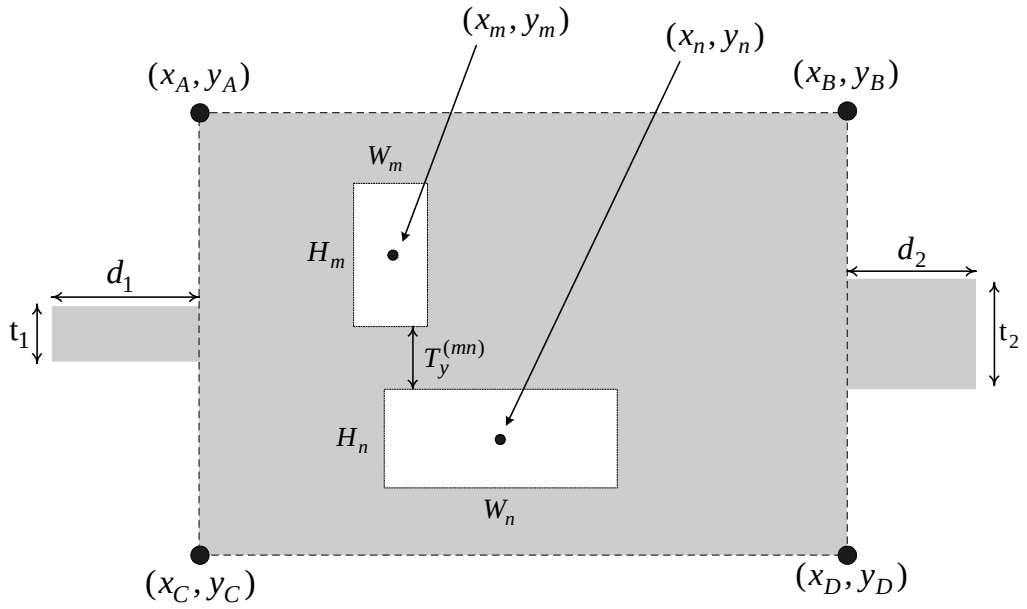

Fig.4.2-4 : Physical microstrip circuit, seen from above, in order to define the subtractive rectangular element y-axis separation constraints.

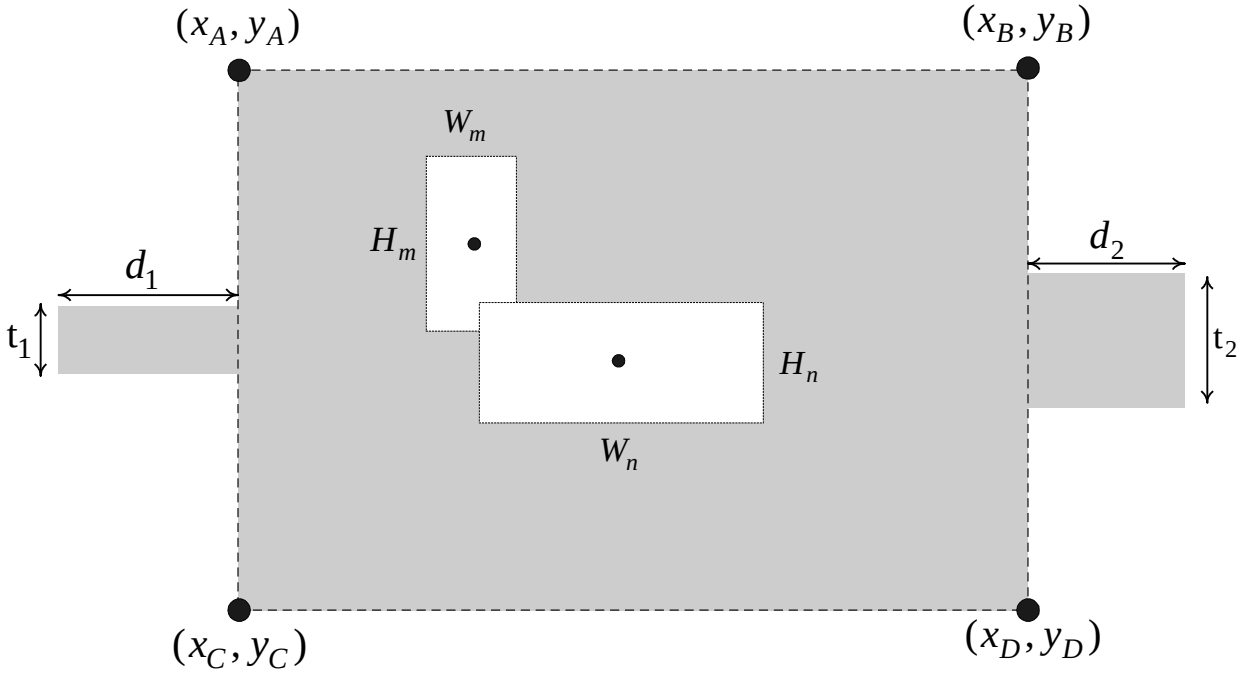

Fig.4.2-5 : Physical microstrip circuit, seen from above, in order to demonstrate that the stated separation constraint allows the overlap situation shown in the present diagram.

(d). In order to ensure that no apertures ('gaps') are formed that are too narrow for the etching process a designer might have in mind, we want

$$H_n > g_{\min} \tag{4.2-13}$$

and

$$W_n > g_{\min} \tag{4.2-14}$$

4.2.5 Inclusion of Fabrication Tolerance Constraints

The constraints in Section 4.2.3 in effect incorporate constraints on the allowed conducting track thicknesses and gap, as illustrated in Fig.4.2-6. Unlike the feature-optimisation approach, where a desired performance can sometimes not be achieved if the tolerances are too loose, the shape optimization can in principle "simply" select another route to try achieve the required performance, in a way that accommodates the fabrication tolerances. The reason is that the design space is larger than that of feature-optimisation; this will be clear from the applications discussed in Chapter 5.

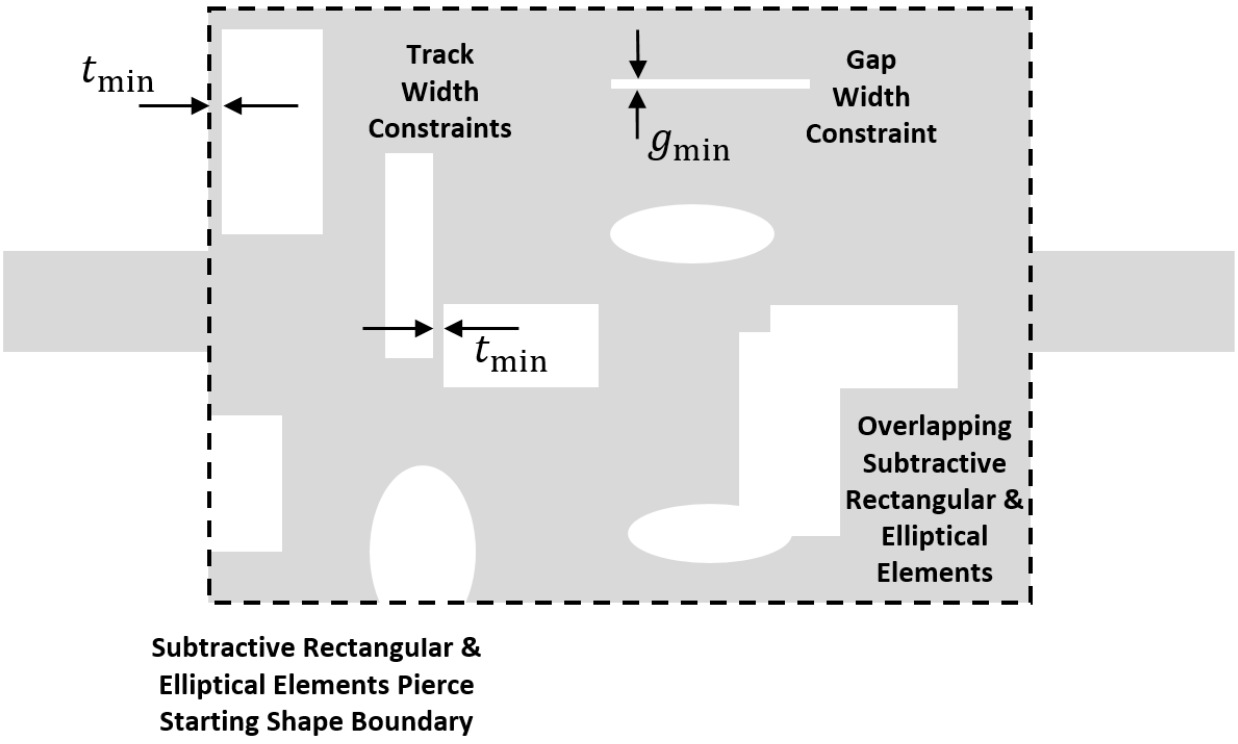

Fig.4.2-6 : Pictorial summary of the incorporation of fabrication tolerances in the subtractive shape synthesis method.

4.3 ENFORCING SYMMETRY IN THE SUBTRACTIVE SHAPE SYNTHESIS OF MICROSTRIP CIRCUITS

4.3.1 Symmetry About the x-Axis

If we intend enforcing symmetry about the x-axis (top/down symmetry), then it makes sense that the starting shape must itself possess such symmetry, as indicated in the figure below[84]. The physical circuit is symmetrical about the line $y = y_{\text{sym}}$.

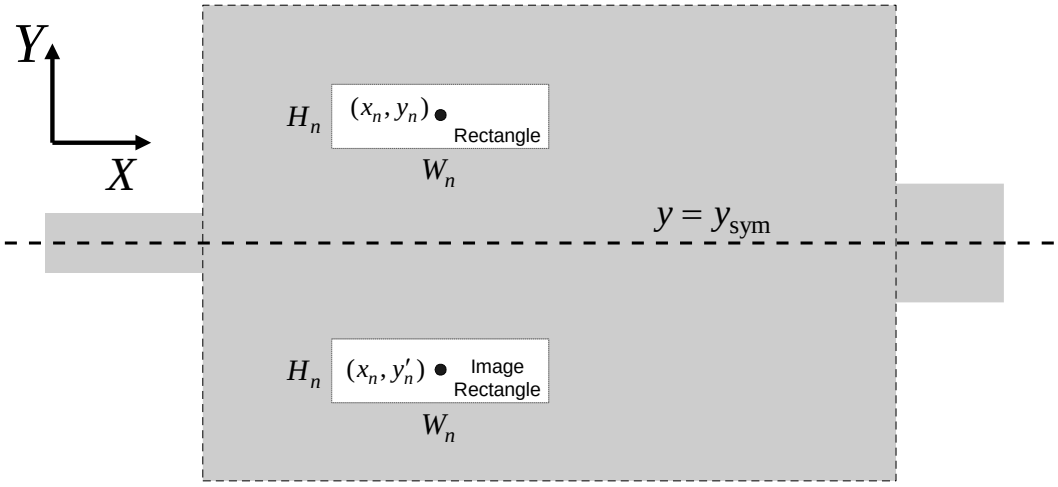

Fig.4.3-1 : Physical microstrip circuit, seen from above, in order to illustrate symmetry about the y-axis.

There are $n = 1, 2, ..., N_{\text{sym}}$ subtractive rectangles, with $N_{\text{sym}} = N / 2$, and associated with each rectangle is a 'image rectangle'. If the designator of the n-th rectangle is $[H_n, W_n, x_n, y_n]$, then that of the n-th image rectangle is $[H_n, W_n, x_n, y_n']$ with

$$y_n' = y_n + 2(y_n - y_{\text{sym}}) \tag{4.3-1}$$

Note that the designator of an image rectangle is known as soon as that for the rectangle itself is known, and so the image rectangle does not add additional optimisation variables to the shaping problem. Each rectangle and its image are subtracted from the starting shape to find a population member.

[84] Which also shows a typical rectangle and its image.

4.3.2 Symmetry About the y-Axis

If we intend enforcing symmetry about the y-axis, then it makes sense that the starting shape must itself possess such symmetry, as indicated in the figure below[85]. The physical circuit is symmetrical about the line $x = x_{\text{sym}}$.

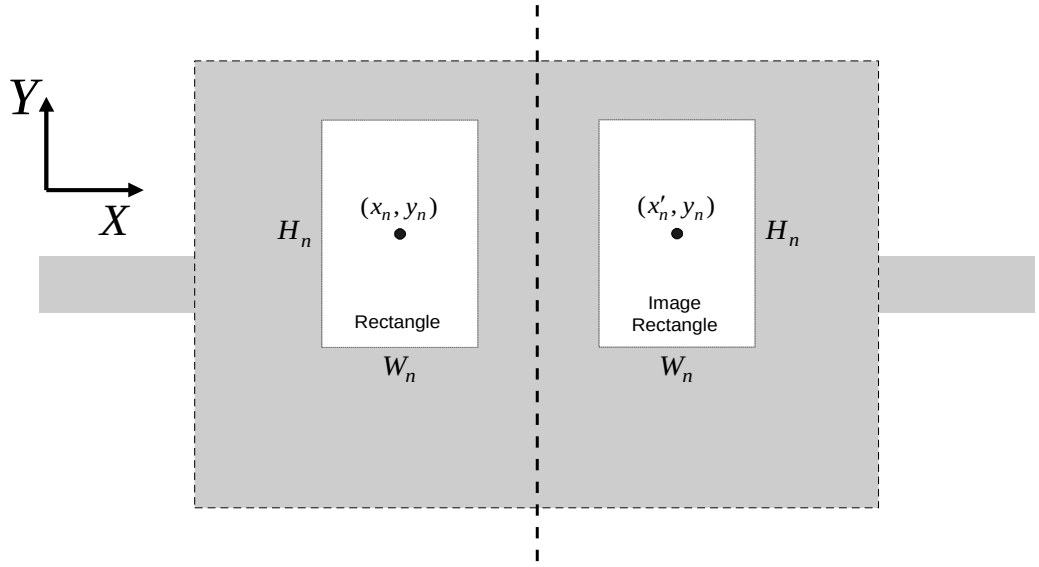

Fig.4.3-2 : Physical microstrip circuit, seen from above, in order to illustrate symmetry about the x-axis.

If the designator of the n-th rectangle is $[H_n, W_n, x_n, y_n]$, then that of the n-th image rectangle is $[[H_n, W_n, x'_n, y_n]]$ with

$$x'_n = x_n + 2(x_n - x_{\text{sym}}) \qquad (4.3\text{-}2)$$

4.3.3 Quadrantal Symmetry

If we intend enforcing symmetry about both the x- and y-axis, then it makes sense that the starting shape must itself possess such symmetry, as indicated in the figure below[86]. The physical circuit is symmetrical about the lines $x = x_{\text{sym}}$ and $y = y_{\text{sym}}$.

[85] Which also shows a typical rectangle and its image.
[86] Which also shows a typical rectangle and its three images.

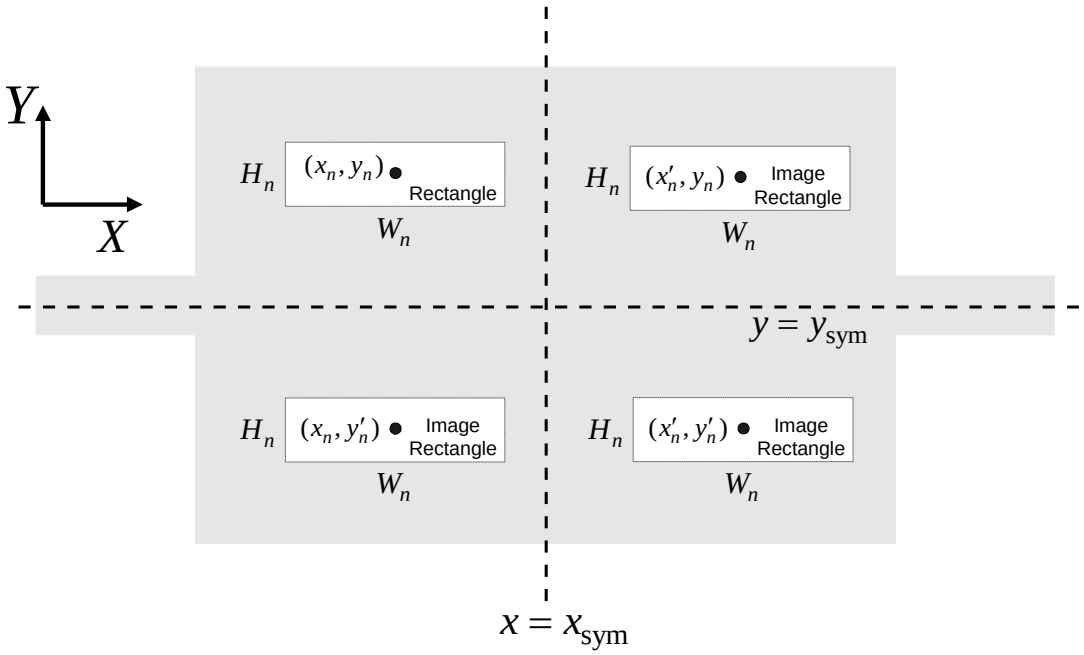

Fig.4.3-3: Physical microstrip circuit, seen from above, in order to illustrate symmetry about the x- and y-axes.

If the designator of the n-th rectangle is $[H_n, W_n, x_n, y_n]$, then that of its three image rectangles are $[H_n, W_n, x'_n, y_n]$, $[H_n, W_n, x_n, y'_n]$ and $[H_n, W_n, x'_n, y'_n]$.

4.4 NON-RECTANGULAR SUBTRACTIVE ELEMENTS

It possible to use other geometrical objects as subtractive elements, such as ellipses (which include a circle as a special case), triangles and even more general shapes[87]. For instance, Fig.4.4-1 shows the n-th subtractive element to be an ellipse of axial dimensions H_n and W_n, with its centroid located at (x_n, y_n). As with subtractive rectangles, its designator can be completely specified as $[H_n, W_n, x_n, y_n]$, which has four degrees of freedom. The special case of a circular subtractive shape is obtained by imposing the constraint $H_n = W_n = A_n$, resulting in a designator $[A_n, x_n, y_n]$ that has three degrees of freedom. The use of both rectangular and elliptical subtractive shapes will be demonstrated in Chapter 5.

[87] As far as the implementation of the method is concerned, one is only limited by what the commercially available CEM engine allows in terms of automated geometry control.

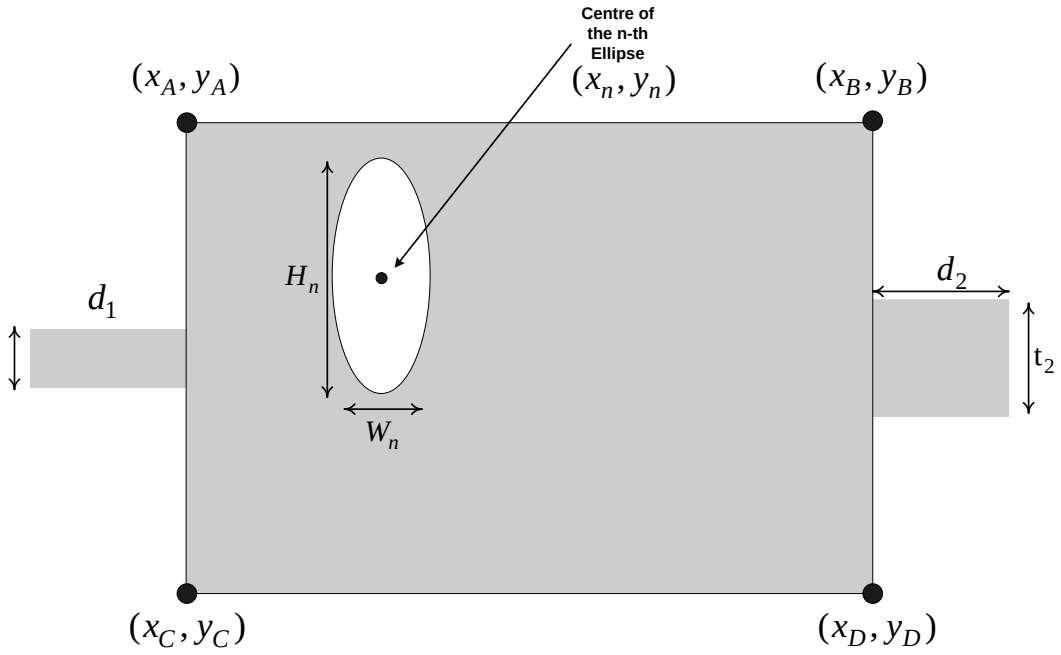

Fig.4.4-1 : Physical microstrip circuit layout, seen from above. The shaded areas are conducting material on the top surface of the finite thickness substrate. The substrate is backed by a conducting groundplane.

4.5 STARTING SHAPE POSSIBILITIES

It is not necessary to require a rectangular starting geometry or any form of geometrical symmetry. We can have varied starting shapes, as illustrated in Fig.4.5-1. The sketch in Fig.4.5-1(a) is meant to show that, unlike many traditional designs (eg. of various types of filter), the subtractive shape synthesis allows us to include ports with non-identical characteristic impedances. These ports need not even be inline, but could be as shown in Fig.4.5-1(b). The starting shape could in fact be chosen as in Fig.4.5-1 (c) and (d), so that the final shape synthesized device perhaps "avoids" certain areas on the substrate occupied by other components. Indeed, the effect of some other known component[88] (its function could be intended to be purely mechanical) could be included in the starting shape, and its presence exploited to achieve the performance required of, or to at least account for its presence on, the physical circuit

[88] Perhaps modelled by a conducting or dielectric block, that is not altered during the shaping process, however the case may be.

being shape synthesized. Thus the shape synthesis method is able to incorporate layout constraints in a flexible way.

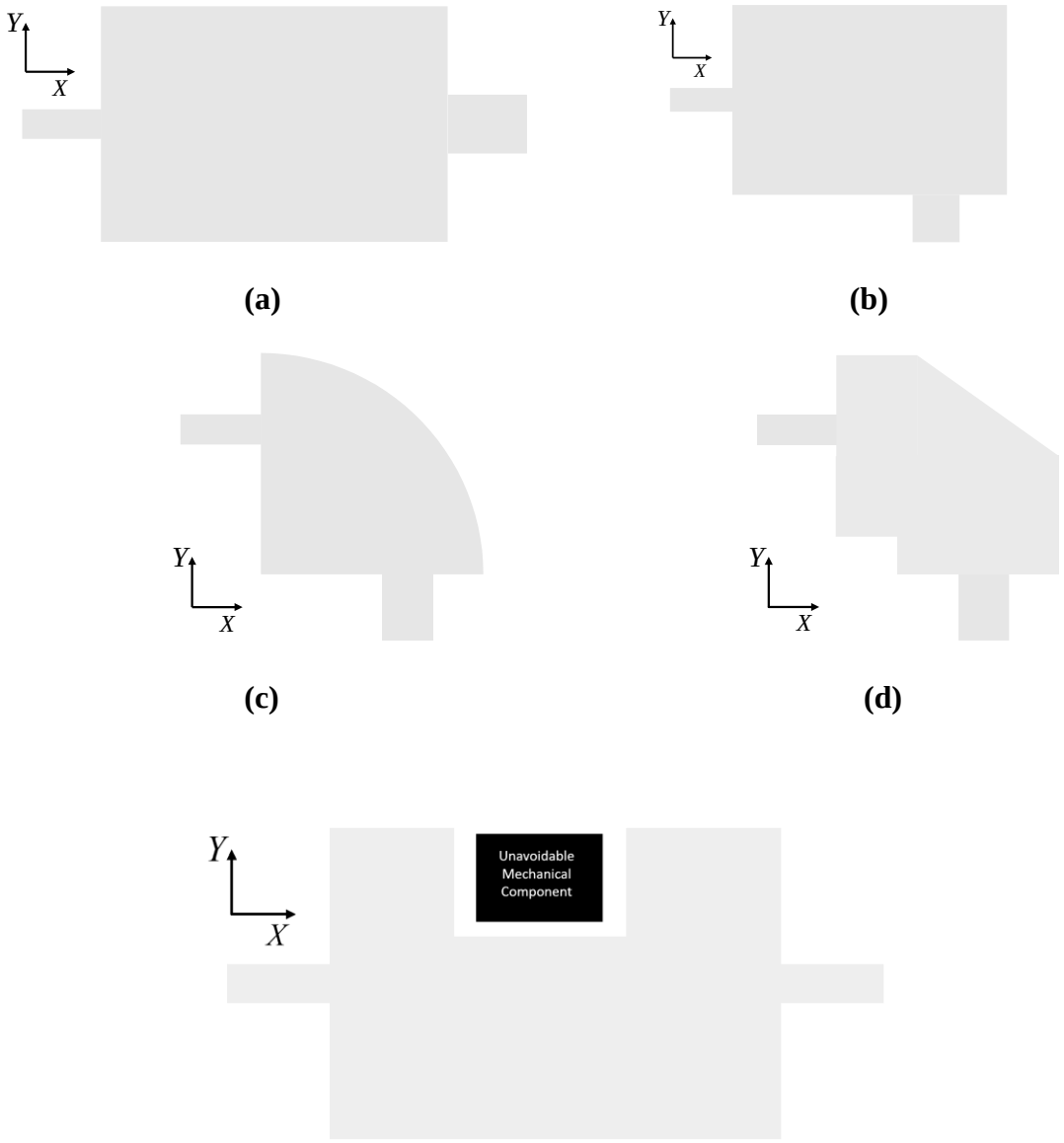

Fig.4.5-1 : Non-exhaustive examples of possible 2-port physical circuit starting shapes.

4.6 SOME TECHNICALITIES ON THE PARTICULAR IMPLEMENTATION OF THE SUBTRACTIVE SHAPE SYNTHESIS METHOD

The new shape synthesis method just outlined in the present chapter is independent of its particular implementation. As CEM and optimization methods improve with time, the efficiency of an implementation could be improved. Nevertheless, comments on the particular implementation (whose development is not a trivial exercise) used here to validate the new subtractive shape synthesis method will be useful. A flowchart for the shaping tool implementation used in this thesis is shown in Fig.4.6-1.

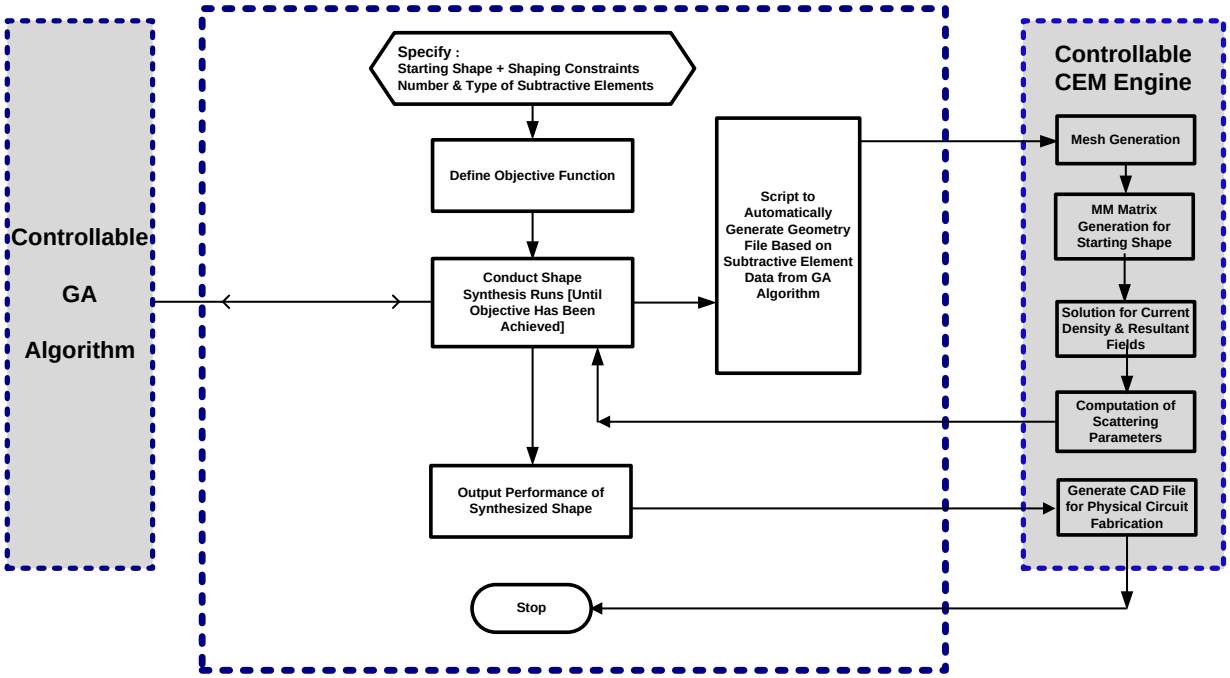

Fig.4.6-1 : Flowchart showing the steps in the particular implementation (of the subtractive shape synthesis method) used in the thesis.

We have principally[89] used the code [FEKO 21] as the controllable engine for the full-wave electromagnetic simulation of the physical microstrip circuits in this thesis. The advantage of being able to use a commercially available code is that the shape synthesis approach can be made available to others, and there is the benefit derived from on-going upgrades to such codes. FEKO

[89] We say "principally" because the code SONNET [SONN 21] was used in the early part of the thesis work, which exposed the weaknesses of the pixelation-based shape synthesis methods, but solely code [FEKO 21] was used in the implementation of the new subtractive shape synthesis method.

in particular allows the user access[90] to geometry resource files that allow one to develop scripts that "etch out" the subtractive shapes (under control of the shaping tool), and thereby implement the subtractive shape synthesis method.

We have implemented the procedure by developing a shape optimisation supervision script in MATLAB that is able to communicate with FEKO resource files, as well as run the optimisation algorithms also available commercially as part of the MATLAB optimisation toolbox[91]. The developed shaping script dictates which parts of the starting geometry may be changed[92], and what symmetries are to be enforced, during shaping. Whenever the optimisation algorithm has, during successive iterations, altered the geometry, the shaping script makes it possible to send this information back to FEKO as a geometry file[93], along with specification of the frequency points, mesh density and required S-parameter output, have it generate a new mesh and MM-matrix, and perform a full-wave analysis from which the objective functions, that allow the optimisation algorithm to take its next decision, are evaluated. The shaping script permits the description of objective functions as desired by the user directly in the shaping script. When performing shaping, it is advisable to begin with a reduced number of degrees of freedom, and then increase this if shaping does not provide a shape whose performance satisfies the specified masks.

In all the results to be presented in this thesis we ensure that the MM mesh densities on the conductor layout on the top of the substrate portions of element layers are sufficiently dense that the CEM model produces accurate results. In full-wave simulations[94] any significant violation of the expected S-parameter relationships in Section 2.4.4, for lossless physical circuits, would be indicative of modelling errors of some sort or the fact that unwanted radiation is taking place. This is monitored by the shaping script as an automatic check on the CEM modelling at all stages, and a flag raised if such modelling error is detected.

[90] This is not the case with all commercial CEM codes we have investigated. Such a capability is needed in order to implement the shape synthesis developed here.
[91] This supplies the "controllable GA algorithm" shown in Fig.4.6-1.
[92] Portions of the starting shape may, for reasons that might arise in some specific design situation, be declared out of bounds to shaping (eg. the feed lines at the ports).
[93] This step is performed through the running *Lua* script editor from MATLAB. *Lua* is a programming language embedded in the FEKO interface and available to FEKO users.
[94] Recall that such models would properly account for radiation, if it takes place.

No details will be given on the pixelation approach discussed in Chapter 3, and used by this author at the start of the research, because an alternative approach has been developed here. We simply mention that we used the commercial code[95] SONNET [SONN 21].

4.7 CONCLUDING REMARKS

We have developed a new shape synthesis method that:

■ Avoids the excessive number of degrees of freedom ("curse of dimensionality") needed by discrete-variable pixelation based shape synthesis methods.

■ Avoids the uncertainties/arbitrariness related to the discrete-to-continuous conversion process needed in continuous-variable pixelation based shape synthesis methods.

■ Permits the implementation of tolerances (eg. on line widths and on gaps).

■ Can be used with surrogate modelling.

■ Can be used with both gradient-based and evolutionary optimization algorithms.

■ Allows the incorporation of layout constraints through the flexibility afforded for the selection of starting shapes and port locations.

Although the development of the script to implement the new subtractive shaping method is far from trivial, it does not need access to the source code type details of the full-wave CEM analysis implementation used. As long as the CEM implementation permits one (complex a task as it is) to perform CAD-like geometry control, often indeed available in commercial CEM software, it is possible to implement the method. This may encourage the wider use of shape synthesis in the design of RF physical circuit layouts and antennas.

Chapter 5 will demonstrate the successful application of the shape synthesis process.

[95] We acknowledge much assistance from Sonnet Inc. in the implementation of the discrete pixelation approach, using their MM-based CEM software, during the early stages of the work on this thesis.

CHAPTER 5
Application of the Subtractive Shape Synthesis Method to Two-Port Physical Microstrip Circuits

5.1 PRELIMINARY REMARKS

Chapter 3 performed a review of shape synthesis techniques as applied to the design of microwave/RF physical circuits and antennas, in a way that provides a broad view of shape synthesis methods in their present form. It identified characteristics (preferences) that would be beneficial if these could be incorporated into an alternative shape synthesis method. Chapter 4 developed such a new shape synthesis method, that we have called subtractive shape synthesis, and that overcomes the shortcomings of pixelation-based methods. It also described a relatively complex tool (developed as part of this thesis work) that implements this subtractive shape synthesis method, and that is (here in Chapter 5) applied to several shape synthesis examples. The objective function used in the majority of the applications is defined in Section 5.2. The successful application of subtractive shape synthesis is demonstrated in Sections 5.3 through 5.6. Section 5.7 briefly mentions some possible extensions of the subtractive shape synthesis technique. Section 5.8 concludes the chapter.

As indicated in Section 4.6, all full-wave CEM modelling referred to in this chapter was performed using [FEKO 21], which has been shown by droves of authors to provide an accurate analysis of physical microwave circuits that agrees very well with actual measurements. **We do not have the burden in this thesis of confirming this[96].** Section 4.6 also pointed out that the relationships between the individual S-parameters are monitored for the implemented subtractive shape synthesis procedure to ensure accurate full-wave CEM modelling (sufficiently dense mesh for the MM use) and that unwanted radiation is not occurring from the shaped physical circuit geometries. This can thus be assumed for all the results shown.

[96] Experimental validation would validate the accuracy of the full-wave simulations rather than the shape synthesis method itself.

5.2 OBJECTIVE FUNCTIONS BASED ON S-PARAMETER MAGNITUDE PERFORMANCE MASKS

5.2.1 Structuring the Definition of Objective Functions[97] for Physical Circuit Shape Synthesis

> "At present no completely satisfactory rule for selecting decision functions is available, and it is not very likely that one will be found in the foreseeable future. Perhaps all that we can reasonably expect is a rule which, in a somewhat equivocal manner, would delimit a set of 'good' designs for a system".
>
> L.A.Zadeh, "What is optimal?", IRE Transactions on Information Theory, pp.3, March 1958.

Objective functions translating performance requirements into a mathematical function whose minimization will actually give a device with a functionality that is close to what we desire. Although any optimization can only proceed once some form of objective function has been committed to, and as a result much has been written about the topic, precisely how these are defined is highly goal-dependent. The goal in this thesis is that of shape synthesis. It will not be known beforehand whether a particular performance is in fact physically possible for a given starting shape. We do not want to initiate the shape synthesis process and then simply "see how small it can make the particular objective function" and then make qualitative arguments as to how well the shaping has done. We would prefer the objective functions to be so defined that they can easily be set to demand less initially and allow the shaping process to declare success (that is, an objective function that has reached its smallest possible value). Only after such a success do we then want to tighten the performance slightly (by altering the some settings in the objective function) and repeating the shape synthesis, and so on until the objective function setting is reached for which the shaping does not reach a clean success.

5.2.2 S-parameter Performance Masks

In many cases only the magnitudes of the S-parameters are of importance. It is then possible to define the desired S-parameter performance in terms of a set of masks. Examples are shown in Fig.5.2-1 and Fig.5.2-2, where the goals for the required behavior of the network are shown

[97] In the evolutionary optimisation algorithm context the objective function is often called the fitness function, but it needs to be recognised that these are one and the same thing [JOHN 99b]. In some disciplines it is also referred to as the penalty function.

specified in terms of upper and lower masks. It is assumed that the performance of the network can be predicted at two separate sets of frequencies[98] namely $\{f_n\}_{n=1}^{N_{11}}$ and $\{f_k\}_{k=1}^{N_{21}}$, for parameters S_{11} and S_{21}, respectively. The mask-related quantities are defined as follows:

■ $\left[T_{ij}^{UpperMask}(f)\right]_{dB} \le 0$ represents the upper bound on the magnitude of S_{ij}, expressed in dB, at frequency f.

■ $\left[T_{ij}^{LowerMask}(f)\right]_{dB} \le 0$ represents the lower bound on the magnitude of S_{ij}, expressed in dB, at frequency f.

■ $\left[S_{ij}^{actual}(f)\right]_{dB} \le 0$ represents the actual value of the magnitude of S_{ij}, in dB, at frequency f.

■ We emphasize that the magnitudes of the S-parameters, and their upper and lower masks, when defined in deciBels as noted above, will be such that, for the passive circuits of interest in this thesis, we have

$$-\infty < \left[S_{ij}^{actual}(f)\right]_{dB} \le 0 \qquad (5.2\text{-}1a)$$

$$-\infty < \left[T_{ij}^{UpperMask}(f)\right]_{dB} \le 0 \qquad (5.2\text{-}1b)$$

$$-\infty < \left[T_{ij}^{LowerMask}(f)\right]_{dB} \le 0 \qquad (5.2\text{-}1c)$$

[98] Several frequencies in the two sets may be identical, but for notational simplicity we will consider them as two separate sets.

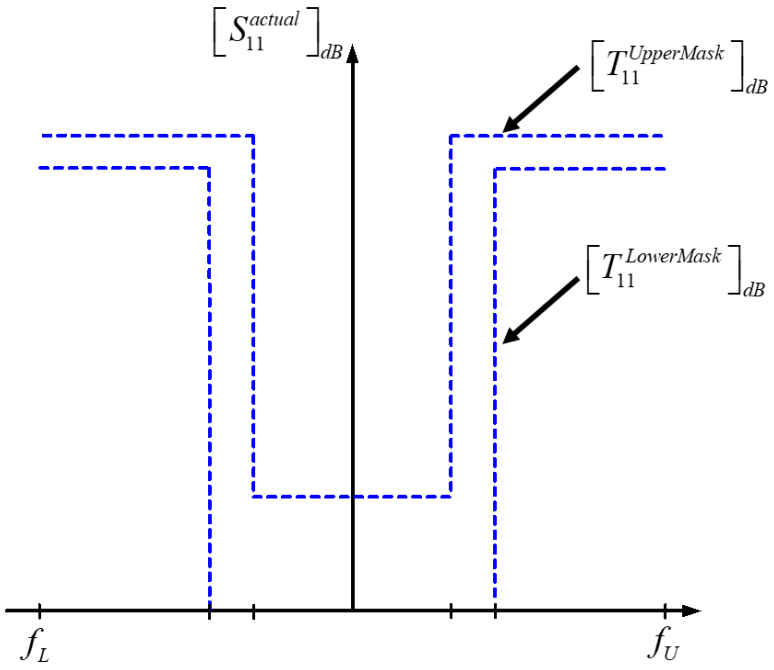

Fig.5.2-1 : Mask for the magnitude of parameter S_{11}.

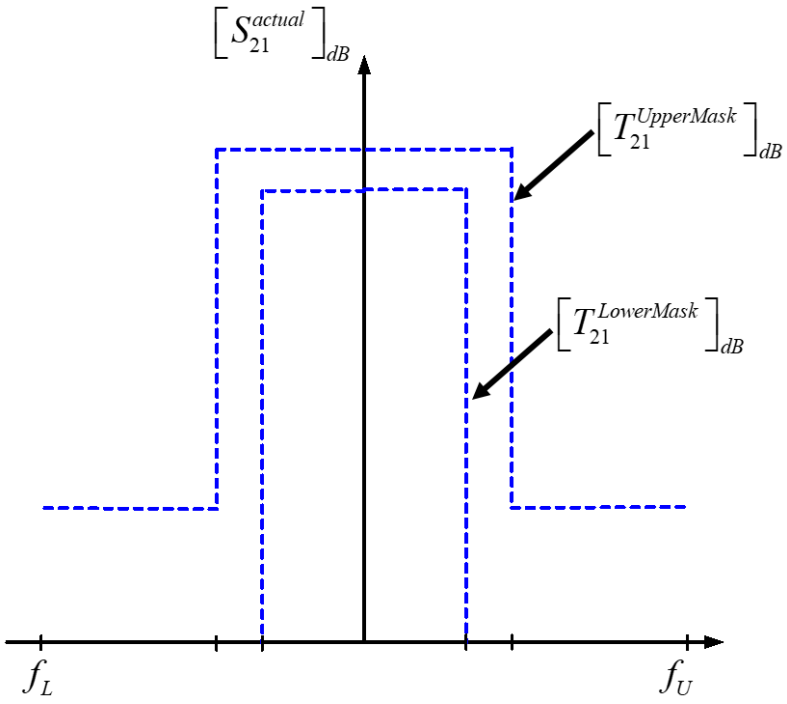

Fig.5.2-2 : Mask for the magnitude of parameter S_{21}.

5.2.3 Objective Function Composed of S-Parameter Magnitude Masks

We next define a number of "error" expressions, in terms of which the objective function will eventually be constructed. We will define them, thereafter explain certain constituent terms, and finally write down the objective function :

A. Error Functions Associated with S_{11}

$n = 1, 2, ..., N_{11}$

$$U_{11}^{(n)} = \begin{cases} \left| \left[S_{11}^{actual}(f_n) \right]_{dB} - \left[T_{11}^{UpperMask}(f_n) \right]_{dB} \right| & if \ \left[S_{11}^{actual}(f_n) \right]_{dB} - \left[T_{11}^{UpperMask}(f_n) \right]_{dB} > Tol_{11}^{U} \\ 0 & if \ \left[S_{11}^{actual}(f_n) \right]_{dB} - \left[T_{11}^{UpperMask}(f_n) \right]_{dB} \le Tol_{11}^{U} \end{cases}$$

(5.2-2)

$$L_{11}^{(n)} = \begin{cases} \left| \left[S_{11}^{actual}(f_n) \right]_{dB} - \left[T_{11}^{LowerMask}(f_n) \right]_{dB} \right| & if \ \left[S_{11}^{actual}(f_n) \right]_{dB} - \left[T_{11}^{LowerMask}(f_n) \right]_{dB} < -Tol_{11}^{L} \\ 0 & if \ \left[S_{11}^{actual}(f_n) \right]_{dB} - \left[T_{11}^{LowerMask}(f_n) \right]_{dB} \ge -Tol_{11}^{L} \end{cases}$$

(5.2-3)

B. Error Functions Associated with S_{21}

$k = 1, 2, ..., N_{21}$

$$U_{21}^{(k)} = \begin{cases} \left| \left[S_{21}^{actual}(f_k) \right]_{dB} - \left[T_{21}^{UpperMask}(f_k) \right]_{dB} \right| & if \ \left[S_{21}^{actual}(f_k) \right]_{dB} - \left[T_{21}^{UpperMask}(f_k) \right]_{dB} > Tol_{21}^{U} \\ 0 & if \ \left[S_{21}^{actual}(f_k) \right]_{dB} - \left[T_{21}^{UpperMask}(f_k) \right]_{dB} \le Tol_{21}^{U} \end{cases}$$

(5.2-4)

$$L_{21}^{(k)} = \begin{cases} \left| \left[S_{21}^{actual}(f_k) \right]_{dB} - \left[T_{21}^{LowerMask}(f_k) \right]_{dB} \right| & if \ \left[S_{21}^{actual}(f_k) \right]_{dB} - \left[T_{21}^{LowerMask}(f_k) \right]_{dB} < -Tol_{21}^{L} \\ 0 & if \ \left[S_{21}^{actual}(f_k) \right]_{dB} - \left[T_{21}^{LowerMask}(f_k) \right]_{dB} \ge -Tol_{21}^{L} \end{cases}$$

(5.2-5)

C. Motivations for the Form of the Error Expressions

The quantity Tol_{ij}^{U} is a positive dB value, by which the actual S_{ij} magnitude may go above the upper mask, whereas Tol_{ij}^{L} is a positive dB value by which it may go below the lower mask, and still be acceptable. It may be set to zero if preferred. However, sometimes we may terminate the shaping process (eg. when it has stagnated) but observe from the current shaped circuit that it almost satisfies the performance mask. In such cases, having quantities Tol_{ij}^{U} and Tol_{ij}^{L} present in F_{obj} allows one to allow some "margin" and re-run the shaping process.

D. Construction of the Objective Function

We can combine the individual terms in a 'sum-of-squares of the errors terms' sense

$$F_{mag} = \frac{\mathrm{w}}{2N_{11}} \sum_{n=1}^{N_{11}} \sqrt{[U_{11}^{(n)}]^2 + [L_{11}^{(n)}]^2} + \frac{(1-\mathrm{w})}{2N_{21}} \sum_{k=1}^{N_{21}} \sqrt{[U_{21}^{(k)}]^2 + [L_{21}^{(k)}]^2} \qquad (5.2\text{-}6)$$

or a 'largest of the error terms sense' as

$$F_{mag} = \mathrm{w} \max_{n=1,2,\ldots} \left\{ U_{11}^{(n)}, L_{11}^{(n)} \right\} + (1-\mathrm{w}) \max_{k=1,2,\ldots} \left\{ U_{21}^{(k)}, L_{21}^{(k)} \right\} \qquad (5.2\text{-}7)$$

with the weight factor $0 \le \mathrm{w} \le 1$. Observe that with $\mathrm{w} = 0$ the mask for the magnitude of S_{11} is ignored, whereas for $\mathrm{w} = 1$ the mask for the magnitude of S_{21} is ignored. Other values of the weight factor place more or less emphasis on one S-parameter or the other[99].

The objective function can then be defined as

$$F_{\text{obj}} = F_{mag} \qquad 0 \le F_{obj} \le \infty \qquad (5.2\text{-}8)$$

or

$$F_{obj} = 1 - \left(\frac{1}{1 + F_{mag}} \right) \qquad 0 \le F_{obj} \le 1 \qquad (5.2\text{-}9)$$

[99] The weight factors can be used to prioritize multiple goals.

E. Further Comments

It is important to recognize that the magnitude masks shown for illustrative purposes in Fig.5.2-1 and Fig.5.2-2 are not the only possibilities. In other words, they need not have the "bandpass" filter form shown, but could be of "bandstop form". The individual sections of the mask need not be horizontal, but of more general form. Furthermore, what has been done for the magnitude of S_{ij} could similarly be done for its phase, and the masks for magnitude $\left|S_{ij}(f)\right|$ and phase $\angle S_{ij}(f)$ need not be the same.

5.3 THE SHAPE SYNTHESIS OF A MATCHING NETWORK USING RECTANGULAR SUBTRACTIVE ELEMENTS

5.3.1 Matching Network with In-Line Ports

As a first application of the proposed subtractive shape synthesis method we consider a transformer to match a $Z_{01}=50\Omega$ ($t_1=4.84\,\text{mm}$) microstrip line to a $Z_{02}=100\Omega$ ($t_2=1.40\,\text{mm}$) line, on a substrate of height 1.575 mm and $\varepsilon_r=2.2$. This is illustrated in Fig.5.3-1, which shows the two lines, plus a starting shape (the "variable" portion) located between these two lines with $b=18.393\,\text{mm}$ and $h=10\,\text{mm}$. We understand that a classical quarter-wave transformer would be used in such a case, but the purpose here is to investigate whether the shape synthesis is able to provide a solution, and will accept the fact that it might not provide precisely the same solutions as the classical quarter-wave transformer.

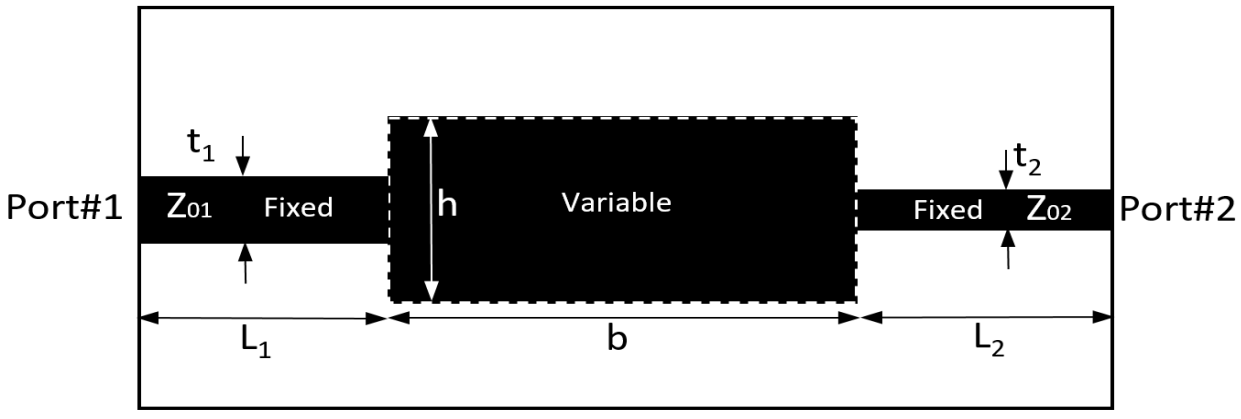

Fig.5.3-1 : $Z_{01}=50\Omega$ **microstrip line (left) and** $Z_{02}=100\Omega$ **line (right) separated by a rectangular starting shape of length** b **and height** h**.**

We use a single subtractive rectangle with designator $[H_n, W_n, x_n, y_n]$, and allow all four quantities (centre-point, height and width) to vary; there are thus four degrees of freedom. Top/down symmetry is assumed, and so there is an image subtractive rectangle as well, but this does not of course add any further degrees of freedom. The smallest width allowed for any conducting track is 0.1mm (i.e. it must be greater than 0.1mm, or not exist at all). The shape synthesized transformers that result can be described by the diagram in Fig.5.3-2. The geometry outcomes of the shaping process are summarized in Table 5.3, and the computed transformer performance (namely S_{11}) in Fig.5.3-3.

Fig.5.3-3 shows the computed[100] $|S_{11}|$ performance of the shape synthesized physical circuit for upper masks[101] whose in-band (2.755 – 3.245 GHz) levels are -18dB, -21dB and -25dB (with the out-of-band level set at -10dB[102]). We notice from Table 5.3 that the shape of the first two cases retains a narrow stub at the Port#1 end, whereas for the -25dB case it does not[103]. We further observe that as the in-band level of the lower mask decreases to -25dB, the $|S_{11}|$ performance also becomes more centered around the center frequency (3 GHz). The above results demonstrate how slight changes in F_{obj} result in changes in the performance of the shape synthesized physical circuits. Fig.5.3-3(d) compares the performance of the shape synthesized network with that of a classical quarter-wave transformer (without any feature optimization).

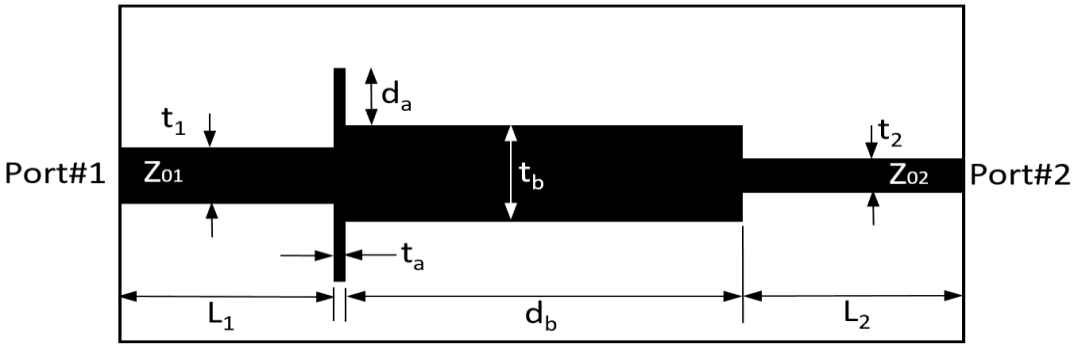

Fig 5.3-2 : Shaped matching network geometry

[100] The computed results shown in the thesis will always be that using a mesh that is sufficiently fine to give a converged result.
[101] There is no lower mask needed for this particular "matching" problem.
[102] The results obtained when this level is set to 0dB are almost identical to those obtained here.
[103] In that case the shaped geometry is that of a classical quarter-wave transformer, with dimensions of the quarter-wave line automatically adjusted by the shape synthesis procedure to account for the step discontinuities. By assigning only 4 degrees of freedom to this application of the subtractive shape synthesis method we have restricted the size of the design space accessible to the method, and so it has presented a design close to the traditional one. This will not be so in the examples to follow.

Table 5.3 : Dimensions of the shape-synthesized transformer when different lower mask levels are used.

In-Band Level of Upper Mask / Relevant Figure	t_a	d_a	t_b	d_b
-18.5 dB / Fig.5.3-3(a)	0.13 mm	1.47 mm	3.53 mm	18.26 mm
-21.0 dB / Fig.5.3-3(b)	0.10 mm	1.78 mm	3.22 mm	18.29 mm
-25.0 dB / Fig.5.3-3(c)	0.0 mm	0.0 mm	3.37 mm	18.39 mm

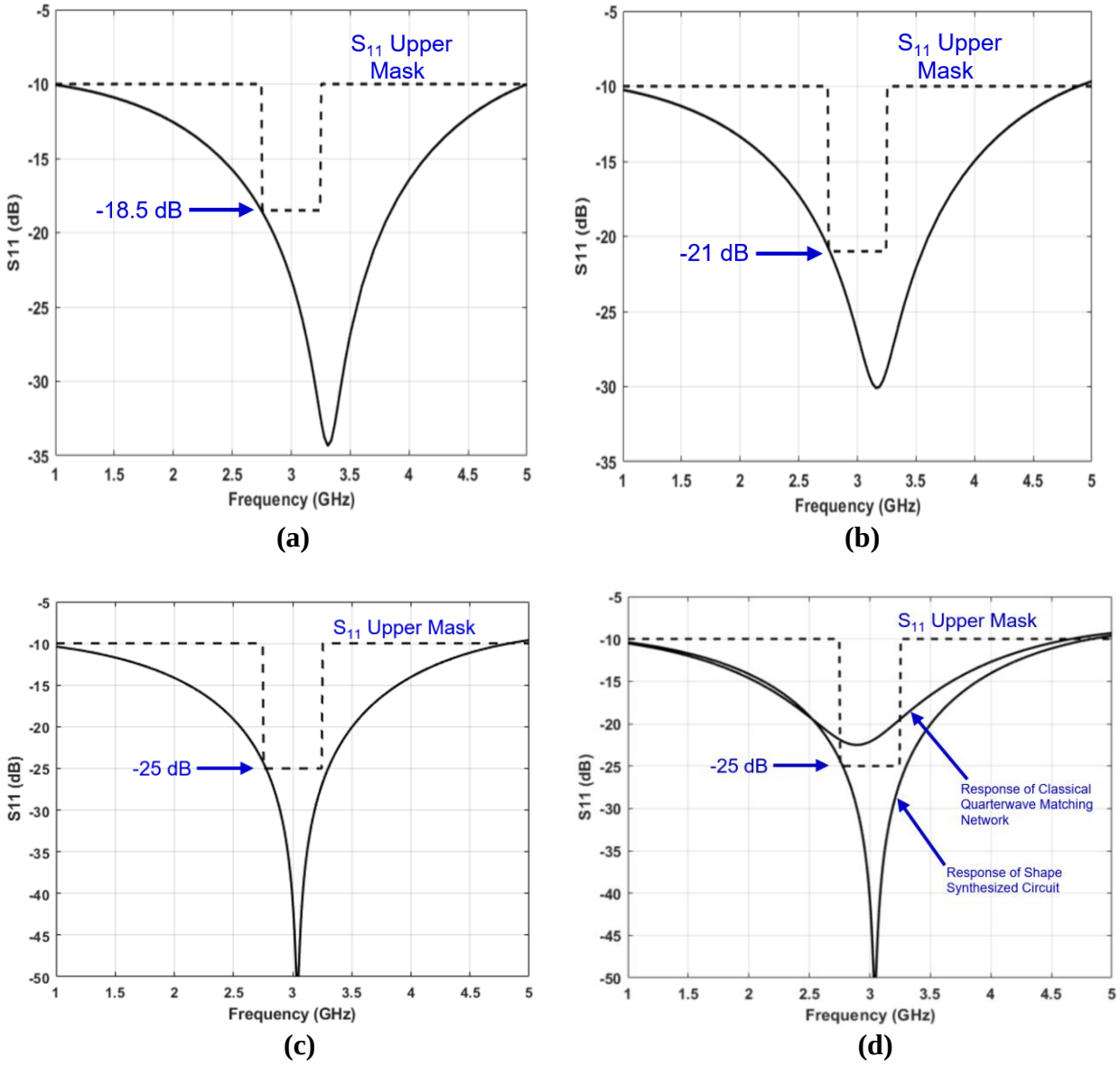

Fig.5.3-3 : Computed S11 magnitude performance for specified in-band mask levels of (a). -18.5 dB, (b). -21.0 dB and (c). -25.0 dB. The performance of a classical quarter-wave transformer is shown in (d).

5.3.2 Matching Network with In-Line Ports & Response Notch

In this problem we wish to shape synthesize a matching network between the same two $Z_{01} = 50\Omega$ and $Z_{02} = 100\Omega$ microstrip lines, on the same substrate, and using the same size starting shape, as in Section 5.3.1. However, in this case we desire $|S_{11}| < -21\text{dB}$ over the band 2.755 – 3.245 GHz, and in addition require a notch at 7 GHz where $|S_{21}| < -25\,\text{dB}$. We use three subtractive rectangles with designators $[H_n, W_n, x_n, y_n]$, $n = 1,2,3$ without any geometrical symmetry enforced. There are thus 12 degrees of freedom.

The resulting shape synthesized geometry is shown in Fig.5.3-4. It is clearly not a geometry that would arise if a traditional design approach had been used; such an approach would have typically cascaded a classical quarter-wave transformer and a notch filter. The subtractive shape synthesis has provided the required performance (shown in Fig. 5.3-5) in a single device of the same length as the classical quarter-wave transformer, albeit wider. The notch is not centered at 7 GHz; the $|S_{21}|$ mask simply stipulated what the level must be (-25 dB) at 7 GHz and this has been obtained.

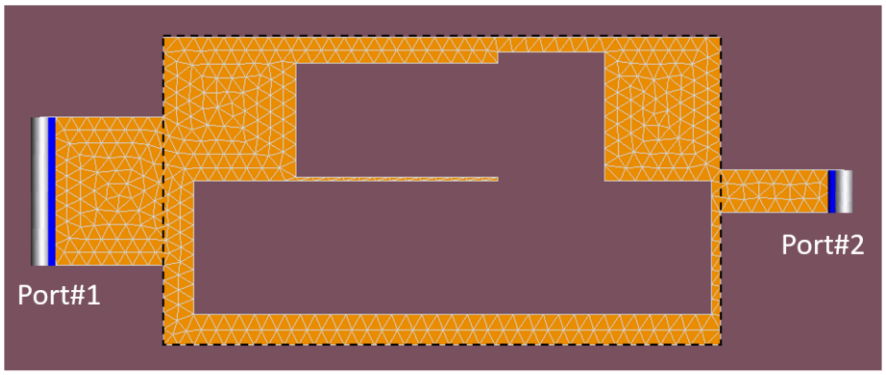

Fig 5.3-4 : Shaped "matching network + notch" geometry. The dashed line is the perimeter of the starting shape.

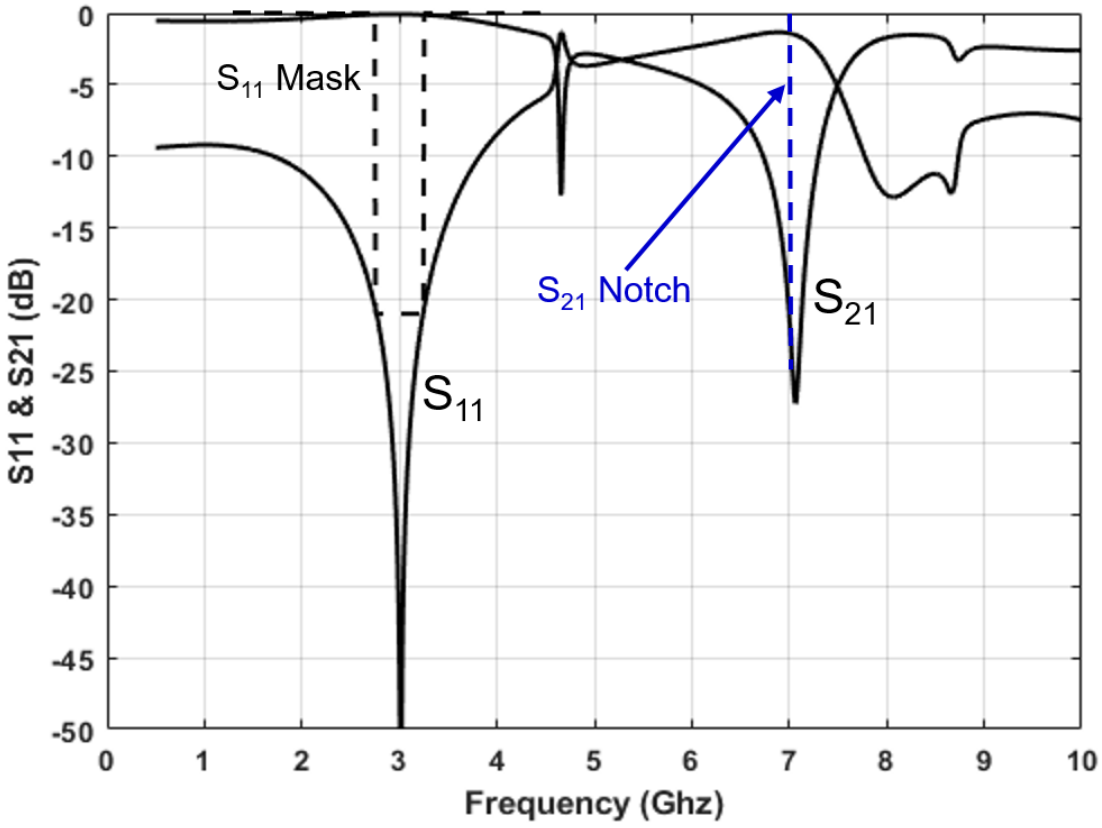

Fig.5.3-5 : Computed S_{11} and S_{21} magnitude performance for "matching network + notch" shape synthesised geometry in Fig.5.3-4.

5.3.3 Matching Network with Ports at 90° Relative With Respect to Each Other & Response Notch

In this problem we wish to shape synthesize a matching network between the same two $Z_{01} = 50\Omega$ and $Z_{02} = 100\Omega$ microstrip lines, on the same substrate. We desire $|S_{11}| < -21\,\text{dB}$ over the band 2.755 – 3.245 GHz, and in addition require a notch at 7 GHz where $|S_{21}| < -25\,\text{dB}$. What is different here is that the two ports are not in-line but are required to be at 90° with respect to each other (eg. perhaps arising to accommodate layout constraints), as shown in the starting shape in Fig.5.3-6, which has $b = 18.393\,\text{mm}$, $h = 10\,\text{mm}$ and $L_3 = 4.998\,\text{mm}$. We use four subtractive rectangles with designators $[H_n, W_n, x_n, y_n]$, $n = 1,2,3,4$ without any geometrical symmetry enforced. There are thus 16 degrees of freedom.

A traditional design approach might have cascaded a classical quarter-wave transformer, a notch filter and a mitred bend, and then used feature optimization for fine-tuning. The shape synthesized geometry shown in Fig.5.3-7 is once more unconventional, and has been found in a design space wider than that available in traditional design. The subtractive shape synthesis has provided the required performance (shown in Fig. 5.3-8) in a single exercise. Once again, the notch is not centered at 7 GHz (in fact now shifted in the opposite direction to that in Fig.5.3-5); the $|S_{21}|$ mask simply stipulated what the level must be (-25 dB) at 7 GHz and this has been obtained.

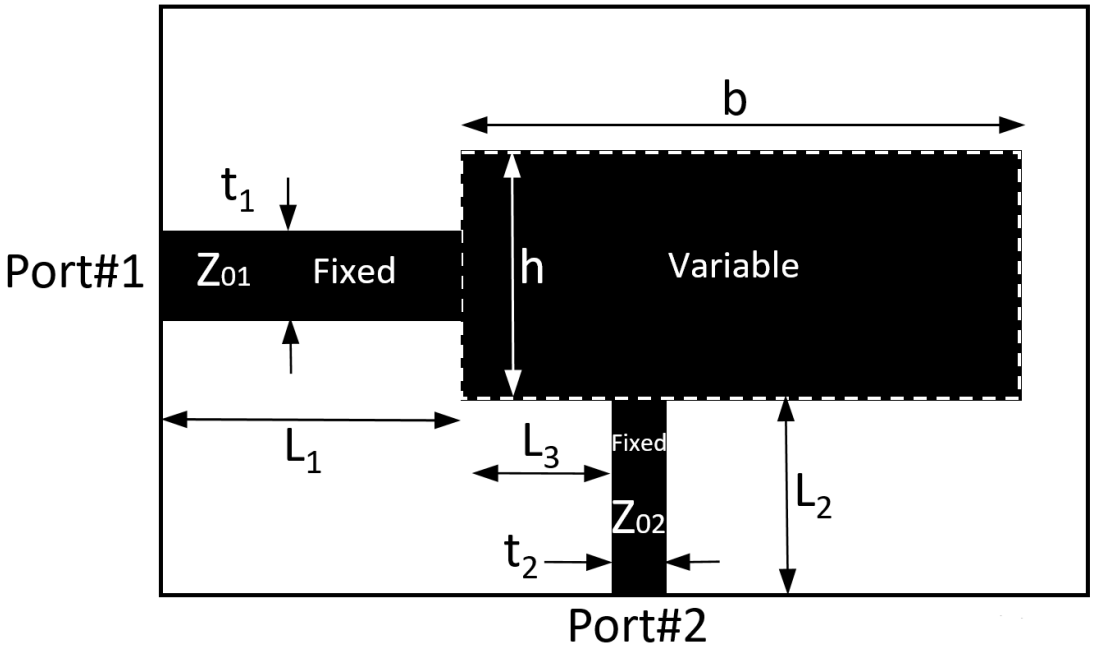

Fig.5.3-6 : $Z_{01} = 50\Omega$ **microstrip line (left) and** $Z_{02} = 100\Omega$ **line (right) separated by a rectangular starting shape of length** b **and height** h**.**

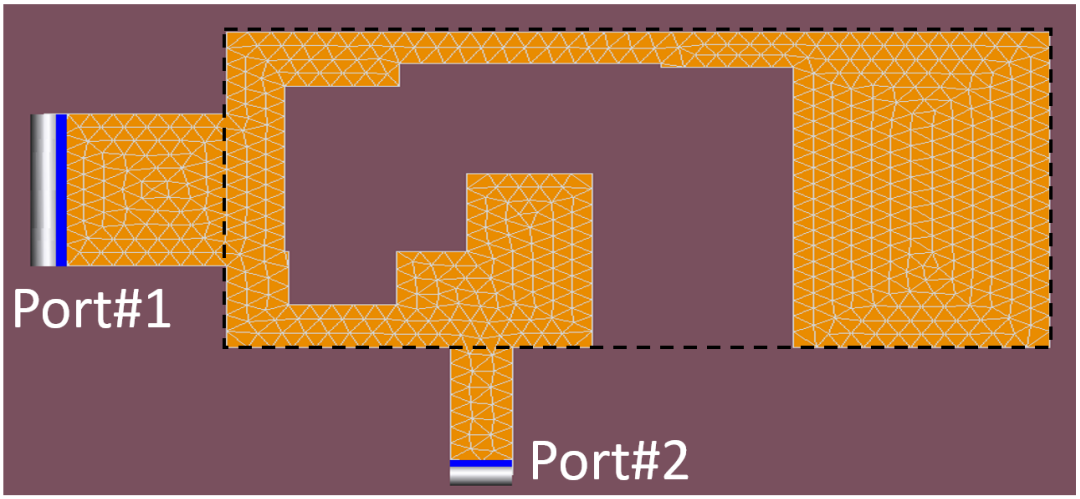

Fig 5.3-7 : Shape synthesized "matching network + notch" geometry on a 90° bend. The dashed line is the perimeter of the starting shape.

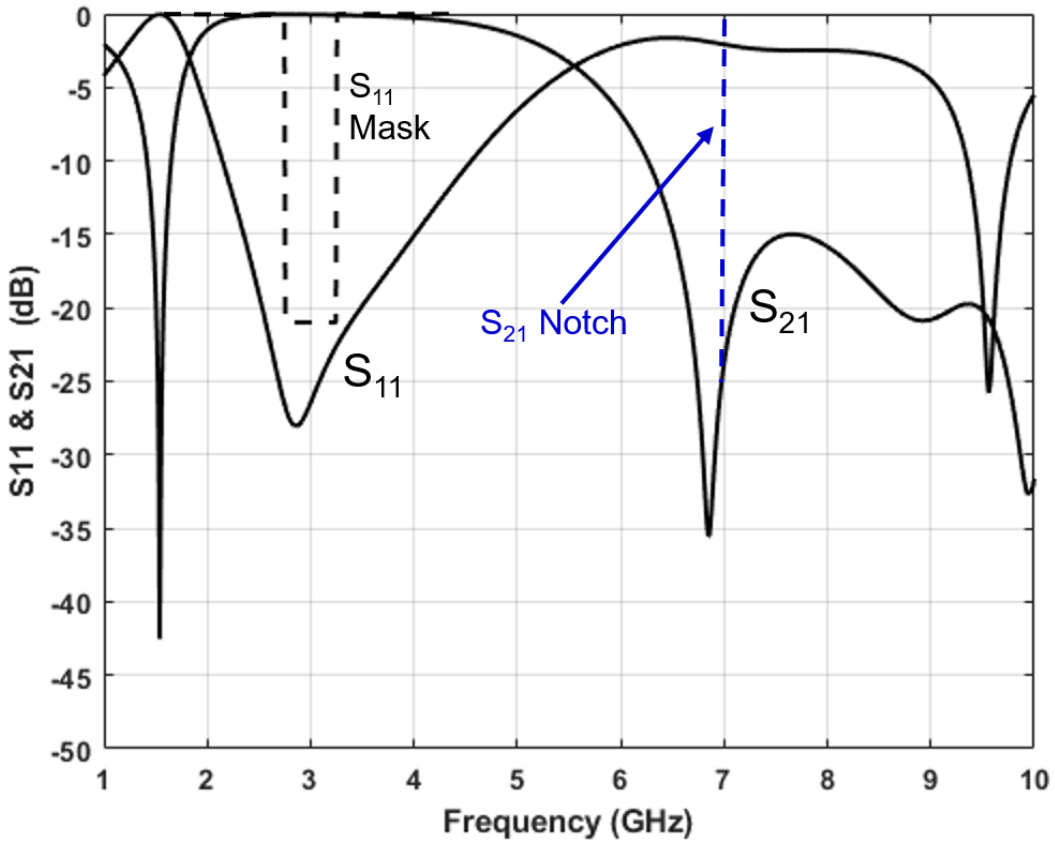

Fig.5.3-8 : Computed S_{11} and S_{21} magnitude performance for "matching network + notch" on a bend (the shape synthesized geometry shown in Fig.5.3-7).

5.4 THE SHAPE SYNTHESIS OF A BANDSTOP FILTER USING RECTANGULAR SUBTRACTIVE ELEMENTS

5.4.1 Traditional ("Feature Optimised") Design

We used a classical procedure to design a bandstop filter using a three quarter–wave open-circuit stubs geometry, with a 2 GHz centre frequency, and 20% bandwidth. The procedure used was that given in [POZA 90]. The microstrip layout of the filter is shown in Fig.5.4-1[104]. The ports consist of microstrip lines with $Z_o = 50\Omega$ at the centre frequency, and uses a dielectric substrate with ε_r = 2.2 and thickness h = 1.27 mm. The computed insertion loss $|S_{21}|$ and return loss $|S_{11}|$ of the bandstop filter over frequency is plotted in Fig.5.4-2, the dimensions of the "paper design" having been adjusted using traditional feature optimisation. Also drawn in, in Fig.5.4-2, are upper and lower masks simply to show what masks are indeed "satisfied" by the filter response. These will be used in all the shape synthesis applications described in this Section 5.4.

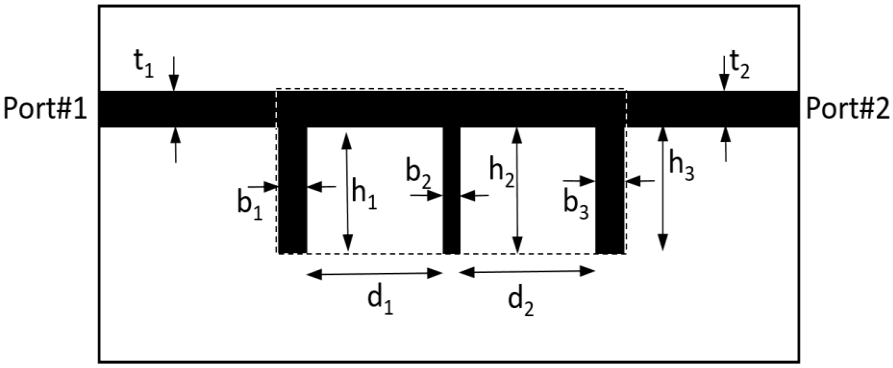

Fig.5.4-1: Microstrip bandstop filter designed using traditional methods. The dimensions are $b_1 = b_3 = 1.628\,\text{mm}$, $b_2 = 0.7008\,\text{mm}$, and $h_1 = h_2 = h_3 = 26.2\,\text{mm}$, $d_1 = d_2 = 24.71\,\text{mm}$ and $t_1 = t_2 = 3.605\,\text{mm}$.

[104] The dashed lines are for later reference and can be ignored for now.

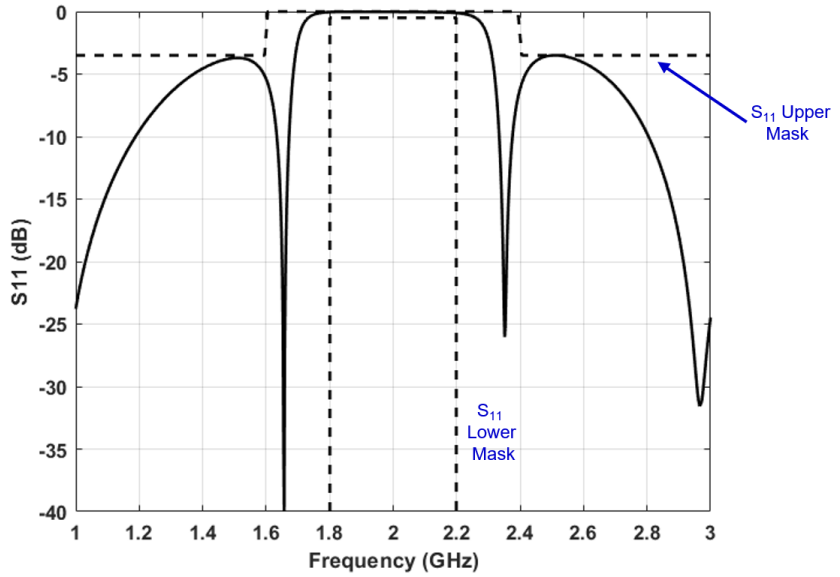

(a)

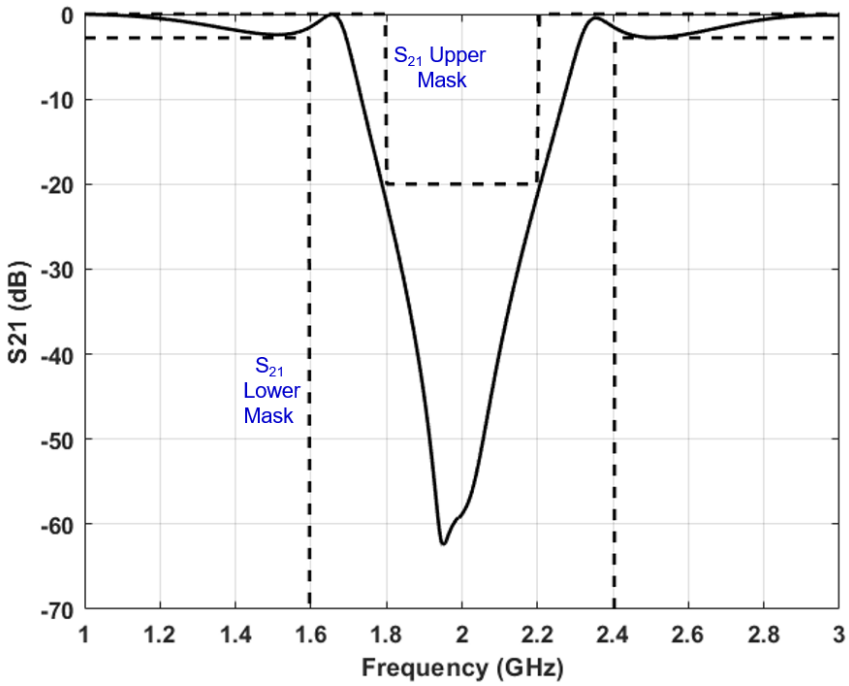

(b)

Fig.5.4-2: Plots of the computed (a) S_{11} magnitude and (b) S_{21} magnitude versus frequency for the microstrip bandstop filter (designed by traditional means) in Fig.5.4-1.

5.4.2 Bandstop Filter Design Using Subtractive Shape Synthesis

With reference to Fig.5.4-3, the fixed portions have $t_1 = t_2 = 3.605\,\text{mm}$ and feedline lengths $L_1 = L_2 = 23.645\,\text{mm}$. The starting shape is of rectangular cross section, indeed the entire region within the dashed lines in Fig.5.4-1, so that $h = 29.8\,\text{mm}$ and $b = 53.3\,\text{mm}$.

The objective function is that in expression (5.2-6), using the upper and lower magnitude masks shown in Fig.5.4-2. The GA was selected as the optimization algorithm, with crossover rate of 0.8, adaptive mutation, a population size of 100 and a tournament selection function. We use four subtractive rectangles with designators $[[H_n, W_n, x_n, y_n]]$, $n = 1, 2, 3, 4$, and thus there are 16 degrees of freedom. Left/right symmetry is enforced, and so there are four image rectangles as well. The constraints used $t_{\min} = g_{\min} = 0.5\text{mm}$.

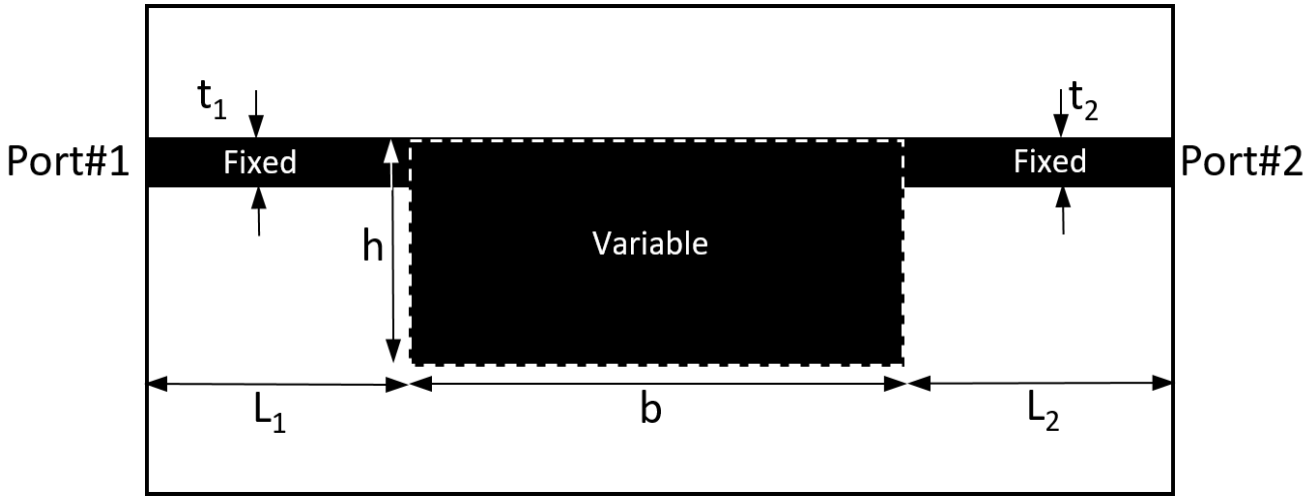

Fig.5.4-3: Diagram showing the fixed and variable (shape-able) portions of the starting geometry for subtractive shape synthesis of the bandstop filter.

The shape synthesized bandstop filter geometry, after 100 iterations, is that in Fig.5.4-4. It is vastly different from that in Fig.5.4-1; it is clear that the design space utilized is not the same. The computed S-parameter performance given in Fig.5.4-5 and Fig.5.4-6.

At the beginning of each shape synthesis run, unless otherwise specified, the GA randomly generates initial values for the degrees of freedom quantities (that is, the designator quantities). In obtaining the shape Fig.5.4-4 this was left up to the GA. The subtractive shape synthesis was then re-run with the same starting shape, but it was once more left up to the GA to generate the

above-mentioned initial values. Since these initial values are generated randomly, for the second run they would have been different. The shaped geometry is now that shown in Fig.5.4-7, which is completely different from the first version in Fig.5.4-4. Although the S-parameter performance of the physical circuit Fig.5.4-7 satisfies the required masks, as evidenced in Fig.5.4-8 and Fig.5.4-9, the response of the two physical circuits are not completely identical. It confirms that many different physical circuits may satisfy a given set of specifications, as previously observed in Section 2.10.

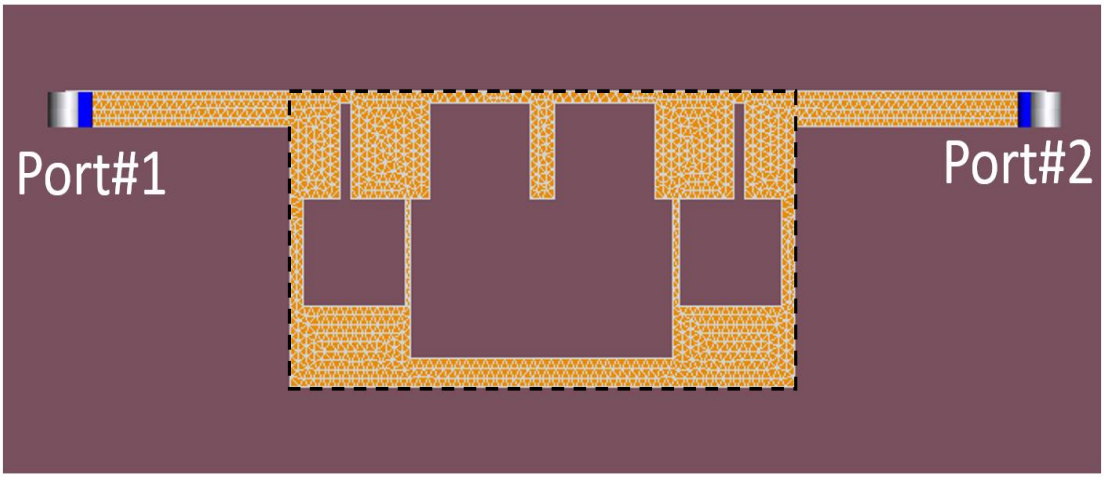

Fig 5.4-4 : Shape synthesized bandstop filter geometry : First version. The dashed line is the perimeter of the starting shape.

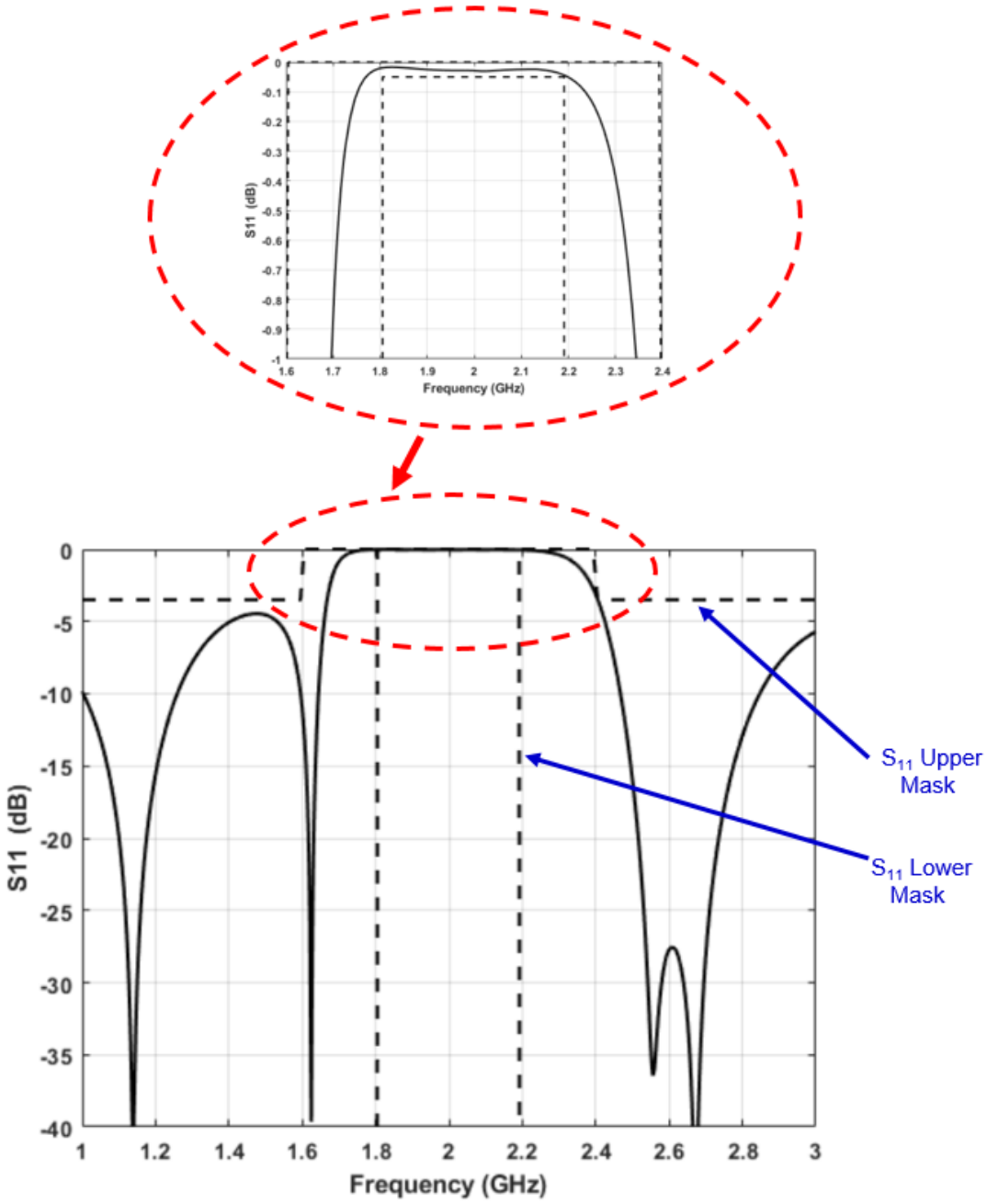

Fig.5.4-5: Computed $|S_{11}|$ of the shape synthesized microstrip bandstop filter shown in Fig.5.4-4.

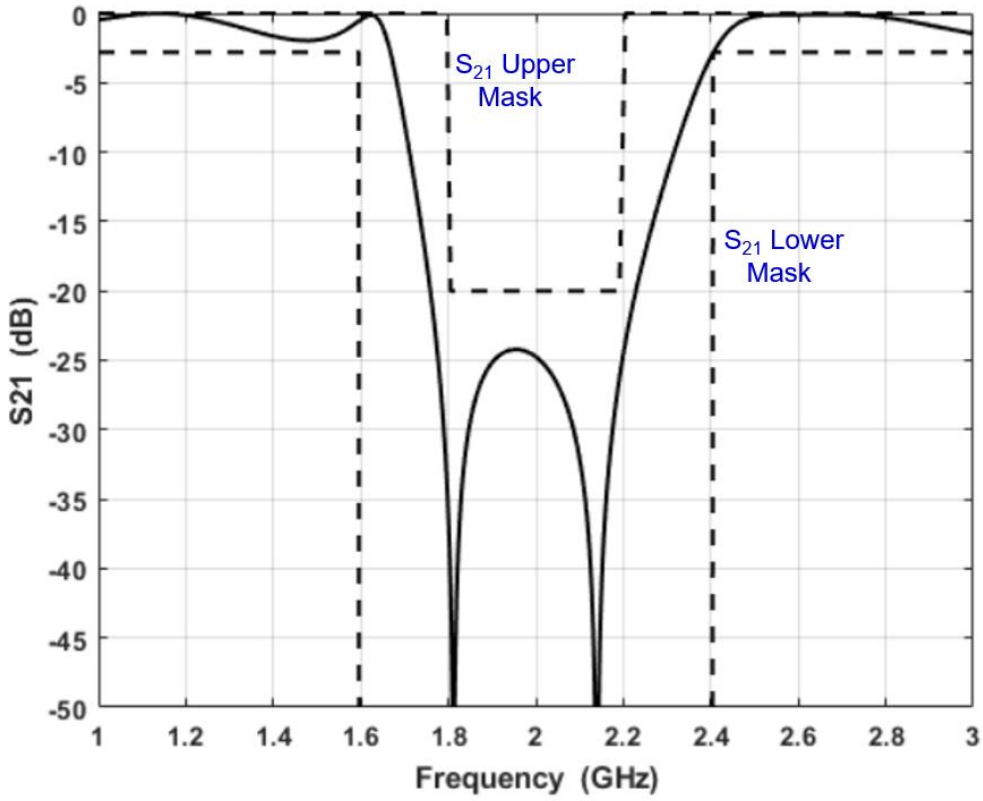

Fig.5.4-6: Computed $|S_{21}|$ of the shape synthesized microstrip bandstop filter shown in Fig.5.4-4.

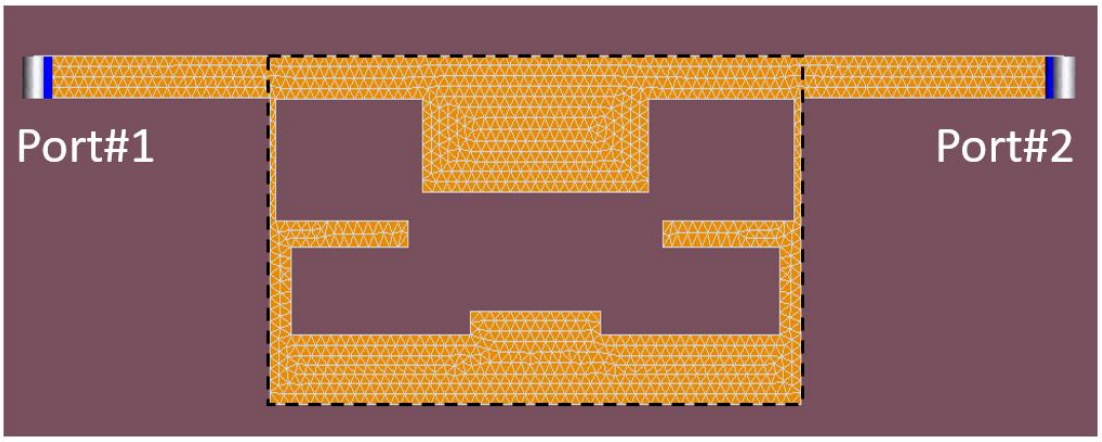

Fig 5.4-7 : Shape synthesized bandstop filter geometry : Second version. The dashed line is the perimeter of the starting shape.

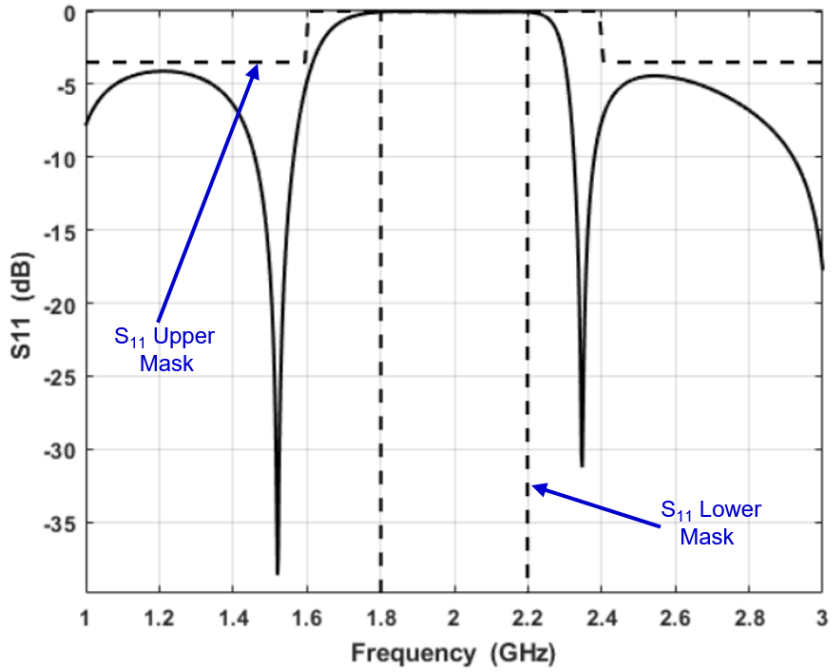

Fig.5.4-8: Computed $|S_{11}|$ of the shape synthesized microstrip bandstop filter shown in Fig.5.4-7.

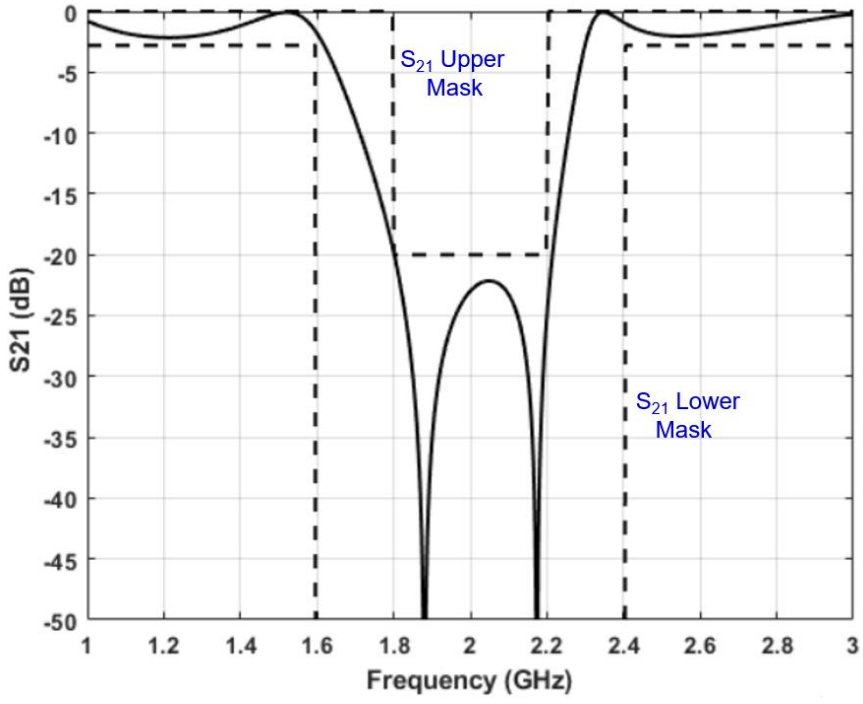

Fig.5.4-9: Computed $|S_{21}|$ of the shape synthesized microstrip bandstop filter shown in Fig.5.4-7.

5.4.3 Bandstop Filter Design Using Subtractive Shape Synthesis & Reduced Starting Shape Size

A comment overheard being made about physical circuit layouts, in an online conference session, by an RF engineer working in the wireless industry, was “we are always trying to shrink it down”. There are no general definitions of what engineers mean by the “compact” or “miniaturized”, and even less so for the inflated term “ultra-compact” that has also been used in the literature. One unambiguous way of clarifying the term “miniaturized” is to take a conventional physical circuit layout that provides a response that is considered desirable, and define this as the reference footprint. If we are able, using the same guiding medium, to obtain a similar S-parameter response using a circuit with a smaller footprint, we can then claim some miniaturization has been achieved.

The subtractive shape synthesis problem described in Section 5.4.2 was repeated with all parameters the same except that the starting shape dimension b in Fig.5.4-3 was reduced by 25% to $b = 40\,\text{mm}$. The shape synthesized resulting geometry (which may be called a compact one) is shown in Fig.5.4-10. Fig.5.4-11 and Fig.5.4-12 confirm that the S-parameter performance masks are satisfied, but once again the details of the responses are not everywhere identical to those of the non-compact shape synthesized bandstop filters in Section 5.4.2. We note that the traditional design procedure mentioned in Section 5.4.1 could not have been used to design such a compact version of the bandstop filter; the subtractive shape synthesis method was able to automatically provide such a design by utilizing a part of the design space inaccessible by traditional design methods. Yet portions of the geometry in Fig.5.4-10 are reminiscent of the long narrow stubs in conventional designs (albeit more complex, and unusually located in the circuit layout) that have emerged quite naturally from the shape synthesis process.

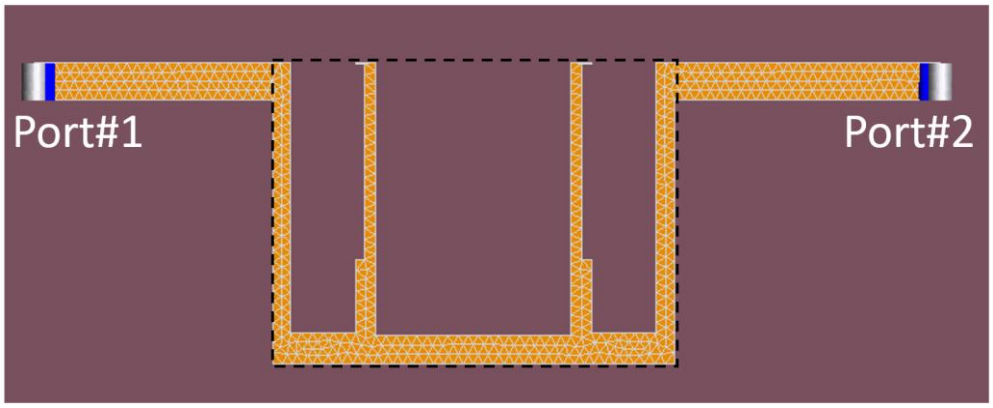

Fig 5.4-10 : Shape synthesized bandstop filter geometry for reduced-size starting shape. The dashed line is the perimeter of the starting shape.

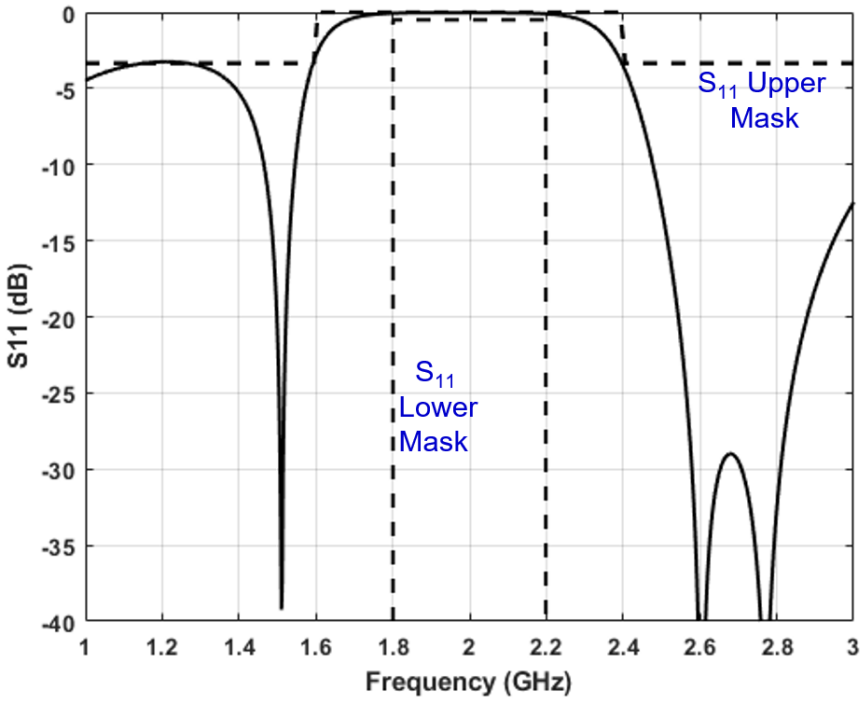

Fig.5.4-11: Computed $|S_{11}|$ of the shape synthesized microstrip bandstop filter shown in Fig.5.4-10.

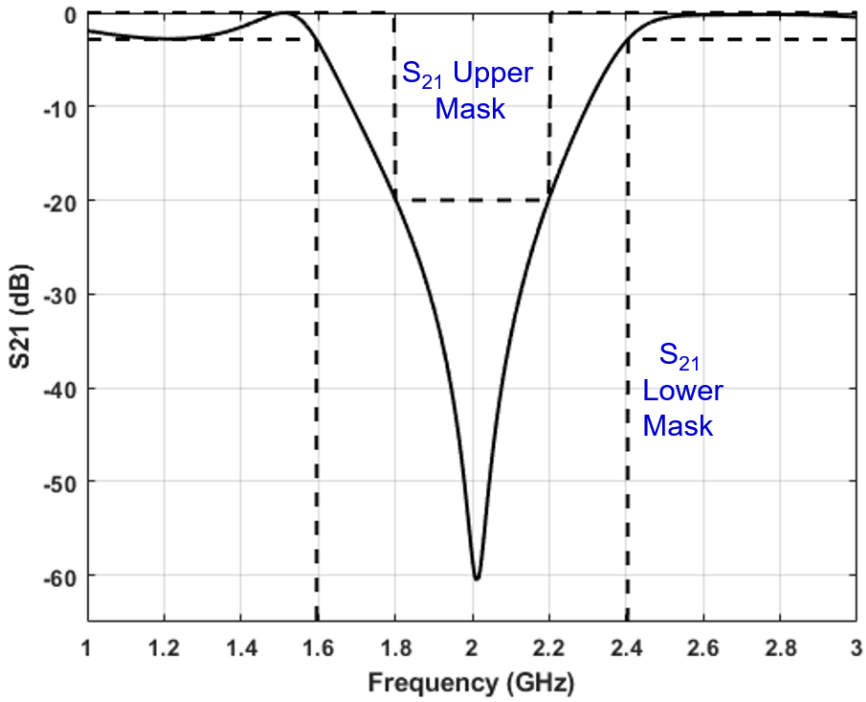

Fig.5.4-12: Computed $|S_{21}|$ of the shape synthesized microstrip bandstop filter shown in Fig.5.4-11.

5.5 THE SHAPE SYNTHESIS OF A BANDSTOP FILTER USING BOTH RECTANGULAR AND ELLIPTICAL SUBTRACTIVE ELEMENTS

5.5.1 Bandstop Filter Design Using Subtractive Shape Synthesis : Port Configuration#1

The subtractive shape synthesis problem described in Section 5.4.2 was repeated with all parameters the same except that non-rectangular subtractive shapes[105] were also used. We use two subtractive rectangles (8 degrees of freedom), two subtractive elliptical shapes (8 degrees of freedom) and a single subtractive circle (3 degrees of freedom), leading to a total of 19 degrees of freedom. Left/right symmetry is enforced, and so there are the same number of image subtractive shapes as well.

The resulting shape synthesized geometry is shown in Fig.5.5-1. Its performance, shown in Fig.5.5-2 and Fig.5.5-3, satisfies the S-parameter masks, and is in fact similar to that obtained in Section 5.4.2 for the other physical circuit geometries "discovered" by the shape synthesis process, except in the details.

[105] As described in Section 4.4.

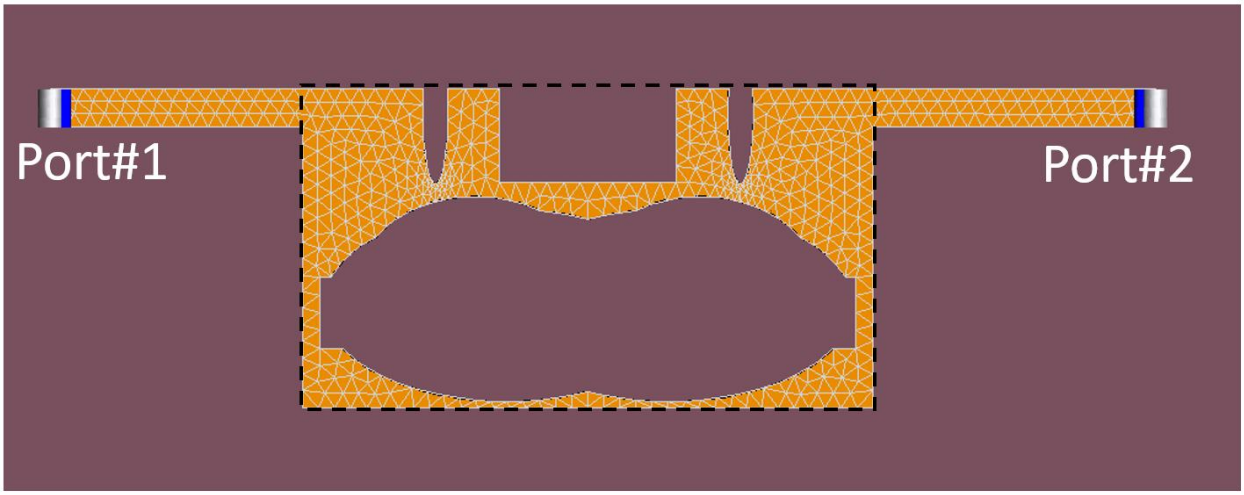

Fig 5.5-1 : Bandstop filter shape synthesized using rectangular and elliptical subtractive elements : First version. The dashed line is the perimeter of the starting shape.

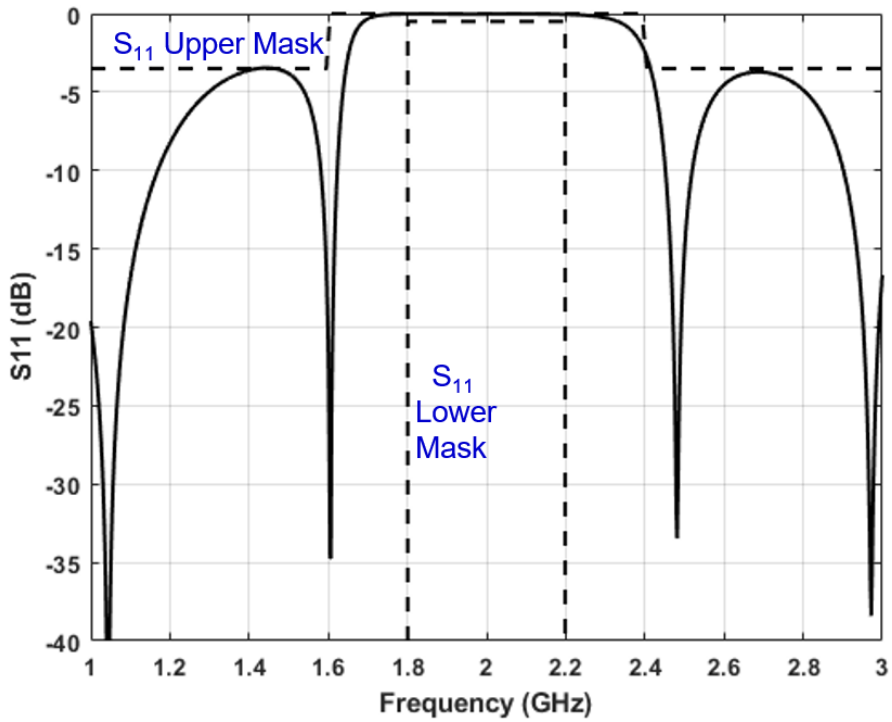

Fig.5.5-2: Computed $|S_{11}|$ of the shape synthesized microstrip bandstop filter shown in Fig.5.5-1.

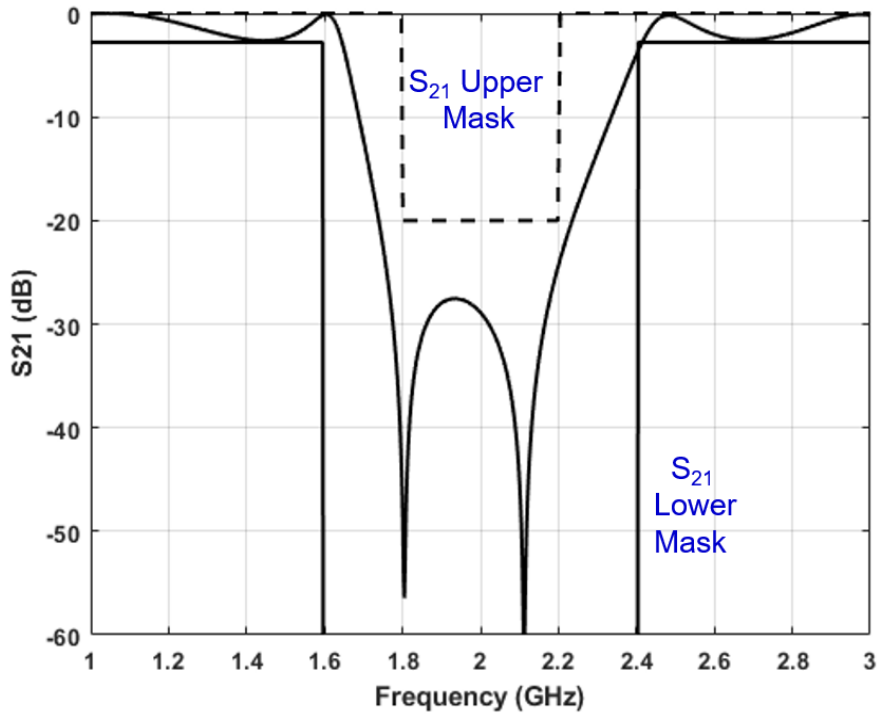

Fig.5.5-3: Computed $|S_{21}|$ of the shape synthesized microstrip bandstop filter shown in Fig.5.5-1.

5.5.2 Bandstop Filter Design Using Subtractive Shape Synthesis : Port Configuration#2

The subtractive shape synthesis problem described in Section 5.5.1 was next repeated with the same S-parameter masks, the same subtractive elements, and with left/right symmetry, so that there remain 19 degrees of freedom. However, the port locations were considered shifted, with the starting shape now that shown in Fig.5.5-4, but with the same *b* and *h* values as in Section 5.4.2 (and hence Section 5.5.1). The resulting shape synthesized geometry is now that shown shown in Fig.5.5-5. Its performance, shown in Fig.5.5-6 and Fig.5.5-7 satisfies the S-parameter masks. The traditional design procedure mentioned in Section 5.4.1 could not have been used to design a bandstop filter with the ports in the position shown, and some type of bend would be needed to position the ports in the location shown. The subtractive shape synthesis method was able automatically provide such a design by accessing a wider design space.

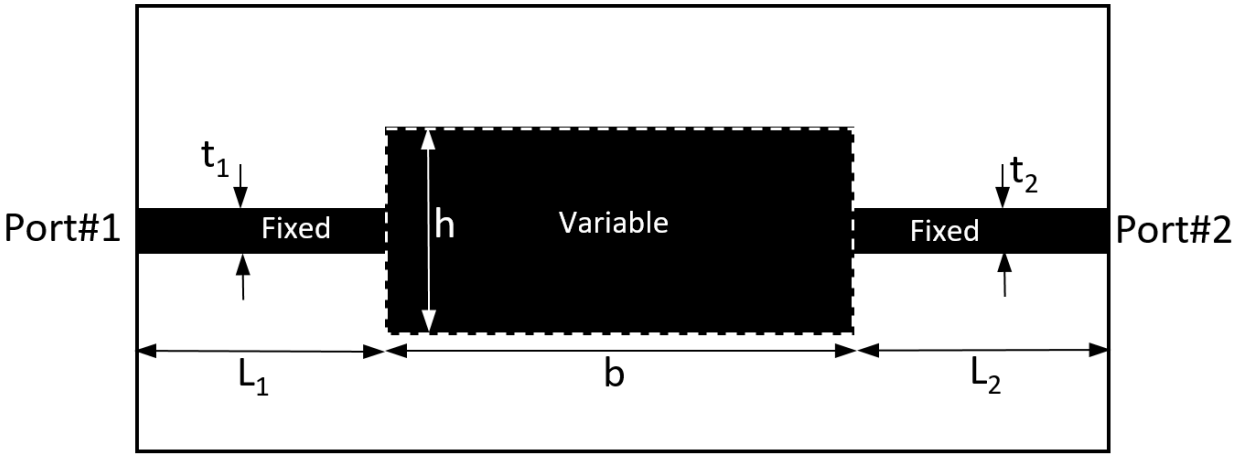

Fig.5.5-4: Diagram showing the fixed and variable (shape-able) portions of the starting geometry for subtractive shape synthesis of the bandstop filter with shifted ports.

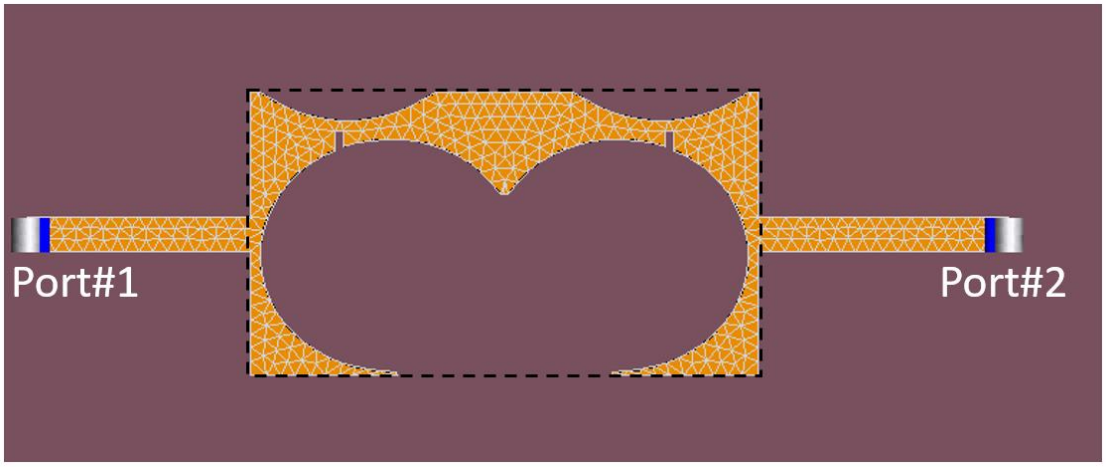

Fig 5.5-5 : Bandstop filter shape synthesized using rectangular and elliptical subtractive elements : Second version. The dashed line is the perimeter of the starting shape.

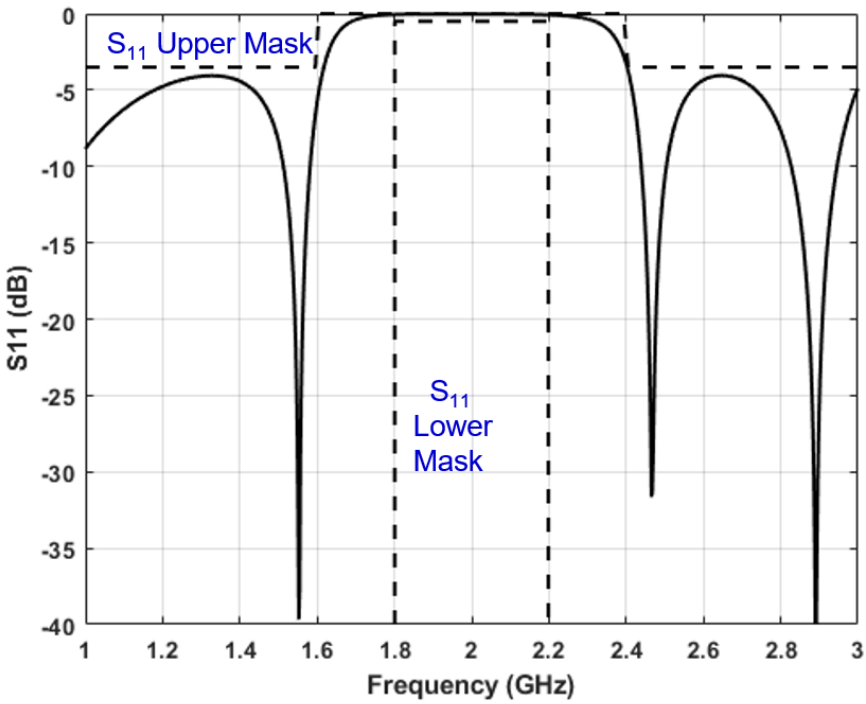

Fig.5.5-6: Computed $|S_{11}|$ of the shape synthesized microstrip bandstop filter shown in Fig.5.5-5.

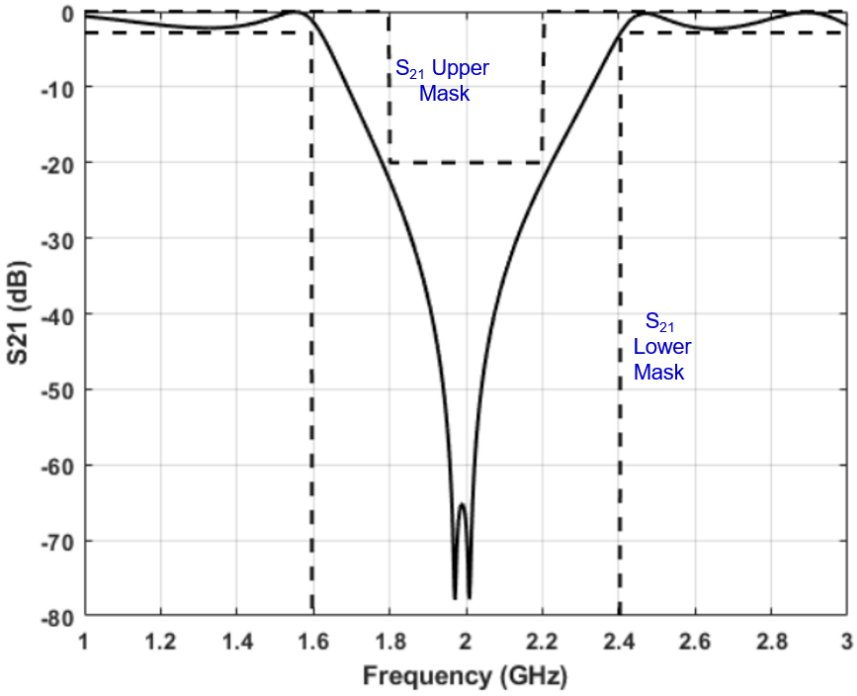

Fig.5.5-7: Computed $|S_{21}|$ of the shape synthesized microstrip bandstop filter shown in Fig.5.5-5.

5.6 ON SUBTRACTIVE SHAPE SYNTHESIS USING GRADIENT-BASED OPTIMISATION

5.6.1 Initial Comments

The application examples shown so far in this chapter confirm the validity of the new subtractive shape synthesis method. It reduces the number of degrees of freedom required and yet provides the necessary geometrical resolution. All the examples utilised the genetic algorithm as the optimizer in the shaping tool. The fact that the degrees of freedom (the adjustable quantities) are continuous geometrical dimensions at once means the surrogate modelling can be utilized. But the goal in this section is to merely demonstrate that, due to the fact that adjustable quantities are continuous variables, gradient-based optimisers can also be used in the shaping tool. Such a gradient-based optimizer[106], which is available in [MATLAB], was incorporated into the shaping tool and applied to the bandstop filter problem with the same parameters and starting shape as in Section 5.4.2.

5.6.2 Continuous Objective Function Composed of S-Parameter Magnitude Masks

As noted in Section 2.5, derivative information (various gradients) of the objective function F_{obj} is needed when using a gradient-based optimization algorithm. The F_{obj} must be defined in a way that such gradient terms are well-defined[107]. The objective functions in Section 5.2 contain the absolute value operation (which has derivative discontinuities), and so are slightly altered here in order to avoid this. The "error" expressions, in terms of which the objective function is be constructed, are now :

A. Error Functions Associated with S_{11}

$n = 1, 2, ..., N_{11}$

$$U_{11}^{(n)} = \begin{cases} \left[S_{11}^{actual}(f_n) \right] - \left[T_{11}^{UpperMask}(f_n) \right] & if \ \left[S_{11}^{actual}(f_n) \right] - \left[T_{11}^{UpperMask}(f_n) \right] \geq 0 \\ 0 & Otherwise \end{cases} \tag{5.6-1}$$

[106] Namely the routine fmincon ("**f**unction **min**imisation with **con**straints"). We have used the option afforded by this routine to determine derivative information numerically.

[107] This is of course not needed by evolutionary optimisation algorithms.

$$L_{11}^{(n)} = \begin{cases} -\left(\left[S_{11}^{actual}(f_n)\right] - \left[T_{11}^{LowerMask}(f_n)\right]\right) & if\ -\left(\left[S_{11}^{actual}(f_n)\right] - \left[T_{11}^{LowerMask}(f_n)\right]\right) \geq 0 \\ 0 & Otherwise \end{cases}$$

(5.6-2)

B. Error Functions Associated with S_{21}

$k = 1, 2, ..., N_{21}$

$$U_{21}^{(k)} = \begin{cases} \left[S_{21}^{actual}(f_k)\right] - \left[T_{21}^{UpperMask}(f_k)\right] & if\ \left[S_{21}^{actual}(f_k)\right] - \left[T_{21}^{UpperMask}(f_k)\right] \geq 0 \\ 0 & Otherwise \end{cases}$$

(5.6-3)

$$L_{21}^{(k)} = \begin{cases} -\left(\left[S_{21}^{actual}(f_k)\right] - \left[T_{21}^{LowerMask}(f_k)\right]\right) & if\ -\left(\left[S_{21}^{actual}(f_k)\right] - \left[T_{21}^{LowerMask}(f_k)\right]\right) \geq 0 \\ 0 & Otherwise \end{cases}$$

(5.6-4)

We can combine the individual terms in a 'sum-of-squares of the errors terms' sense as

$$F_{obj} = F_{mag} = \frac{\mathrm{w}}{2N_{11}} \sum_{n=1}^{N_{11}} \sqrt{[U_{11}^{(n)}]^2 + [L_{11}^{(n)}]^2} + \frac{(1-\mathrm{w})}{2N_{21}} \sum_{k=1}^{N_{21}} \sqrt{[U_{21}^{(k)}]^2 + [L_{21}^{(k)}]^2} \qquad (5.6\text{-}5)$$

5.6.3 Outcomes of the Subtractive Shape Synthesis Utilising a Gradient-Based Optimisation Algorithm

With the gradient-based optimiser used in the shaping tool we arrive at the shape synthesized geometry in Fig.5.6-1. The associated $|S_{21}|$ response is that in Fig.5.6-2. This implementation obviosly clearly shows that the subtractive shape synthesis method can accomodate gradient-based optimisers. However, the shaping process stagnates at the results just shown in Fig.5.6-1 and Fig.5.6-2. Apparently, the gradient-based optimiser has found a local minimum and then is unable to move out of it; this is often a problem with such optimisers, and is one reason users often prefer evolutionary ones, in spite of their relative slowness. It should be recalled that, as

noted in Section 2.10, feature optimisation (that so effectively uses gradient-based optimsers) has the advantage of the 'warm start' afforded by the traditional design geometry that it merely has to fine-tune (and so starts with a peformance already close to the desired one). With shape sythesis there is no such 'warm start' to rely on. Some additional comments on the issue are given in Chapter 6.

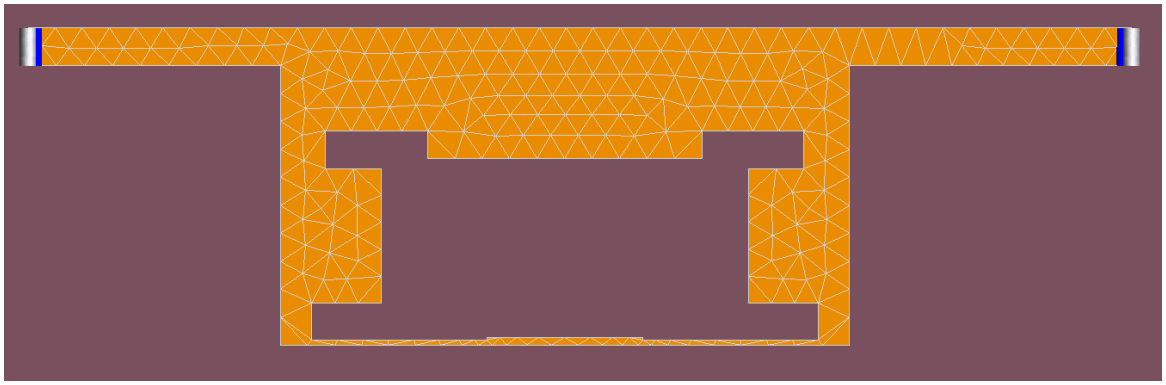

Fig 5.6-1 : Bandstop filter using rectangular subtractive elements in the subtractive shape synthesis procedure utilizing a gradient-based optimisation algorithm.

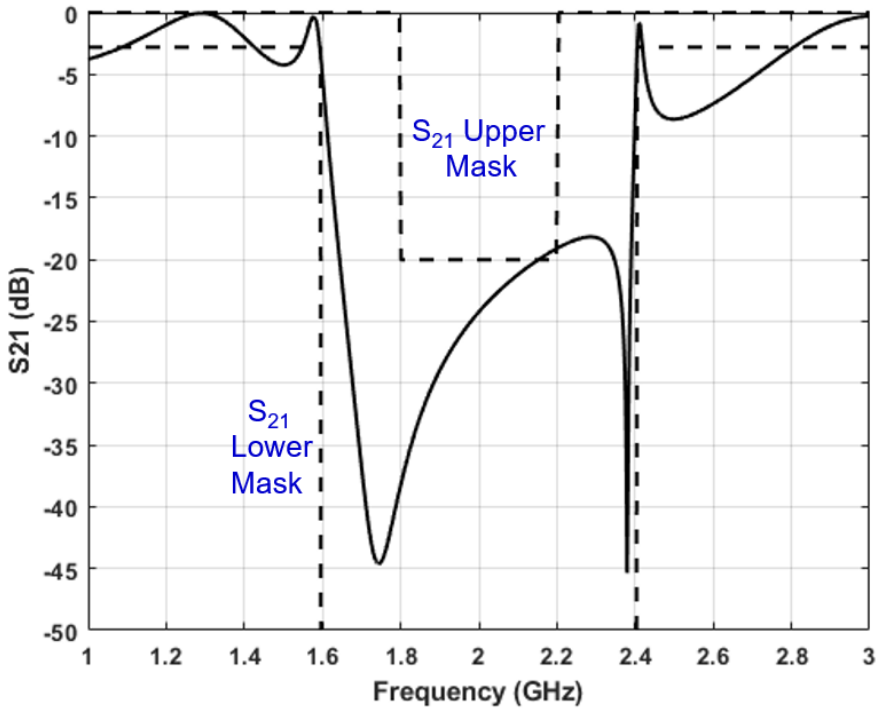

Fig.5.6-2: Computed $|S_{21}|$ of the shape synthesized microstrip bandstop filter shown in Fig.5.6-1.

5.7 PROSPECTS FOR THE SUBTRACTIVE SHAPE SYNTHESIS APPROACH : POSSIBLE EXTENSIONS

The subtractive shaping method is not limited to 2-port physical circuits. It can be applied to multi-ports, to antenna design work (eg. to shape an antenna to obtain both radiation pattern and input/output port requirements), and to multi-layer physical circuits (eg. the groundplane and intermediate conducting layers could be shaped as well), as long as the CEM engine used permits these configurations. Often microstrip circuits make judicious use of vias; the subtractive shaping method could be extended (in fact in an additive sense) by allowing, along with the subtractive elements, one or more vias of some fixed diameter but variable location (x_v, y_v) to be additional degrees of freedom[108]. Although we have validated the new method using microstrip type physical circuits, the idea is sufficiently general that it would be possible to apply the method to other media (eg. waveguide circuitry; coplanar waveguide circuits), as long as the chosen CEM engine allows automated control of the associated geometry by the shaping controller tool. Because the new subtractive shape synthesis method uses continuous geometrical parameters as the adjustable variables, it could be used for many of the tasks currently available using feature optimization methods (eg. surrogate modelling; loss minimization; yield maximization), and yet provide access to a much broader design space.

5.8 CONCLUDING REMARKS

The examples discussed in this chapter have successfully demonstrated the application of the new subtractive shape synthesis method that has been devised in this thesis as a result of experience that revealed the shortcomings of pixelation-based methods. Some of the examples show that such shape synthesis can arrive at a design that would not be directly possible using well-known traditional (feature optimization) procedures. The resulting physical circuit geometries are entirely unconventional, which confirms that the new approach is able to access a wider design space, and hence can provide increased flexibility for RF designers.

Although we have shown examples whose operating frequencies are in the lower GHz range, over different frequency ranges the physical size of the circuits will be different, but the electrical size will not. Thus the CEM analysis we have used will still be feasible. The fact that

[108] Some other ways in which such shape synthesis could allow designs not available using traditional design-library routes were suggested earlier in Section 4.5.

we are able to restrict line widths and gaps (which may turn out to be physically very small for conventional designs at mm-wave frequencies, for example) is a plus. In mm-wave applications one could include power losses in the objective function and design to achieve the mask performance with the minimum loss.

CHAPTER 6
General Conclusions

This research set out to examine existing shape synthesis methods for physical microstrip circuits in an effort to identify why such methods have not yet become mainstream approaches in engineering practice, and then perhaps suggest improvements that might make its more widespread use desirable. Once the shortcomings of existing shape synthesis methods had been identified, it became clear that an entirely new approach was needed. This has been achieved by the contributions of this thesis.

The principal original contributions of the thesis are as follows:

■ A new shape synthesis method, that we have called **subtractive shape synthesis**, has been devised, that overcomes the limitations of existing shape synthesis methods. This approach has not been reported by others. It uses geometrical objects (eg. rectangles, ellipses) that for continuity of terminology could be called generalized pixels/voxels, in that both their centroid locations and their dimensions (size) are not fixed but are continuous variables of the shaping process. At any stage of the shaping process the object being shaped is defined by the starting shape with the subtractive[109] geometrical objects removed. It is this new idea that allows one to obtain the geometrical resolution needed for high-performance RF physical circuits without there being an unmanageable number of degrees of freedom.

■ The details of this new method have been fleshed out and implemented.

■ Importantly, through definition of the starting geometry, the physical circuits can be constrained to fit within some intended layout (eg. not occupying certain parts of the substrate, and having specified port locations). The constraints on the subtractive objects can also be selected so that the resulting physical circuit is favourable (eg. does not require extremely tight tolerances) as regards fabrication. The presence of nearby objects, such as some non-electrical component in the overall layout on which the shape synthesized circuit is to be located, could be accounted for in the shape synthesis.

[109] We realise that there could be additive elements, if this were to prove advantageous, in future developments of the method.

■ The implementated subtractive shape synthesis method has been demonstrated through its successful application to several microstrip circuit examples, such as a matching network and a bandstop filter. These confirmed the viability of the new method. Some of the examples show that such shape synthesis can arrive at a design that would not be directly possible using well-known traditional (feature optimization) procedures. The resulting physical circuit geometries are unconventional, which confirms that the new approach is able to access a wider design space, and hence can provide increased flexibility for RF designers. Yet some geometries reveal features (eg. reveal long stubs and slots, albeit not standard ones) that are reminiscent of what is found in conventional designs.

■ The implementation of the shaping tool itself, apart from being needed to validate the shaping process, is a contribution in its own right. It has purposefully been fully implemented using commercially available software for both the computational electromagnetics and the optimization algorithm. The shaping tool script manages the entire shaping process by permitting the definition of different objective functions, allowing specification of the starting shape and designation of those portions of the starting geometry that may not be altered during shaping, with easy adaption to different problem types and requirements. The shaping tool also communicates and manages the CEM engine and optimization engine. The advantage of being able to use such commercial codes is that the approach becomes more accessible to others.

Some may be of the opinion that the shape synthesis approach is too computer-time-consuming to be of wider interest. But such work should be forward-looking, and so will (like computational electromagnetics, often considered to be ‘ivory-tower’ research in the 1960s/1970s) with continued development, eventually become a standard tool in future RF design. We believe that the new subtractive shape synthesis approach “discovered” by this thesis work can play a key role on advancing the topic.

Unlike existing shape synthesis methods, it can (because of the relatively small number of adjustable variables needed, and the fact that they are continuous) be used directly with surrogate modelling and gradient-based optimization algorithms. It is recommended that future work incorporate surrogate modelling to greatly speed up the subtractive shape synthesis process.

Although[110] we found that gradient-optimizers were not helpful in this work because one does not have a 'warm start' in shape synthesis work, there are emerging studies (currently in disciplines other than electrical engineering) on ways of utilizing evolutionary and gradient-based optimisers in combination "so as to get the best of both worlds" [POUR 18][GHOL 20]. This route could also help speed up the subtractive shape synthesis process. Ways of extending the type of applications of the subtractive shape synthesis process have also been provided in Section 5.7.

[110] As discussed in Section 5.6.3.

References

[AAGE 17] N.Aage and V. Egede Johansen, “Topology optimization of microwave filters”, Int. J. for Numerical Methods in Engineering, Vol.112, pp.283-300, May 2017.

[ALAK 21] A.Alakhras and D.A.McNamara, “The shape synthesis of 3D electrically-small conducting surface antennas”, Electronics Letters, Vol.57, No.8, pp.311-313, April 2021.

[ALJA 17] A.Aljanah and D.A.McNamara, “The shape synthesis of unit elements for transmitarray antennas”, IEEE AP-S Int. Symp. Digest, San Diego, USA, July 2017.

[ALJA 18] A.Aljanah and D.A.McNamara, “Shape synthesis of 3-layer transmitarray elements”, IEEE Int. Antennas & Propagat. Symp. Digest, Boston, USA, July 2018.

[ALJA 21] A.Alajanah, E.Almajali and D.A.Mcnamara, “Some observed outcomes of the shape synthesis of dual-band transmitarray elements”, IEEE Int. Antennas & Propagat. Symp., Singapore, December 2021.

[ALRO 20] H.Alroughani & D.A.McNamara, “The shape synthesis of dielectric resonator antennas”, IEEE Trans. Antennas Propagation, Vol.68, No.8, pp.5766-5777, Aug.2020.

[ALTS02] E. Altshuler, "Electrically small self-resonant wire antennas optimized using a genetic algorithm," IEEE Transactions on Antennas and Propagation, vol. 50, no. 3, pp. 297-300, 2002.

[AOKI 11] Y. Aoki, H. Deguchi, and M. Tsuji, “Reflectarray with arbitrarily-shaped conductive elements optimized by genetic algorithm”, IEEE Antennas and Propagation International Symposium, Spokane, Washington, USA, July 2011.

[ASSA 06] A.Assadihaghi, S.Bila, C.Durousseau, D.Bailiargeat, M.Auborg, S.Verdeyme, M.Rochette, J.Puech and L.Lapierre, “Design of microwave components using topology gradient optimization”, 36th European Microwave Conf., Manchester, UK, pp.462-465, Sept. 2006.

[ASSA 08] A.Assadihaghi, S.Bila, D.Bailiargeat, M.Auborg, S.Verdeyme, C.Boichon, J.Puech and L.Lapierre, “Optimization of microwave devices combining topology gradient and genetic algorithm”, Int. J. RF and Microwave Computer-Aided Engineering, pp.454-463, May 2008.

[BAND69] W. Bandler, “Optimization methods for computer-aided design,” IEEE Transactions on Microwave Theory and Techniques, vol. mtt-17, 1969.

[BAND 88] J.W.Bandler and S.H.Chen, “Circuit optimization : The state of the art”, IEEE Trans. Microwave Theory Tech., Vol.36, No.2, pp.424-443, Feb.1988.

[BAND 93] J.W.Bandler, S.H.Chen, R.M.Biernacki, L.Gao, K.Madsen and H.Yu, “Huber optimization of circuits : A robust approach”, IEEE Trans. Microwave Theory Tech., Vol.41, No.12, pp.2279-2287, Dec.1993.

[CAMP 21] S.D.Campbell, R.P.Jenkins, O.J.O’Connor and D.H.Werner, “The explosion of artificial intelligence in antennas and propagation”, IEEE

Antennas and Propagation Magazine, pp.16-27, June 2021.

[CAPE 19] M.Capek, L.Jelinek and M.Gustafsson, “Shape synthesis based on topology sensitivity”, IEEE Trans. Antennas Propagation, Vol.67, No.6, pp.3889-3901, June 2019.

[CELU 00] M.Celuch-Marcysiak, W.Gwarek, P.Miazga, M.Sypniewski and A.Wieckowski, “Automatic design of high frequency structures using 3-D FDTD simulator in an optimization loop”, 13th Int. Conf. Microwaves, Radar and Wireless Communications (MIKON), Wroclaw, Poland, May 2000.

[CHOO 00] H. Choo, A. Hutani, L. C. Trintinalia and H. Ling, "Shape optimisation of broadband microstrip antennas using genetic algorithm," in Electronics Letters, vol. 36, no. 25, pp. 2057-2058, 7 Dec. 2000.

[COLL 92] R.E.Collin, Foundations for Microwave Engineering (McGraw-Hill, 1992).

[DAVI 84] W.A.Davis, Microwave Semiconductor Circuit Design (Van Nostrand Reinhold Co., 1984)

[DELA 97] C. Delabie, M. Villegas, and O. Picon, “Creation of new shapes for resonant microstrip structures by means of genetic algorithms”, Electronics Letters, Vol. 33, No. 18, pp. 1509-1510, Aug. 1997.

[EDWA 01] T.C.Edwards and M.B.Steer, Foundations of Interconnect and Microstrip Design (Wiley, 2001).

[EREN11] A. Erentok and O. Sigmund, "Topology optimization of sub-wavelength antennas," IEEE Transactions on Antennas and Propagation, vol. 59, no. 1, pp. 58-69, 2011.

[ETHI 12] J. Ethier and D. McNamara, "A sub-structure characteristic mode concept for antenna shape synthesis," *Electronics Letters*, vol.48, no.9, 2012.

[ETHI 14a] J.Ethier, D.A.McNamara, J.Shaker & R.Chaharmir, “Reflectarray synthesis with similarity-shaped fragmented sub-wavelength elements”, IEEE Trans. Antennas Propagation, Vol.62, No.9, pp.4498-4509, Sept.2014.

[ETHI 14b] J.Ethier and D.A.McNamara, “Antenna shape synthesis without prior specification of the feedpoint locations”, IEEE Trans. Antennas Propagation, Vol.62, No.10, pp.4919-4934, Oct.2014.

[FEKO 21] FEKO, Altair Inc. (www.altair.com).

[GHOL 20] S.Gholizadeh, M.Danesh and C.Gheyratmand, “A new Newton metaheuristic algorithm for discrete performance-based design optimization of steel moment frames”, Computers and structures, Vol.234, July 2020.

[GOSA 17] G.Gosal, E.Almajali, D.A.McNamara and M.Yagoub, “Transmitarray antenna design using forward and inverse neural network modelling”, IEEE Antennas & Wireless Propagation Letters, Vol.15, pp.1483-1486, 2016.

[GOUD 17] S. Goudos, "Antenna design using binary differential evolution," IEEE Antennas and Propagation Magazine, pp.74-93, Feb.2017.

[GROU 19] V.Grout, M.O.Akinsolu, B.Liu, P.I.Lazaridis, K.K.Mistry and Z.D.Zaharis, “Software solutions for antenna design exploration”, IEEE

Antennas and Propagation Magazine, pp.48-59, June 2019.

[HASS 14] E. Hassan and M. Berggren,"Topology optimization of metallic antennas", IEEE Transactions on Antennas and Propagation, vol.62, no.5, pp.2488-2500, May 2014.

[HASS 20] E.Hassan, B.Scheiner, F.Michler, M.Berggren, E.Wadbro, F.Röhrl, "Multilayer topology optimization of wideband SIW-to-waveguide transitions", IEEE Transactions on Microwave Theory and Techniques, Vol.68, No.4, pp.1326-1339, April 2020.

[HONG 01] J.Hong and M.J.Lancaster, Microstrip Filters for RF/Microwave Applications (Wiley, 2001)

[HAUP 10] R.L.Haupt, T.H.O'Donnell and H.L.Southal, "Biological Antenna Design Methods", Chap.6 in : F.Gross (Edit.), Frontiers in Antennas (McGraw-Hill, 2010)

JENS 11 J.S.Jensen and O.Sigmund, "Topology optimization for nano-photonics", Laser Photonics Review, Vol.5, No.2, pp.308-321, 2011.

[JIN 21] J.Jin, F.Feng, J.Zhang, J.Ma and Q.J.Zhang, "Efficient EM topology optimization incorporating advanced matrix Padé via Lanczos and genetic algorithm for microwave design", IEEE Trans. Microwave Theory & Techniques, Available via IEEE Early Access, 2021.

[JOHN 96] A.John and R.H.Jansen, "Evolutionary generation of M(MIC) component shapes using 2.5D EM simulation and discrete genetic optimization", IEEE MTT-S International Symposium Digest, pp.745-748, San Francisco, California, USA, June 1996.

[JOHN 97] J. Johnson and Y. Rahmat-Samii, "Genetic algorithms in engineering electromagnetics", IEEE Transactions Antennas Propagation Magazine, vol. 39, pp. 7-21, 1997.

[JOHN 99a] J. Johnson and Y.Rahmat-Samii, "Genetic algorithms and method of moments (GA/MOM) for the design of integrated antennas", IEEE Transactions on Antennas and Propagation, vol.47, pp.1606-1614, 1999.

[JOHN 99b] J. Johnson and Y. Rahmat-Samii, "Evolutionary designs of integrated antennas using genetic algorithms and method of moments (GA/MoM)", Electromagnetic Optimization by Genetic Algorithms (Wiley, 1999).

[KIDO 07] A. Kido, H. Deguchi, M. Tsuji and M. Ohira, "Multi-resonator generation in arbitrarily-shaped planar-circuit filters by genetic optimization", 2nd European Microwave Integrated Circuits Conference, October 2007.

[KIDO 08] T. Kido, H. Deguchi, M. Tsuji and M. Ohira, "Compact high-performance planar bandpass filters with arbitrarily-shaped conductor patches and slots", 38th European Microwave Conference, October 2008.

[KOZA 98a] A.Kozak and W.Gwarek, "Unrestricted arbitrary shape optimization based on 3D electromagnetic simulation", IEEE MTT-S International Symposium Digest, Baltimore, Maryland, June 1998.

[KOZA 98b] A.Kozak and W.Gwarek, "Automatic arbitrary shape optimization based on 3D FDTD solver and perturbation theory applied for synthesis of resonators", 13th Int. Conf. Microwaves, Radar and Wireless Communications (MIKON), Poland, May 1998.

[LI 18] R.Li, D.A.McNamara, G.Wei & J.Li, "Increasing radiation efficiency using antenna shape optimization approach", IEEE Antennas Wireless Propagat. Letters, Vol.17, No.3, pp.393-396, March 2018.

[LIND 99] D. Linden and E. Altshuler, "Design of wire antennas using genetic algorithms", Chapter 8 in : Y. Rahmat-Samii and E. Michielssen (Edits.), Electromagnetic Optimization by Genetic Algorithms (Wiley, 1999).

[LIU 16] H. Liu and M. Yan, "Electrically small loop antenna standing on compact ground in wireless sensor package," IEEE Antennas and Wireless Propagation Letters, vol. 15, pp. 76-79, 2016.

[MAHD 15] [MAHD 15] N. Mahdi, S. Bila, M. Aubourg, C. DUrousseau, J. Puech, and D. Baillargeat, "Shape Optimization of Planar Microwave Components", IEEE MTT-S International Conference on Numerical Electromagnetic and Multiphysics Modeling and Optimization (NEMO), Ottawa, Canada, Aug. 2015.

[MATLAB] MATLAB R2016b, Optimization Toolbox 7.5. www.mathworks.com

[MATT 21] M.Matthaiou, O.Yurduseven, H.Q.Ngo, D.Morales-Jimenez, S.L.Cotton and V.F.Fusco, "The road to 6G : Ten physical layer challenges for communications engineers"" IEEE Communications Magazine, pp.64-69, Jan.2021.

[MIAZ 97] P.Miazga and W.Gwarek, "Improved design of passive coaxial components using electromagnetic 2-D solver in an optimization loop", IEEE Transactions on Microwave Theory and Techniques, Vol.45, No.6, pp.858-861, June 1997.

[MIRH16] S. Mirhadi and M. Soleimani, "Ultra wideband antenna design using discrete Green's functions in conjunction with binary particle swarm optimisation," IET Microwaves, Antennas & Propagation, vol. 10, no.2, pp.184-192, 2016.

[MITC 99] M. Mitchell, *"An Introduction to Genetic Algorithms" (MIT Press, 1999).*

[NISH 02] T. Nishino and T. Itoh, "Evolutionary generation of microwave line-segments circuits by genetic algorithms," IEEE Trans. Microwave Theory Tech., vol. 50, pp. 2048–2055, Sept. 2002.

[NISH 03] T. Nishino and Tatsuo Itoh, "Evolutionary generation of 3-D line-segment circuits with a broadside-coupled multiconductor transmission-line model," IEEE Transactions on Microwave Theory and Techniques, vol. 51, no. 10, pp. 2045-2054, Oct. 2003.

[NOMU 13] T.Nomura, M.Ohkado, P.Schmalenberg, J.Lee, O.Ahmed and M.Bakr, "Topology optimization method for microstrips using boundary condition representation and adjoint analysis", 43rd European Microwave Conf., pp.632-635, Nuremberg, Germany, Oct.2013.

[OHIR 06] M. Ohira, H. Deguchi, M. Tsuji, and H. Shigesawa, "Planar-circuit bandpass filters consisting of arbitrarily shaped elements", European Microwave Integrated Circuits Conference, May 2006.

[OHIR 07] M. Ohira, H. Deguchi, M.Tsuji, and H. Shigesawa, "Planar-circuit bandpass filters consisting of arbitrarily shaped elements," Electronics and Communications in Japan, Part 2, Vol. 90, No. 2, 2007.

[OZGU 03] O. Ozgun and S. Mutlu, "Design of dual-frequency probe-fed microstrip

antennas with genetic optimization algorithm," in IEEE Transactions on Antennas and Propagation, vol. 51, no. 8, pp. 1947-1954, Aug. 2003.

[PETE 97] A.Peterson, S.Ray and R.Mittra, Computational Methods for Electromagnetics (IEEE Press, 1997).

[POUR 18] A.Pourchoit and O.Sigaud, “Combining evolutionary and gradient-based methods for policy search”, Computer Science, Sept.2018.

[POZA 90] D.M.Pozar, Microwave Engineering (Addison-Wesley Publ. Co., 1990)

[RAHM 07] Y. Rahmat-Samii, Reflector Antennas, Chapter 15 in: J. L. Volakis (Edit.), Antenna Engineering Handbook (McGraw-Hill, 2007), 4th Edition.

[RAHM12] Y.Rahmat-Samii, J.M.Kovitz and H.Rajagopalan, “Nature-inspired optimization techniques in communication antenna designs", Proc.IEEE, Vol.100, No.7, pp.2132-2144, July 2012.

[RAMO 45] S.Ramo, Introduction to Microwaves (McGraw-Hill, 1945).

[RAO 82] S.M.Rao, D.R.Wilton and A.W.Glisson, "Electromagnetic scattering by surfaces of arbitrary shape", IEEE Transactions on Antennas and Propagation, vol.30, pp.409-418, May 1982.

[RAO 13] S. Rao, L. Shafai, and S. K. Sharma (Edits.), Handbook of Reflector Antennas and Feed Systems, Vol. I, II, and III (Artech House, 2013).

[SALU 18] M. Salucci, F.Robol, N.Anselmi, M.A.Hannan, P.Rocca, G.Olivieri, M.Donelli and A.Massa, "S-Band spline-shaped aperture-stacked patch antenna for air traffic control applications," IEEE Transactions on Antennas and Propagation, vol. 66, no. 8, pp. 4292-4297, 2018.

[SAZO 82] D. M. Sazanov, A. N. Gridin, and B. A. Mishustin, Microwave Circuits (Mir Publ., 1982), pp.74-75.

[SHAR 20] Y.Sharma, H.H.Zhang and H.Xin, “Machine learning techniques for optimizing design of double T-shaped monopole design”, IEEE Transactions on Antennas and Propagation,, vol.68, No.7, pp.5658-5663, July 2020.

[SONN 21] SONNET, Sonnet Software Inc., www.sonnetsoftware.com

[SORR 10] R.Sorrentino and G.Bianchi, Microwave and RF Engineering (Wiley, 2010)

[STEE 02] M. B. Steer, J. W. Bandler and C. M. Snowden, "Computer-aided design of RF and microwave circuits and systems," in IEEE Transactions on Microwave Theory and Techniques, vol. 50, no. 3, pp. 996-1005, Mar.2002.

[STEE 13] M.Steer, Microwave & RF Design : A Systems Approach (Scitech Publishing, 2013)

[SUMO 21] Surrogate Modelling Lab, Ghent University, Belgium. http://sumo.intec.ugent.be

[THOR 05] B. Thors, and H. Holter, "Broadband fragmented aperture phased array element design using genetic algorithms", IEEE Transactions Antennas propagate vol. 53, pp. 3280-3287, 2005.

[TOIV 10] J. Toivanen and P. Ylä-Oijala, “Gradient-based shape optimization of ultra-wideband antennas parameterized using splines,” IET Microwaves, Antennas & Propagation, vol. 4, pp. 1406-1414, 2010.

[TOIV 09] J. I. Toivanen, R.A.E.Makinen, S.Jarvenpaa, P. Ylä-Oijala and J.Rahola, "Electromagnetic sensitivity analysis and shape optimization using method of moments and automatic differentiation", IEEE Transactions on Antennas and Propagation, Vol. 57, No.1, pp. 168-175, Jan. 2009.

[VOLA 12] J.Volakis and K.Sertel, Integral Equation Methods for Electromagnetics (SciTech Publ., 2012)

[WANG 04] W.Wang, Y.Lu and J.S.Fu, "Arbitrary planar microwave filter design by the FEM-GA approach", Microwave & Optical Technology Letters, Vol.41, No.4, pp.276-279, May 2004.

[WANG 05] W.Wang, Y.Lu, J.S.Fu and Y.Z.Xiong, "Particle swarm optimization and finite-element based approach for microwave filter design", IEEE Trans. Magnetics, Vol.41, No.5, pp.1800-1803, May 2005.

[WANG20a] Z.Wang, J.Dong, M.Wang and J.Mo, "Antenna topology optimization based on binary bat algorithm", Int. Conf. Microwave & Millimeterwave Technology, Shanghai, China, Sept.2020.

[WANG20b] Z.Wang, J.Dong, M.Wang and J.Mo, "Antenna topology optimization based on angle-modulated bat algorithm", IEEE MTT-S Int. Conf. Numerical Electromagnetic & Multiphysics Modeling and Optimization (NEMO), Hangzho, China, Dec.2020.

[WEIL 97] D. Weile and E. Michielssen, "Genetic algorithm optimization applied to electromagnetics: a review," IEEE Transactions on Antennas and Propagation, vol. 45, pp. 343-353, 1997.

[WOLP 97] Wolpert, D.H., William, G.M.: 'No free lunch theorems for optimization', IEEE Trans. Evol. Comput., 1997, 1, pp. 67–82.

[YAMA09] T. Yamamoto and T. Tsukagoshi, "Efficient antenna miniaturization technique by cut off of chromosome-length in genetic algorithm," Asia Pacific Microwave Conference, Singapore, pp. 1837-1840, 2009.

[YANG16a] B. Yang and J. Adams, "Systematic shape optimization of symmetric MIMO antennas using characteristic modes", IEEE Transactions on Antennas and Propagation,, vol.64, pp.2668-2678, 2016.

[YANG16b] B. Yang and J. Adams, "A modal approach to shape synthesis and feed placement for planar MIMO antennas," IEEE International Symposium on Antennas and Propagation, Fajardo, pp. 15-16, 2016.

[YANG19] B. Yang and J. Adams, "A shape-first, feed-next design approach for compact planar MIMO antennas," Progress In Electromagnetics Research, Vol. 77, 157–165, 2019.

ZHU 20 S.Zhu, X.Yang, J.Wang, N.Nie and B.Wang, "Mutual coupling reduction of ±45º dual-polarized closely spaced MIMO antenna by topology optimization", IEEE Access, Vol.8, pp.29089-29098, Feb.2020.

[ZHAN 21] Q.J.Zhang, E.Gad, B.Nouri, W.Na and M.Nakhla, "Simulation and automated modelling of microwave circuits : State-of-the-art and emerging trends", IEEE J. Microwaves, Vol.1, No.1, pp.494-507, Jan. 2021.

APPENDIX I

Some Details on a Particular Discrete-Pixelation Shape Synthesis Case Referred to in Part H of Section 3.7.2

The "hairpin" bandpass filter configuration [HONG 01] is shown in Fig.I-1, obtained using feature optimization. The S-parameter performance we computed using [SONN 21] is shown in Fig.I-2 and Fig.I-3. The upper and lower masks are also shown. We noted that changes of only 0.1mm in the lengths of the coupled resonators in Fig.I caused the S-parameter performance to change by noticeable amounts. The discrete-variable pixelation based method was then used to shape synthesize a bandpass filter that satisfies the same mask. The starting shape was a rectangle of conductor that fits between the two ports and just encloses the actual hairpin layout, shown by the blue dashed line in Fig.I-1.

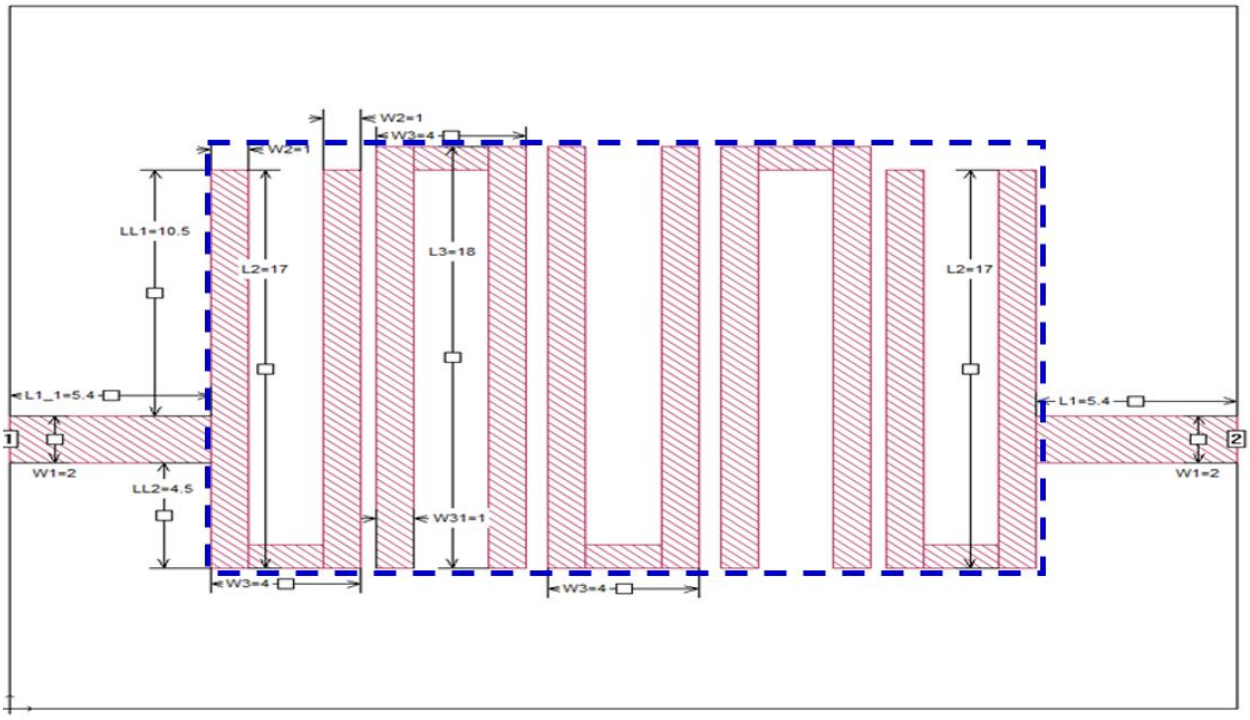

Fig. I-1 : Feature-optimized 5-pole hairpin bandpass filter microstrip physical circuit. The substrate thickness is 1.27mm and the relative permittivity 6.15.

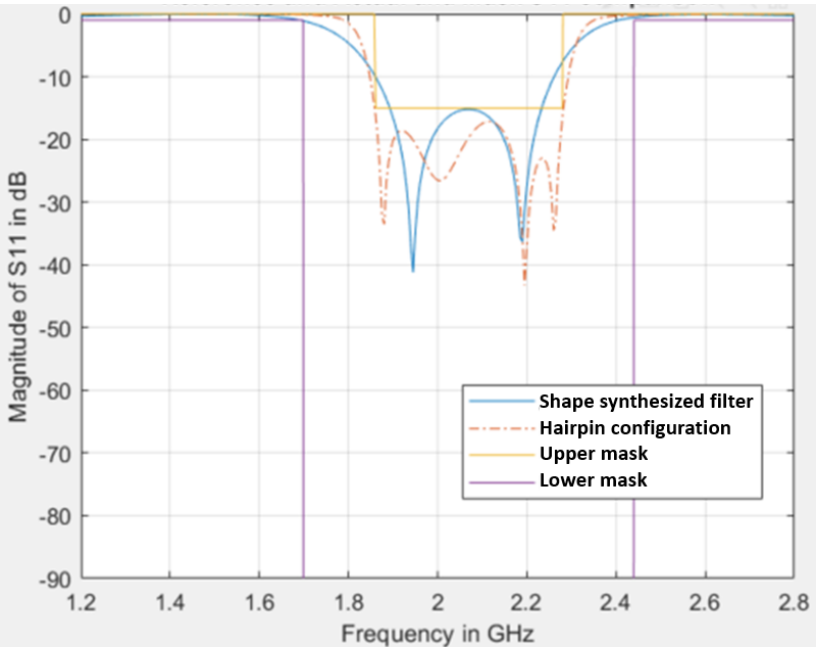

Fig. I-2 : Computed S_{11} magnitude of the hairpin configuration, and shaped synthesized, bandpass filter.

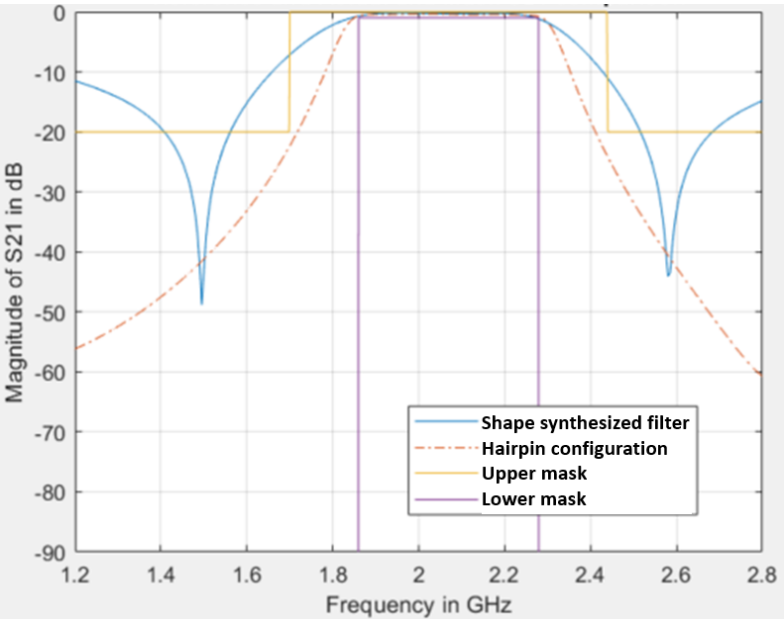

Fig. I-3 : Computed S_{21} magnitude of the hairpin configuration, and shaped synthesized, bandpass filter.

When performing the shape synthesis, if the pixel size is selected to 0.1mm per side, the number of pixels required[111] (degrees of freedom assigned for shaping) is roughly 10000, whereas a cell

[111] This is also then the resulting chromosome length when using the GA optimiser.

size of 0.5mm per side reduces this to 1584[112]. Even with this much smaller number, the shape synthesis runs for several weeks without the shaped designs satisfying the specified masks. The process was halted when the shaped filter was as shown in Fig.I-4. The GA optimizer had stagnated. Its S-parameter performance is also shown in Figs. I-2 and I-3. The mask has not yet been satisfied.

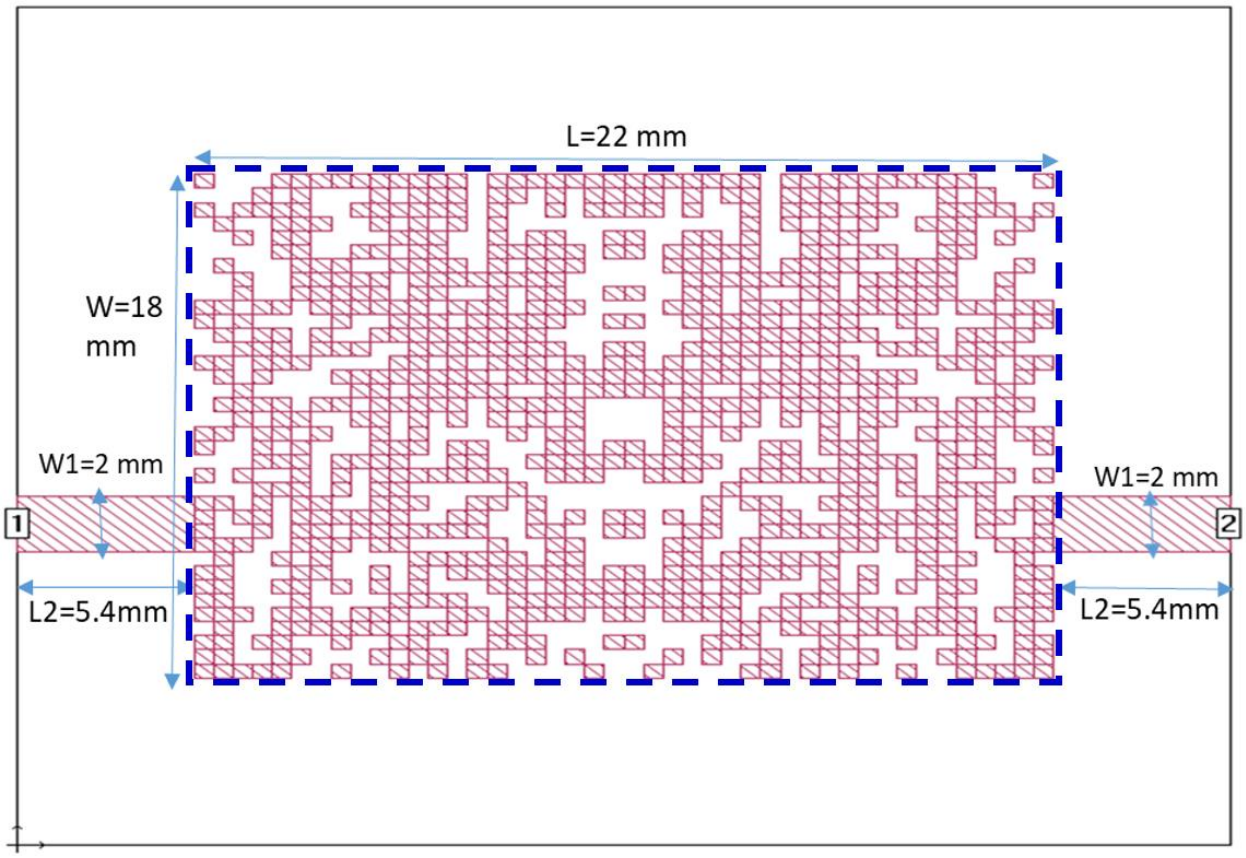

Fig. I-4 : Discrete-pixelation shape synthesized bandpass filter.

[112] It may be for this reason that (see Part G of Section 3.7.2) the authors of [MAHD 15] shaped the resonators of their hairpin filter individually to obtained the special performance they required, rather than the complete hairpin filter, although the authors do not say this.